

**UNIVERSITY OF THE WITWATERSRAND**

School of Civil and Environmental Engineering



UNIVERSITY OF THE  
WITWATERSRAND,  
JOHANNESBURG

**Effect of corrosion of lap-spliced steel reinforcement on the  
flexural strength of reinforced concrete beams**

**Anele Emanuel Mahlawe**

A research report submitted to the Faculty of Engineering and the Built Environment, University of the Witwatersrand, in partial fulfilment of the requirements for the degree of Master of Science in Engineering

October, 2020

**Johannesburg**

## DECLARATION

I declare that this research report is my own, unaided work. It is being submitted for the Degree of Master of Science to the University of the Witwatersrand, Johannesburg. It has not been submitted before for any degree or examination to any other University.



.....  
Anele Emanuel Mahlawe

**05 October 2020**

Date

## ABSTRACT

The study aimed to investigate the effect of corrosion on the flexural strength of reinforced concrete (RC) beams with steel lap-splicing in the central constant moment region. A total of 24 RC  $100 \times 165 \times 1500$  mm beams were cast each for SANS10100-1 and Eurocode 2. Out of the 24 RC beams, 12 RC beams were cast for each design code (6 with lap-splicing and 6 without spliced flexural reinforcement). Accelerated chloride-induced corrosion was used to induce steel corrosion in the in the central constant moment region. Only 6 RC beams were corroded for each design code, the remaining 6 were used for reference purposes.

All beams were tested for ultimate strength using a 4-point bending configuration. The applied load, mid-span deflection and mode of failure were recorded until failure load was reached. The results showed an increase in deflection and a decrease in ultimate strength in the corrosion-damaged specimens. The failure mode of non-lapped beams remained ductile, while on lap-spliced beams the failure mode changed from ductile to brittle. The corroded bars were physically measured using a Vernier Caliper for the determination of corrosion degree.

## **DEDICATION**

To my beloved family, my wife and my children.

## ACKNOWLEDGEMENTS

I would like to express my sincere gratitude towards the following people for their immense contribution towards the accomplishment of this research project:

- My supervisor, Dr. Mike Otieno for his support, guidance and encouragement given during the entire study period. This work would not have been possible without his direction and support.
- My wife Fundiswa and my children Zinathi and Zongeziwe for their invaluable encouragement, support and patience during my study. Without them, none of this would have been possible.
- To my mother and all my siblings for their support and encouragement. In particular I would like to thank my brother Nceba, who was always happy to lend a helping hand during casting of beams.
- My late father. He and my mother have always given unwavering encouragement and support towards all my academic endeavours.
- To Hillman building staff for their willingness to always assist.
- To my fellow postgraduate colleagues in the Cement and Concrete Research Group for their support and encouragement.
- My employer, Department of Environmental Affairs for funding my studies and for granting me time off to conduct laboratory experiments.
- To The Concrete Institute, AfriSam and National Research Foundation for their support in various ways during the experimental work.

Above all and before anything else, I thank the Almighty for making the completion of this research project possible.

## NOMENCLATURE

PC	Portland cement
RC	Reinforced concrete
w/b	Water to binder ratio
SANS	South African National Standard
EC2	Eurocode 2

### Concrete beam series labels

SANS – NS – NC 10100-1	Non-corroded/non-spliced beams designed according to SANS 10100-1
SANS – S – NC	Non-corroded/ spliced beams designed according to SANS 10100-1
EC2 – NS – NC	Non-corroded/non-spliced beams designed according to Eurocode 2
EC2 – S – NC	Non-corroded/ spliced beams designed according to Eurocode 2
SANS – NS – C	Corroded/non-spliced beams designed according to SANS 10100-1
SANS – S – C	Corroded/ spliced beams designed according to SANS 10100-1
EC2 – NS – C	Corroded/non-spliced beams designed according to Eurocode 2
EC2 – S – C	Corroded/ spliced beams designed according to Eurocode 2

## TABLE OF CONTENTS

<b>DECLARATION .....</b>	<b>i</b>
<b>ABSTRACT .....</b>	<b>ii</b>
<b>DEDICATION .....</b>	<b>iii</b>
<b>ACKNOWLEDGEMENTS .....</b>	<b>iv</b>
<b>NOMENCLATURE .....</b>	<b>v</b>
<b>LIST OF FIGURES.....</b>	<b>x</b>
<b>LIST OF TABLES.....</b>	<b>xii</b>
<b>CHAPTER 1: INTRODUCTION .....</b>	<b>1</b>
1.1    Background .....	1
1.2    Splicing of steel reinforcement in flexural RC members .....	2
1.3    Problem Statement .....	3
1.4    Aim and objectives of the study .....	3
1.5    Motivation and significance of the research.....	4
1.6    Scope and limitations .....	5
1.7    Layout of the report.....	5
1.8    References .....	6
<b>CHAPTER 2: LITERATURE REVIEW .....</b>	<b>9</b>
2.1    Introduction .....	9
2.2    Transport mechanisms in concrete .....	9
2.2.1    Capillary suction .....	9
2.2.2    Diffusion .....	9
2.2.3    Permeation .....	10
2.2.4    Migration .....	11
2.3    Mechanism of steel reinforcement corrosion in concrete .....	11
2.3.1    Causes of reinforcement corrosion in concrete.....	12

2.3.2	Stages of steel corrosion in reinforced concrete structures.....	15
2.3.3	Mechanical properties of corroded steel bars and effect of steel corrosion on flexural strength of beams .....	16
2.3.4	Effect of corrosion on steel-concrete interface bond .....	17
2.3.5	Factors affecting reinforcement corrosion .....	19
2.3.6	Accelerated corrosion .....	28
2.4	Need for lap-splicing of steel reinforcement in concrete .....	30
2.4.1	Code stipulations on lap splicing of flexural steel reinforcement.....	31
2.5	Summary .....	32
2.6	References .....	33
<b>CHAPTER 3: EXPERIMENTAL METHODOLOGY .....</b>		<b>40</b>
3.1	Introduction .....	40
3.2	Materials.....	40
3.2.1	Cement .....	40
3.2.2	Aggregates .....	40
3.2.3	Reinforcing steel .....	42
3.2.4	Formwork.....	42
3.3	Concrete mix proportions.....	44
3.4	Specimen type and sample size .....	44
3.5	Mixing, casting and curing of specimens.....	46
3.6	Corrosion acceleration experimental set-up.....	47
3.7	Specimen testing .....	51
3.7.1	Compressive strength tests.....	51
3.7.2	Flexural strength tests .....	52
3.8	Assessment of corrosion in corroded RC beams.....	53
3.9	Conclusion.....	53
3.10	References .....	54
<b>CHAPTER 4: RESULTS AND DISCUSSION.....</b>		<b>57</b>
4.1	Introduction .....	57



4.2	General observations .....	57
4.2.1	Corrosion induced cracking .....	57
4.2.2	Steel corrosion morphology .....	59
4.3	Determination of corrosion-inducing current.....	61
4.4	Compressive strength tests .....	62
4.5	Flexural strength tests.....	62
4.5.1	Testing set-up.....	62
4.5.2	Load-midspan deflection behaviour of reference beams .....	63
4.5.3	Load-midspan deflection behaviour of corroded beams.....	67
4.5.4	Mode of failure .....	70
4.2.3	Determination of corrosion level / Actual degrees of corrosion.....	74
4.5.5	Effect of degree of corrosion on flexural capacity of RC beams.....	76
4.5.6	Effect of corrosion on ductility of RC beams .....	79
4.5.7	General findings and comparison of SANS 10100-1 and Eurocode 2 on the performance of lap-spliced RC beams.....	80
4.6	Comparison with results from other researcher's .....	81
4.7	General discussion of results.....	82
4.8	References .....	84
<b>CHAPTER 5: CONCLUSIONS AND RECOMMENDATIONS .....</b>		<b>86</b>
5.1	Introduction .....	86
5.2	Conclusions .....	86
5.2.1	Influence of corrosion of lap-spliced steel on the flexural performance of RC beams .....	86
5.2.2	Flexural ductility of steel corrosion-damaged RC beams.....	87
5.2.3	Failure mode of steel corrosion-damaged RC beams .....	88
5.2.4	Practical implications of the study findings.....	88
5.3	Recommendations for future studies.....	89
<b>APPENDIX A: SPECIMEN DESIGN.....</b>		<b>90</b>
A.1	SANS 10100-1 design.....	90

A.2	Eurocode 2 design .....	94
<b>APPENDIX B: DETAILS OF AGGREGATES AND CONCRETE MIX DESIGN ... 97</b>		
B.1	Fine aggregate grading analysis and grading curve .....	97
B.2	Coarse aggregate grading analysis and grading curve .....	98
B.3	Concrete Mix Design .....	99
<b>APPENDIX C: EXPERIMENTAL RESULTS ..... 101</b>		
C.1	Compressive Strength and Density Results .....	101
C.2	Corrosion Acceleration Tests .....	103
C 2.1	Estimation of required current inducing corrosion .....	103
C 2.2	Corrosion degree results .....	104
C 2.3	Voltage-time curves .....	106
C 2.4	Theoretical vs Experimental load .....	110
C 2.5	Flexural strength vs corrosion results .....	111
C 2.6	Ductility vs corrosion results .....	112
	School of Civil Engineering and Environmental Engineering Ethics Committee: Ethics Waiver.....	113

## LIST OF FIGURES

Figure 2. 1: Convection zone in concrete (Ballim, et al., 2009).....	10
Figure 2. 2: Illustrates the corrosion of reinforcement in concrete (Ahmad, 2003).....	12
Figure 2. 3: The carbonation “front” (Ballim <i>et al.</i> , 2009).....	13
Figure 2. 4: Corrosion damage model (Tuutti, 1982).....	15
Figure 2. 5: Bond strengths of corroded specimens (Al-Sulaimani <i>et al.</i> , 1990; Cabrera, 1996).....	18
Figure 2. 6: Effect of concrete cover on the diffusion of oxygen (Bentur <i>et al.</i> , 1997).....	23
Figure 2. 7: Average chloride-induced corrosion rates (Otieno, 2008).....	26
Figure 3. 1: Grading curve of fine aggregate.....	41
Figure 3. 2: Photograph of moulds prior to concrete casting .....	43
Figure 3. 3: Photograph of moulds post concrete casting.....	43
Figure 3. 4: Type A RC beams geometry and reinforcement details (according to SANS10100-1) .....	46
Figure 3. 5: Type B RC beams geometry and reinforcement details (according to Eurocode 2).....	46
Figure 3. 6: Accelerated corrosion set-up of beam specimens .....	48
Figure 3. 7: Photograph showing accelerated corrosion set-up.....	49
Figure 3. 8: Photograph showing longitudinal cracks on concrete surface .....	50
Figure 3. 9: Photograph showing corrosion products.....	51
Figure 3. 10: Photograph showing support conditions and loading arrangement .....	52
Figure 3. 11: Flow chart showing experimental details.....	54
Figure 4. 1: Schematic diagram of RC beam specimens .....	58
Figure 4. 2: Cracking on the ponded surface.....	58
Figure 4. 3: Cracking on the vertical side of beam.....	59
Figure 4. 4: Corrosion distribution on non-lap steel bars .....	60
Figure 4. 5: Corrosion distribution on lap-spliced bars .....	60
Figure 4. 6: Voltage-Time curve for lap-spliced RC beams.....	61
Figure 4. 7: Compressive Strength Test Results .....	62
Figure 4. 8: Loading test arrangement.....	63

Figure 4. 9: Load-midspan deflection curves of non-corroded beams .....	64
Figure 4. 10: Flexural crack pattern developed on SANS 10100-NS-NC beams .....	65
Figure 4. 11: Cracking pattern developed on SANS 10100-S-NC beams.....	66
Figure 4. 12: Flexural crack pattern developed on EC2-NS-NC beams .....	67
Figure 4. 13: Flexural crack pattern developed on EC2-S-NC beams .....	67
Figure 4. 14: Load-midspan deflection curves of corroded beams .....	68
Figure 4. 15: Flexural and splitting bond failure on non-spliced control beams.....	72
Figure 4. 16: Flexural and splitting bond failure on lap-spliced control beams.....	72
Figure 4. 17: Flexural and splitting bond failure on SANS non-spliced and lap-spliced beams .....	73
Figure 4. 18: Flexural and splitting bond failure on EC2 non-spliced corroded beams.....	73
Figure 4. 19: Flexural and splitting bond failure on EC2 lap-spliced corroded beams.....	73
Figure 4. 20: Flexural Strength results for SANS 10100-1 and Eurocode 2 beams.....	76
Figure 4. 21: Mid-span deflection ductility factors for SANS 10100-NS beams.....	79
Figure B. 1: Grading curve of fine aggregate.....	97
Figure B. 2: Grading curve of coarse aggregate.....	98
Figure C. 1: Voltage-Time curve for SANS 10100-1 non-spliced beams.....	106
Figure C. 2: Voltage-Time curve for SANS 10100-1 lap-spliced beams.....	107
Figure C. 3: Voltage-Time curve for Eurocode 2 non-spliced beams.....	108
Figure C. 4: Voltage-Time curve for Eurocode 2 lap-spliced beams.....	109
Figure C. 6: Flexural strength and steel cross-sectional loss.....	111
Figure C. 7: Flexural ductility and steel cross-sectional loss .....	112

## LIST OF TABLES

Table 2. 1: Influence of w/b and binder content on corrosion rates (Mangat & Molloy, 1992) .....	19
Table 2. 2: Effect of binder type on chloride binding (Arya et al., 1990) .....	21
Table 2. 3 : Relationship between resistivity and corrosion risk (Andrade & Alonso, 1996) .....	24
Table 2. 4: Stipulated minimum anchorage length.....	31
Table 3. 1: Typical oxide composition of Plain Portland Cement (Afrisam datasheet, 2017) .....	40
Table 3. 2: Typical characteristics of Andesite (Alexander & Mindess, 2005) .....	42
Table 3. 3: Concrete mix proportions .....	44
Table 3. 4: Specimens details .....	45
Table 4. 1: Presentation of RC beam specimens .....	57
Table 4. 2: Applied loads vs mid-span deflections of non-corroded beams .....	65
Table 4. 3: Applied loads vs mid-span deflections of corroded beams .....	69
Table 4. 4: Observed failure modes for each beam. ....	71
Table 4. 5: Corrosion degree in SANS 10100-1 and Eurocode 2 beams .....	75
Table 4. 6: Corrosion and flexure capacity of SANS-NS-C beams .....	77
Table 4. 7: Corrosion and flexure capacity of SANS-S-C beams .....	77
Table 4. 8: Corrosion and flexure capacity of EC2-NS-C beams .....	78
Table 4. 9: Corrosion and flexure capacity of EC2-S-C beams .....	78
Table 4. 10: Summary of flexural test results for SANS 10100-1 beams .....	83
Table 4. 11: Summary of flexural test results for Eurocode 2 beams .....	83
Table 5. 1: Reduction in flexural capacity due to corrosion .....	87
Table B. 1: Grading analysis of Fine Aggregate .....	97
Table B. 2: Grading analysis of Coarse Aggregate .....	98
Table C. 1: 7 day Compressive strength results .....	101
Table C. 2: 28 day Compressive strength results .....	102
Table C. 3: SANS 10100-1 beams corrosion degree results .....	104

Table C. 4: Eurocode 2 beams corrosion degree results..... 105  
Table C. 5: Theoretical and experimental load-carrying capacity of control RC beams ... 110

## CHAPTER 1: INTRODUCTION

### 1.1 Background

Concrete is the most common material used in the construction industry due to its durability, availability, economy and versatility. Concrete has high compressive strength but low tensile strength, therefore the reinforcement is used in conjunction with concrete to improve the tensile strength of concrete (Robberts & Marshall, 2005). One of the biggest challenges with reinforced concrete (RC) structures is their deterioration due to corrosion of the embedded reinforcement. This brings about a reduction in the load-carrying capacity of structural members (Castel *et al.*, 2000).

Concrete is known to provide a good protection to the embedded reinforcement due to the high alkaline environment in concrete (Elbusaefi, 2014). The alkaline environment of concrete (pH >12) results in the formation of a passive layer on the surface of the reinforcement bar, thus providing the reinforcement steel with some degree of corrosion protection (Glass & Buenfeld, 2000). According to Neville (1995), the passive layer is self-generated after the hydration of cement has started, consists of gamma ferric-oxide adhering tightly to the steel. When harmful substances (e.g. carbon dioxide or chlorides) penetrate the concrete cover to the steel level, the passive layer can be destroyed and reinforcement steel corrosion is initiated. Corrosion may propagate if moisture and oxygen are available at the steel surface (Bertolini *et al.*, 2016).

Azad *et al.* (2010) alluded that the corrosion of reinforcement is widely reported as the primary cause of deterioration of reinforced concrete structures. Corrosion is the destructive attack of a metal by chemical or electrochemical reaction with its environment and is caused by the inherent instability of metals in their metallic form (Alexander *et al.*, 2012). The detrimental effects of reinforcement corrosion are loss of steel cross-sectional area and thereafter the bond loss between steel and concrete. The formation of rust in the embedded reinforcement leads to a reduction in bond strength, cracking and spalling of the concrete (Cheng *et al.*, 2005). The oxides are loosely attached and spall off from the surface of steel leading to degradation of the bond between concrete and reinforcing steel (Almusallam *et al.*, 1996). During the process of corrosion, the mass of the steel

reinforcement decreases as the depth of corrosion layer increases. The extent of reinforcement corrosion has a significant effect on strength, deformational behaviour, ductility, bond strength and mode of failure of reinforced concrete (RC) structures. Cabrera (1996) suggests that reduction in the cross-sectional area together with the weakening of the bond and anchorage between concrete and reinforcement negatively affects the serviceability and ultimate strength of reinforced concrete members.

With respect to concrete structures reinforced with lap-spliced steel reinforcement, their performance is affected by many factors such as surface deformation of reinforcing bars, embedment length, concrete cover, bar diameter and concrete strength. These factors influence bond strength at concrete-steel interface, thus damaging the RC structure and reducing the load-carrying capacity. Damage of the concrete structure may manifest in the form of an increased number of cracks, increased crack widths and an increase in the deflection (Alyousef, 2016).

## **1.2 Splicing of steel reinforcement in flexural RC members**

The use of spliced steel reinforcement in concrete structures is inevitable due to reasons such as steel fabrication, transportation limitations, steel workshop fabrication (limited available length) and construction joints. The required length of steel bars may exceed standard stock length of 13 m, or the steel bar may be too long to be transported conveniently. Splicing of reinforcement steel is provided by several means such as welding, mechanical couplers, bar overlapping with a minimum length specified by design codes (Tarabia et al., 2016). The various splicing methods ensure a safe load transfer from one bar through the surrounding concrete. A lap-spliced method which requires the overlapping of two parallel bars is considered as the most economical and practical technique commonly used to transfer forces between lapped steel bars in a reinforced concrete member. This study will examine the influence of corroded lap-spliced reinforcement on flexural strength of reinforced beams. In this study a comparison of lap length requirements will be carried out between the SANS 10100 – 1 and the Eurocode 2.



### 1.3 Problem Statement

Almost all tensile stresses in reinforced concrete flexural members are carried by the steel reinforcement. When the steel corrodes, concrete cover cracking and spalling occurs, the cross-sectional area of the reinforcing steel reduces, and there is a reduction of the bond between the steel and the surrounding concrete (Azad *et al.*, 2007).

One of the most important parameters providing the composite action in reinforced concrete elements is the bond between reinforcement and concrete as the load transfer is achieved by means of transferring bond stresses in the interaction zone. The bond stress is the shear stress developing between the steel and the concrete. The bond disruption between the concrete and steel due to the reinforcement corrosion will weaken the bond strength, thus reducing the load-carrying capacity of a reinforced concrete member (Ballim & Reid, 2003). Tachibana *et al.* (1991) indicated that the corrosion of only  $5 \mu\text{m}$  of parent material is sufficient to cause a disruption of the concrete and consequently the bond strength. Several researchers have, however, found that low corrosion levels ( $< 2\%$  mass loss of reinforcing bars) can produce a firmly adherent layer of rust that may contribute to an enhancement in bond strength (Kivell *et al.*, 2011).

Similarly, the primary corrosion problem affecting concrete members reinforced with lap-spliced steel bars is failure of bond at the concrete-steel interface. This is caused by a reduction in cross-sectional area and deterioration of rebar ribs which changes the surface area of steel bar. These problems lead to a significant reduction of load-carrying capacity and ductility at the ultimate limit state, thus affecting the service life of the structure (Castel *et al.*, 2000). This may lead to brittle-like mode of failure, which may have not been taken into account during the design of RC element.

### 1.4 Aim and objectives of the study

The aim of this study was to investigate the effect of corrosion of spliced steel reinforcement on the flexural performance of reinforced concrete beams.

To achieve this aim, the following objectives were fulfilled:

- Inducing accelerated corrosion in the area corresponding to reinforcement steel lap splices;
- Testing and compiling data of corroded concrete specimens to assess residual flexural capacity;
- Comparing the test results of corroded beams to those of non-corroded beams in order to assess the flexural behaviour of spliced reinforcement affected by corrosion.
- Comparing the flexural test results of beams with reinforcement non-lap-spliced, lap-spliced in accordance with SANS 10100-1 and to those of beams with lap-spliced in accordance with Eurocode 2.

### **1.5 Motivation and significance of the research**

As previously mentioned, many reinforced concrete structures are constructed using spliced reinforcement due to the existence of construction joints, limited available lengths, and transportation limitations. A lap-spliced reinforcement steel provides a simple, cost effective, and efficient connection method commonly used to transfer the stress between spliced bars in a reinforced concrete element. As lap splices develop their strength from the surrounding concrete, the corrosion damage to reinforcement steel and the surrounding concrete in lapped zones weakens the bond between the steel and concrete, thus leading to decrease in the strength and ductility of the spliced reinforcement (ACI 318, 2008).

In the study, the South African Standard, the structural use of concrete SANS 10100-1 (2000) is compared with the Eurocode Standard for design of concrete structure EN 1992-1-1 (2004). The South African Standard was developed based the British Standard BS 8110 which has since been withdrawn and replaced with EN 1992-1-1. The withdrawal and replacement of the British standards with the Eurocode Standard for design of concrete structure EN 1992-1-1 brought the need to align South African Standard, the structural use of concrete SANS 10100-1 with Eurocode 2. The comparison of the two design codes will help to understand the implications and differences in results obtained when applying the two codes.

Although several researchers (Theron , 1994; Almusallam, 2001 and Azad, *et al.*, 2010) have conducted considerable work on the effect of reinforcement steel corrosion on

flexural strength of RC beams, to author's knowledge there is still limited literature on the effect of corroded lap-spliced reinforcement steel on flexural strength. Therefore this study seeks to make a contribution on the effect of corrosion of lap-spliced flexural steel reinforcement corrosion in beams on flexural capacity.

## **1.6 Scope and limitations**

The scope of this research is limited to the following aspects:

- a. The corrosion acceleration of the reinforcement steel will be limited to chloride induced corrosion using impressed current technique. Carbonation induced corrosion will not be investigated but is briefly covered in the literature review.
- b. Three types of test specimens (lapped according to SANS guidelines, lapped according to Eurocode 2 guidelines and non-lap reinforcement) will be used.
- c. The corrosion acceleration was not carried out under sustained loading.

## **1.7 Layout of the report**

This research report is divided into five chapters as follows:

*Chapter one* gives a general introduction with emphasis on steel reinforcement corrosion in RC structures due to chlorides. A brief overview is given on durability and service life prediction of RC structures, with a focus on cracked concrete.

*Chapter two* is a literature review of research related steel reinforcement corrosion, transport mechanism in concrete, causes of steel reinforcement corrosion, its effect on flexural strength of RC members and techniques used to induce corrosion. Although the carbonation induced corrosion is briefly covered, the emphasis of the literature review is on chloride induced corrosion which is the focus of this study.

*Chapter three* presents the experimental details and methodology employed in this study to achieve the research objectives.

*Chapter four* presents the experimental results of this study and the discussion thereof.

*Chapter five* provides the conclusions based on literature review and the experimental results. This chapter also contains recommendations for future study.

## 1.8 References

- ACI 318. (2008). *Building code requirements for structural concrete (ACI 318-08) and commentary*.
- Alexander, M., Beushausen, H., & Otieno, M. (2012). Corrosion of Steel in reinforced concrete: Influence of binder type, water/binder ratio, cover and cracking. *CoMSIRU, University of Cape Town*.
- Almusallam, A. A. (2001). Effect of degree of corrosion on the properties of reinforcing steel bars. *Construction and Building Materials*, 15(8), 361–368.
- Almusallam, A. A., Al-Gahtani, A. S., & Aziz, A. R. (1996). Effect of reinforcement corrosion on bond strength. *Construction and Building Materials*, 10(2), 123–129.
- Alyousef, R. (2016). *The Fatigue Behaviour of Tension Lap Spliced Reinforced Concrete Beams Strengthened with Fibre Reinforced Polymer Wrapping*.
- Azad, A. K., Ahmad, S., & Azher, S. A. (2007). Residual strength of corrosion-damaged reinforced concrete beams. *ACI Materials Journal*, 104(1), 40.
- Azad, K., Ahmad, S., & Al-Gohi, B. (2010). Flexural strength of corroded reinforced. *Magazine of Concrete Research*, 62(6), 405–414.
- Ballim, Y., & Reid, J. (2003). Reinforcement corrosion and the deflection of RC beams—an experimental critique of current test methods. *Cement and Concrete Composites*, 25(6), 625–632.
- Bertolini, L., Carsana, M., Gastaldi, M., Lollini, F., & Redaelli, E. (2016). *Corrosion of Steel in Concrete and Its Prevention in Aggressive Chloride-Bearing Environments*.
- Cabrera, J. (1996). Deterioration of concrete due to reinforcement steel corrosion. *Cement and Concrete Composites*, 18(1), 47–59.

- Castel, A., François, R., & Arliguie, G. (2000). Mechanical behaviour of corroded reinforced concrete beams—Part 1: Experimental study of corroded beams. *Materials and Structures*, 33(9), 539–544.
- Cheng, A., Huang, R., Wu, J.-K., & Chen, C.-H. (2005). Influence of GGBS on durability and corrosion behavior of reinforced concrete. *Materials Chemistry and Physics*, 93(2–3), 404–411.
- Elbusaefi, A. A. (2014). The effect of steel bar corrosion on the bond strength of concrete manufactured with cement replacement materials. *PHD Studies, Cardiff University*.
- EN 1992-1-1. (2004). Eurocode 2: Design of concrete structures—Part 1-1: General rules and rules for buildings. *European Committee for Standardization (CEN)*.
- Glass, G., & Buenfeld, N. (2000). The influence of chloride binding on the chloride induced corrosion risk in reinforced concrete. *Corrosion Science*, 42(2), 329–344.
- Kivell, A., Palermo, A., & Scott, A. (2011). *Effects of bond deterioration due to corrosion in reinforced concrete*. 081–088.
- Neville, A. M. (1995). *Properties of concrete* (4th ed, Vol. 4). Longman.
- Robberts, J. M., & Marshall, V. (2005). *Analysis and Design of Concrete Structures*. Nuclear Structural Engineering.
- SANS 10100 -1. (2000). *The Structural Use of Concrete. Part 1: Design*. South African Standard Code of practice.
- Tachibana, Y., Kajikawa, Y., & Kawamura, M. (1991). Behaviour and punching strength of RC slabs damaged by corrosion of reinforcement. *Doboku Gakkai Ronbunshu*, 1991(426), 65–74.

Tarabia, A. M., Mahmoud, Z. I., Shoukry, M. S., & Abudina, A. A. (2016). Performance of RC slabs with lap splices using headed bars. *Alexandria Engineering Journal*, 55(3), 2729–2740.

Theron, G. D. V. (1994). Effects of reinforcement corrosion on the structural performance of reinforced concrete beams. *MSc Dissertation, Department of Civil Engineering, University of Cape Town*.

## **CHAPTER 2: LITERATURE REVIEW**

### **2.1 Introduction**

The literature review presented in this chapter covers the principles of steel reinforcement corrosion with the focus on chloride-induced corrosion. The chapter covers transport mechanism in concrete, mechanism of steel reinforcement corrosion and its causes. Also covered in this chapter are various techniques used to accelerate corrosion and stipulations by various codes of practice including SANS 10100 – 1 and Eurocode 2 on minimum lap lengths for reinforcement steel in flexural members.

### **2.2 Transport mechanisms in concrete**

The deterioration of concrete involves some form of fluid and ionic flow as deterioration mechanisms such as leaching, chloride ingress and carbonation are all related to the ease with which a fluid or ions can move through the concrete. The flow of fluid through the concrete microstructure relates to its penetrability. Penetrability may be defined as the degree to which the concrete permit gases, liquids and chloride ions to move through its pore structure (Richardson, 2002).

The transportation of chloride ions through concrete takes place in the water phase in the form of mechanisms such as capillary suction, diffusion, permeation, and migration (Broomfield, 2007). These are briefly covered in the following sections.

#### **2.2.1 Capillary suction**

Capillary suction occurs for dry or partially dry concrete, it is the dominant mechanism for concrete exposed to drying and wetting cycles. Bertolini, *et al.*, (2004) stated that this is an important mechanism for marine concrete in the tidal and splash zone as well as in the case of concrete in road applications where de-icing salts are used.

#### **2.2.2 Diffusion**

This is the main transport of chlorides when concrete is saturated such as in submerged conditions. Diffusion is defined as the process by which liquid, gas or ions move through

a porous material under the action of a concentration gradient (Ballim *et al.*, 2009). The process of diffusion is predominant in concrete structures that are fully submerged in sea water or exposed to salts. Diffusion is modelled by Fick's second law of diffusion which concerns the rate of change of concentration with respect to time. Models based on Fick's second law of diffusion have been developed by several researchers (Maage *et al.*, 1996; Weyers, 1998) to predict the length of the corrosion initiation period under various circumstances. Fick's second law of diffusion is stated as follows:

$$\frac{\partial C(x,t)}{\partial t} = D \frac{\partial^2 C(x,t)}{\partial x^2} \quad (2.1)$$

where:  $C(x,t)$  = concentration of diffusing substance at depth  $x$  and time  $t$ ,  $t$  = time,  $D$  = diffusion coefficient,  $x$  = depth coordinate from the concrete surface into the concrete.

As shown in Figure 2.1, the diffusion zone is found beyond the convection zone. The convection zone is defined as the depth at which continuous cycles of wetting and drying occur (Ballim *et al.*, 2009). In the convection zone, the water carrying dissolved chlorides moves in and out.

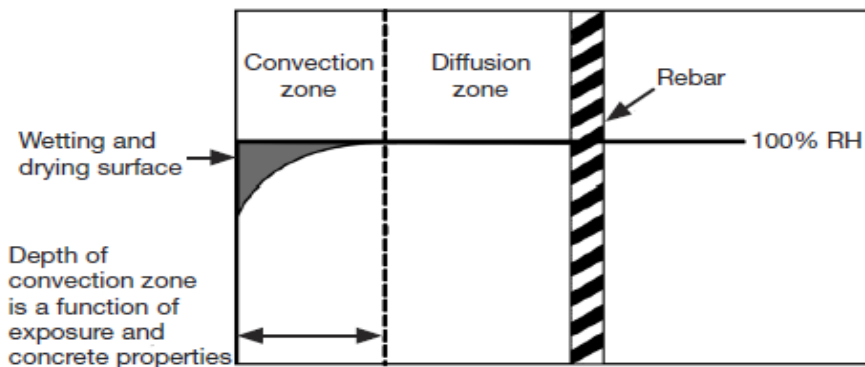


**Figure 2. 1: Convection zone in concrete (Ballim, *et al.*, 2009)**

### 2.2.3 Permeation

Permeation is the penetration of liquid or gas into a solid by a pressure head and is related to material property, the coefficient of permeability. Ballim., *et al.*, (2009) described permeation as the process of movement of fluids through the pore structure under an externally applied pressure while the pores are saturated with the particular fluid. Permeability is a measure of the capacity for concrete to transfer fluids by permeation.



The permeability of concrete is dependent on the concrete microstructure, the moisture condition of the material and the characteristics of the permeating fluid.

#### 2.2.4 Migration

Migration (also referred to as accelerated diffusion, electro-diffusion, or conduction) is described as the movement of ions in a solution under an electrical field. It is the transport mechanism most often used in laboratory accelerated chloride tests and is described by the Nernst-Planck equation (Ballim *et al.*, 2009).

### 2.3 Mechanism of steel reinforcement corrosion in concrete

Ballim *et al.*, (2009) define corrosion of steel in the presence of electrolytes as an electrochemical process mediated by the formation of cathodic and anodic areas on the surface of the steel. For the electrochemical reaction to occur, the presence of oxygen and moisture is required. The site where the metal dissolution takes place is called the anode. During the electrochemical process, iron is oxidized at the anode to ions that pass into pore solution and at the cathode, oxygen is reduced to hydroxyl ions. The anode and the cathode form a corrosion cell, with the flow of electrons in the steel and of ions in the concrete pore solution leading to the corrosion of reinforcement. Stansbury & Buchanan (2000) suggested the use of following equations for the corrosion half-cell reactions for iron:



The presence of sufficient chloride ions or calcium carbonates into the reinforced concrete, tends to attack the existing passive nature, thereby promoting the corrosion process. In the case where the corrosion is caused by a chloride attack or carbonation, the chemical reaction remains the same but the chloride ions which have the same charge as the  $\text{OH}^{-}$  competes with it to form films with  $\text{Fe}^{2+}$  (Broomfield, 2007 and Neville, 1995).

Figure 2.2 illustrates the reinforcement corrosion in concrete:

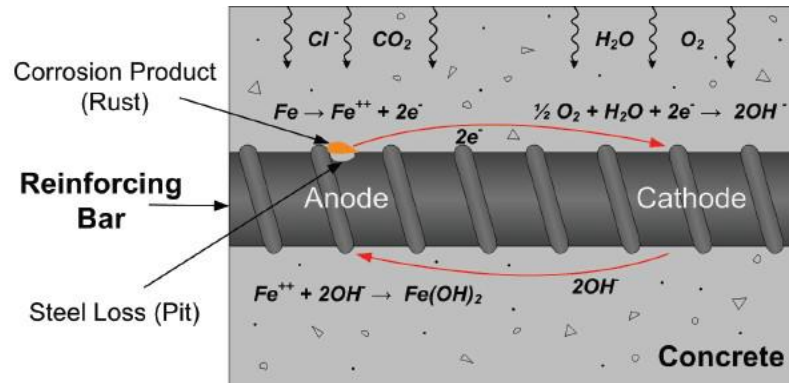
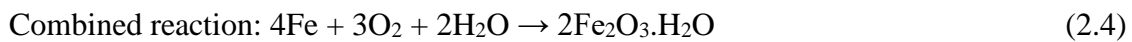


**Figure 2. 2: Illustrates the corrosion of reinforcement in concrete (Ahmad, 2003)**



The volume of corrosion products such as ferric oxide ( $\text{Fe}_2\text{O}_3$ ) is two times greater than the steel it substitutes, and upon hydration, the ferric oxide becomes porous as a result of the expansion it undergoes, this produces the flaky rust layer on the surface of the reinforcing bar and can result in cracking and spalling of the cover concrete (Broomfield, 2007).

### 2.3.1 Causes of reinforcement corrosion in concrete

The reinforcement corrosion in concrete occurs due to several factors such as the presence of stray currents or the presence of dissimilar metals with carbonation induced and chloride-induced corrosion being the main causes of corrosion. Although this study focusses on chloride-induced corrosion, a brief description of carbonation induced corrosion is provided.

#### 2.3.1.1 Carbonation induced corrosion

Carbonation is the formation of calcium carbonate by a chemical reaction in the concrete. Ballim *et al.*, (2009) define carbonation as the process whereby atmospheric carbon dioxide ( $\text{CO}_2$ ) enters the pore structure of hardened cement paste and reacts with  $\text{Ca}(\text{OH})_2$  to form calcium carbonate ( $\text{CaCO}_3$ ). This involves the following chemical reaction:



For the above reaction to take place, carbon dioxide first dissolves in water to form carbonic acid:



Ballim *et al.*, (2009) alluded that the carbonation process reduces the pH of the pore solution from  $>12$  to  $<8$ . The depth up to which the pH has dropped to  $<8$  is called the carbonation depth. The reduction of the pH value leads to de-passivation of the reinforcement steel, which leaves the reinforcement steel vulnerable to corrosion.

Ballim *et al.*, (2009) further stated that carbonation moves as a “front” into the concrete and is a slow process with a rate dependent on the porosity and permeability of the concrete cover. This front does not advance beyond a particular point until all the  $\text{Ca}(\text{OH})_2$  at that point has been converted to  $\text{CaCO}_3$ . Hence, the amount of  $\text{Ca}(\text{OH})_2$  in the pore structure of the concrete also has an influence on the rate of carbonation. Corrosion of steel reinforcing is initiated when the carbonation ‘front’ reaches the steel level and the movement of the carbonation “front” is shown in Figure 2.3:

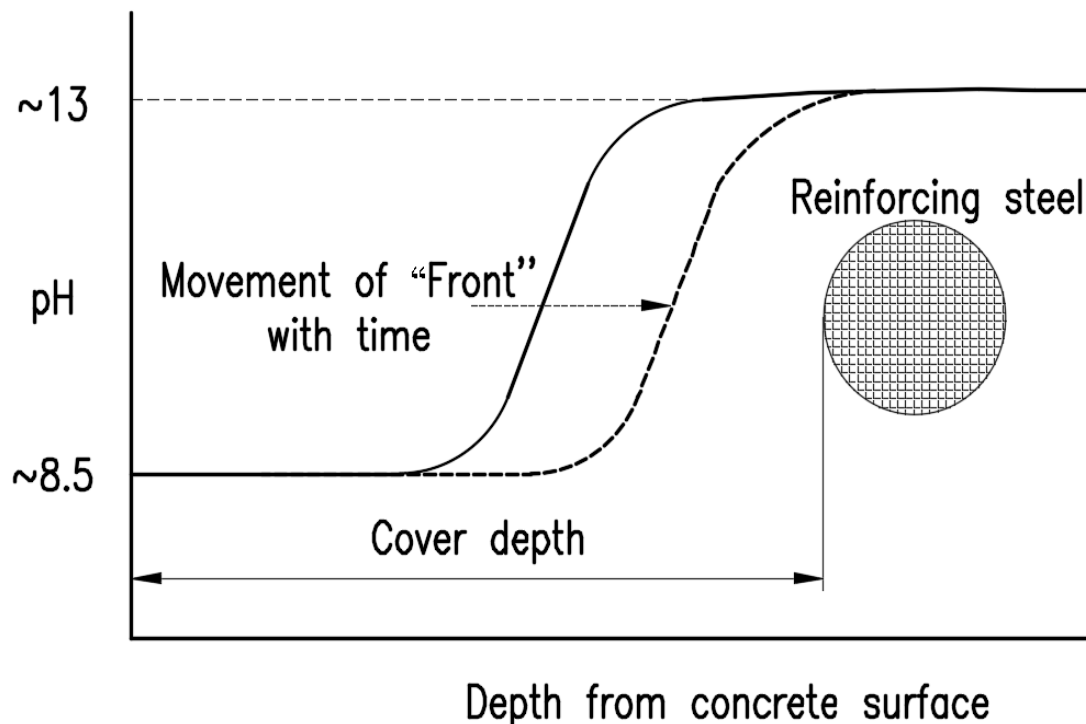


**Figure 2. 3: The carbonation “front” (Ballim *et al.*, 2009)**

Ballim *et al* (2009) modelled the advance rate of carbonation front as follows:

$$x = D\sqrt{t} \quad (2.7)$$

where:

$x$  = depth of carbonation

$t$  = time of exposure

$D$  = carbonation coefficient

For carbonation to spread, fresh carbon dioxide from the surface needs to be supplied continuously and deeper into the concrete (Ballim, *et al.*, 2009).

Carbonation of concrete is common in the inland environments and in parking structures. It occurs slowly in concrete structures with good concrete quality and adequate cover and does not occur if the concrete is water-saturated or in very dry conditions as the rate of carbonation is strongly affected by the moisture content of the concrete pore structure. The moisture in concrete is required to form the carbonic-acid that attacks the steel passivating layer. This type of corrosion is characterised by microcell/homogenous corrosion (Boddy *et al.*, 1999).

### **2.3.1.2 Chloride-induced corrosion**

Chloride-induced corrosion is a localized type of corrosion that occurs when the concentration of chlorides at the steel level reaches a critical value called the chloride threshold (Martín-Pérez, 1999). The mechanism of chloride attack in RC is usually divided into several stages: transport of chloride ions through the concrete cover, passive film breakdown on rebar, pitting corrosion (Bertolini & Redaelli, 2009). Chloride-induced corrosion is dominant in structures exposed to chloride-containing environment, such as structures built in the marine environment. Chlorides can also be present in the concrete through the use of contaminated aggregates (sea-dredged aggregates), seawater and admixtures containing calcium chloride ( $\text{CaCl}_2$ ) (Roberge, 2000). In studies conducted by several researchers, corrosion was observed using various chloride threshold values. Broomfield (2007) stated that a chloride threshold concentration of 0.4% chlorides by mass of cement is the level at which the passive layer on reinforcement is broken down and corrosion may initiate, while in a study conducted by Hausmann (1967), the corrosion was routinely observed when the chloride concentration exceeded

0.6% of the hydroxyl concentration. Once the chloride threshold is reached, the passive layer is attacked by chlorides and result in pitting corrosion. Pitting corrosion is mostly associated with chloride-induced corrosion (Elbusaefi, 2014). It occurs at discrete sites along the reinforcing bar, often causing deep pits. Pitting corrosion can completely penetrate the cross-section of steel reinforcement in a relatively short period of time. Consequently, this leads to a very rapid and significant loss of the cross-sectional area of the steel bar (Batis & Rakanta, 2005).

Reinforced concrete structures that are continuously submerged in seawater are less susceptible to reinforcement corrosion compared to concrete exposed to wetting/drying cycles, since, under submerged conditions, there is not enough oxygen available to sustain active corrosion (Ballim *et al.*, 2009).

### 2.3.2 Stages of steel corrosion in reinforced concrete structures

The service life of reinforced concrete structures is characterised according to the classic model proposed by Tuutti (1982), wherein the two-stage service life model with respect to reinforcement corrosion was developed. The corrosion of steel reinforcement is divided into two distinct phases, namely the corrosion initiation phase and the corrosion propagation phase as shown in Figure 2.4:

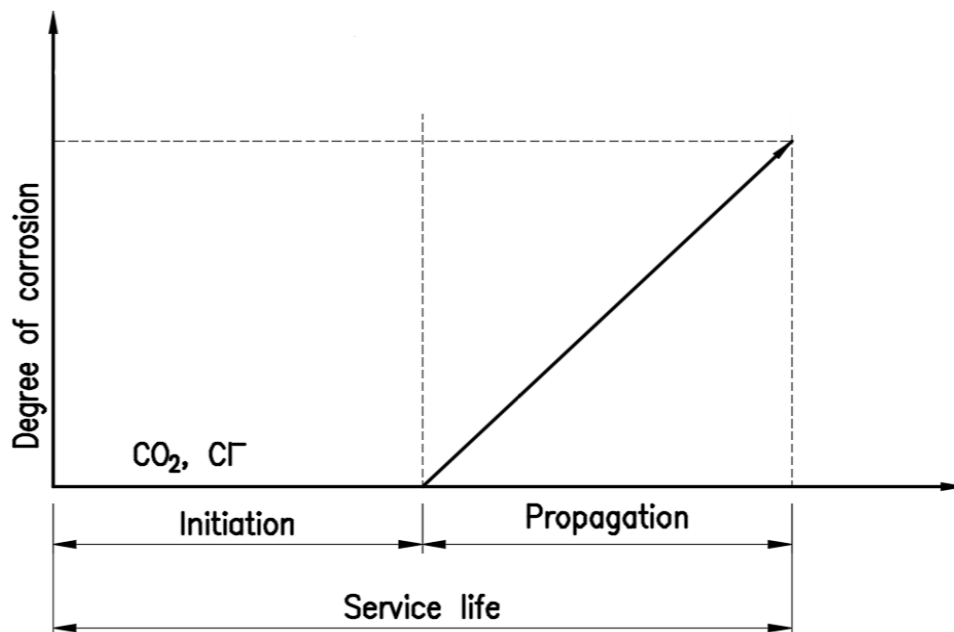


**Figure 2. 4: Corrosion damage model (Tuutti, 1982)**

### **a. The initiation phase**

Tuutti (1982) described the initiation phase as the process by which aggressive substances, (carbon dioxide and chlorides), destroy the passive protective film on the steel surface, thus rendering it liable to corrode.

In the case of chloride-induced corrosion, the initiation stage corresponds to the period of time during which chlorides penetrate the concrete without observed damage, until the chloride threshold value is reached (Martín-Pérez, 1999). For carbonation-induced corrosion, this phase corresponds to the time taken for the carbonation front to reach the steel reinforcement and breakdown the passive layer (Ballim *et al.*, 2009).

### **b. The propagation phase**

During this period, the reinforced concrete structure deteriorates due to the loss of steel reinforcement cross-sectional area and the accumulation of corrosion products around the steel surface. This phase lasts until an unacceptable degree of corrosion damage has occurred when the structure is no longer considered to be acceptable on the grounds of structural integrity, serviceability or appearance (Tuutti, 1982).

### **2.3.3 Mechanical properties of corroded steel bars and effect of steel corrosion on flexural strength of beams**

Corrosion of reinforcement steel leads to the reduction of steel cross-sectional area which can reduce the flexural capacity of the member. Several researchers (Andrade *et al.*, 1991; Castel *et al.*, 2000) investigated the effects of corrosion on the mechanical behaviour of steel reinforcing. According to Andrade, *et al.* (1991), a reduction in bar section between 10 % and 25 % in the critical zones of the structure will result in the reduction of its residual service life, while a 5% reduction (including concrete cracking and spalling) will indicate the early stage of deterioration.

Al-Sulaimani *et al.*, (1990) conducted a study to investigate the effect of steel reinforcement corrosion on the flexural behaviour of RC beams. In the study, 24 RC beams with the dimensions of 150 x 150 x 1000 mm were designed. These beams were reinforced with 2  $\phi$ 10 mm top bars, 1  $\phi$ 12 mm bottom bar and 6 mm diameter links spaced

at 50 mm centres. The steel reinforcement corrosion on the bottom bar was accelerated by applying a constant current density of  $2000 \mu\text{A}/\text{cm}^2$ . After conducting flexural tests, the authors reported that the loss of a cross-sectional area ranging between 9.4 and 10.4% reduced the load-carrying capacity of RC beams by 10%.

The mechanical properties of corroded steel bars were investigated in a study conducted by Almusallam (2001). In the study, two bar diameters (6 mm and 12 mm) were used and corroded to different levels. The results indicated that the increase in corrosion degree reduces the elongation of steel bars at maximum load, compared to non-corroded steel bars. Reinforcing steel bars with a minimum corrosion degree of 12.6% showed a brittle behaviour. The study reported a reduction in the tensile strength with increasing degree of steel corrosion.

The above finding is supported by a study conducted by (Zhang *et al.*, 2009). Their study concluded that the decrease in the elongation of steel bar will increase its brittleness, thereby reducing the ductility of corroded steel bars.

#### **2.3.4 Effect of corrosion on steel-concrete interface bond**

The bond between reinforcement steel and the surrounding concrete is of the most important as it ensures the composite action between concrete and reinforcement steel. For reinforced concrete structures situated in highly corrosive environment, the bond between concrete and reinforcement steel can be weakened by the formation of rust and other corrosion products, resulting in a volume expansion of steel that generates tensile stresses in the concrete. Cracking and spalling of concrete occurs, thus resulting in the loss of bond strength between the steel and concrete. Such damage may lead to an increase of corrosion rate, thus a significant reduction of steel parameters such as yielding and ultimate stresses (Fernandez *et al.*, 2016).

Cabrera (1996) conducted an investigation on the effect of reinforcement steel corrosion on the steel and concrete bond. In the investigation, 150 mm concrete cubes with 12 mm diameter steel reinforcement bar centrally embedded in the cube were used for pull-out tests. The specimens were subjected to varying corrosion degrees. The results from pull-out tests are presented in Figure 2.5.

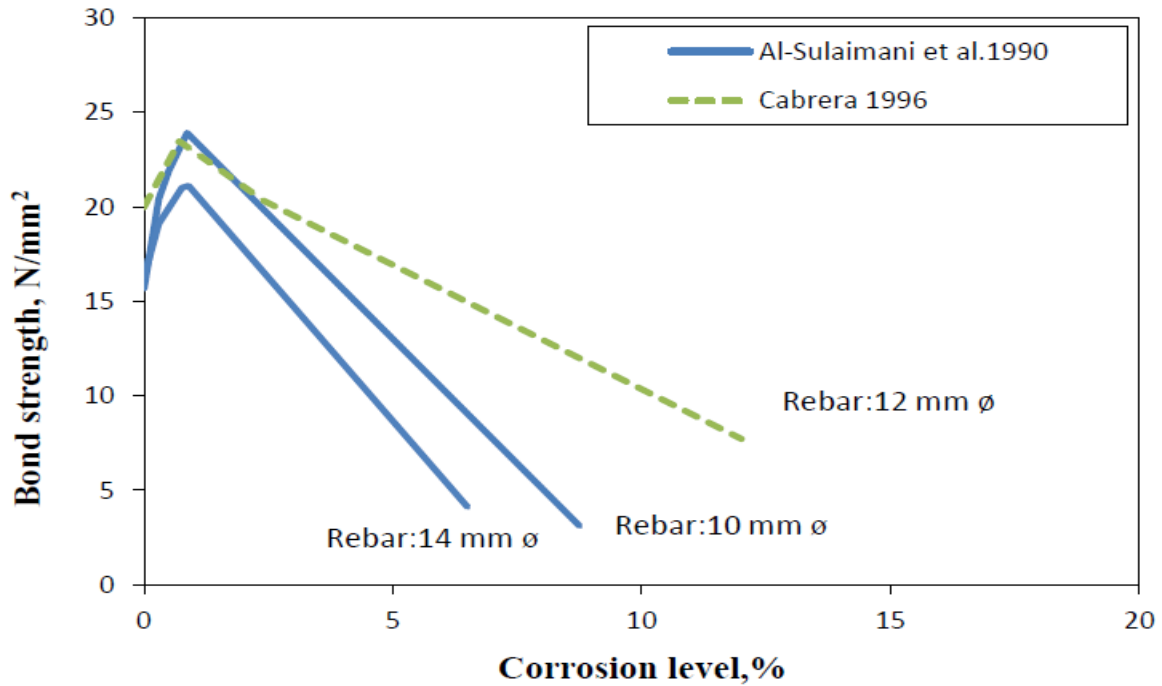


**Figure 2. 5: Bond strengths of corroded specimens (Al-Sulaimani *et al.*, 1990; Cabrera, 1996)**

The results from pull-out tests revealed the initial increase in bond strength when corrosion increased up to 1% section loss. However, there was a bond strength reduction of 23.8% at the corrosion rate of 12.6%. It was concluded that the bond strength initial increase was due to the friction created by the larger volume occupied by corrosion products. At the corrosion rate of 12.6%, the reinforcing steel ribs were destroyed and this resulted in the loss of bond. This is in agreement with experimental study conducted by Al-sulaimani *et al.*, (1990) which also showed an increase in bond strength during the initial corrosion level to about 1%.

Similar trends were observed on results from the recent study conducted by Kearsley & Joyce (2014) where pull-out tests were carried out in cylinder specimens. In their results, an increase in bond strength was observed for corrosion levels lower than 2%. The control specimens reached a maximum bond strength value of 3.2 MPa, whereas the specimens with an estimated percentage mass loss of 1.9% reached a value of 3.8 MPa. These results indicate that the well adherent rust layer formed at low corrosion levels helps the bond between concrete and steel reinforcement.



## 2.3.5 Factors affecting reinforcement corrosion

### 2.3.5.1 Effect of concrete quality

Concrete quality (binder type and w/b ratio) has a strong bearing on the start and sustenance of steel reinforcement corrosion as it influences the resistance of concrete to the ingress of aggressive substances such as chlorides, carbon dioxide, oxygen and water (Broomfield, 2007).

Concrete quality is controlled by parameters such as water-to-cement ratio, binder type, binder content and aggregate type.

#### (a) Water/binder (w/b) ratio and binder content

The w/b ratio is the most important factor governing the quality of concrete due to its influence on the permeability of concrete. Less permeable concrete limits the ingress of aggressive substances (oxygen, chloride ions and moisture) and increase the concrete resistivity (Scott, 2004).

The South African concrete design code SANS 10100-2 (2014) and Eurocode 2 specify a maximum w/b ratio of 0.55 for RC structures situated in aggressive environments. Mangat and Molloy (1992) conducted a study to investigate the corrosion rates of a 12 mm deformed rebar cast in concrete, with a cover depth of 10 mm, three different w/b ratios and cement contents were used in the study. The results obtained from the investigation are shown in Table 2.1.

**Table 2. 1: Influence of w/b and binder content on corrosion rates (Mangat & Molloy, 1992)**

w/b	Binder content (kg/m <sup>3</sup> )	$i_{corr}$ (uA/cm <sup>2</sup> )	Cl <sup>-</sup> % mass cem.
0.45	430	0.13	1.4
0.58	430	0.65	2.0
0.76	430	2.16	2.3
0.58	330	0.62	1.73
0.58	530	0.52	1.21

The study found that the w/b ratio has a significant effect on the corrosion rate of steel, with the total binder content being less significant. The highest corrosion rate was observed to occur in the specimen with 0.76 w/b ratio with the highest chloride content, while the lowest corrosion rate was observed to occur in the specimen with 0.45 w/b despite having a higher chloride content than the 0.58 w/b with 530 kg cement. The lower w/b ratio reduces the penetrability of the concrete sample and increase the concrete resistivity.

#### **(b) Binder type**

The use of Portland cement in conjunction with cement extenders such as fly ash, ground granulated blast-furnace slag and condensed silica fume can significantly improve the corrosion resistance in reinforced concrete and reduce the permeability of concrete (Grieve, 2009).

Several researchers, (Arya *et al.*, 1990; Arya & Xu, 1995; Cabrera, 1996; Scott & Alexander, 2007; Scott, 2004) have studied the effect of binder types on reinforcement corrosion steel bars embedded in concrete. In a study conducted by Cabrera (1996) where he investigated the effect of fly ash on the rate of reinforcement corrosion by using, up to 30% low calcium fly ash. The results revealed greater corrosion resistance for concrete where fly ash was used compared to concrete where only plain Portland cement was used. This is due to the fact that fly ash reduces the penetrability of concrete as well as the rate of chloride diffusion through concrete (Grieve, 2009). This was supported by a study conducted by Scott and Alexander (2007) where corrosion rates were measured on concrete specimens with crack widths of 0.2 mm and 0.7 mm and fly ash of 30%, resulted in a corrosion rate reduction of 40% compared to plain Portland cement.

The results from another study conducted by Arya *et al.*, (1990) to investigate the influence of cement type on chloride binding in concrete showed an increased chloride binding capacity of fly ash and slag blended cements compared to 100 % PC mixes for admixed chlorides. Their results are summarised in Table 2.2.

**Table 2. 2: Effect of binder type on chloride binding (Arya *et al.*, 1990)**

<b>Binder Type</b>	<b>Total <math>Cl^-</math></b>	<b>Free <math>Cl^-</math></b>	<b>Bound <math>Cl^-</math></b>	<b>% Bound</b>
PC	1.635	0.831	0.804	50
30% FA	1.887	0.818	1.069	57
70% Slag	1.750	0.830	0.920	53
10% SF	1.265	0.684	0.581	46

As illustrated in Table 2.2, 30% fly ash showed a greater binding capacity (57%) compared with 70% slag (53%). Both fly ash and slag blended cements had a greater binding capacity than 100 % PC mix.

### **(c) Aggregate type**

Concrete is produced using different types of aggregate added to cement paste. These are known to have a considerable effect on the concrete quality with significant effects on its permeability and strength. The permeability of concrete is mainly influenced by the permeability of the cement paste, especially at the interface with aggregates whilst aggregates have a significant effect on concrete strength by providing rigidity and stiffness to the material to resist applied loads without undue deformations (Alexander & Mindess, 2005).

With respect to electrical resistivity, electrical current can easily flow through the pore system of the cement paste, but aggregates are known to provide a higher electrical resistivity compared to hardened cement paste due to their lower porosity (Azarsa & Gupta, 2017).

Sengul (2014) studied the effect of aggregate type on electrical resistivity measurements. In his experimental study a comparison was made between concrete containing crushed limestone and with concrete containing gravel. Higher electrical resistivity values were reported on concrete produced with crushed limestone aggregates. He reported that obtained values for the electrical resistivity of concrete were attributed to aggregate type. Gravel aggregates were rounded shaped with smooth surface whereas the crushed limestone aggregates had irregular shape and rough surface texture. The use of rounded

gravel aggregates resulted in poor bonding between gravel and cement paste as opposed to crushed limestone aggregates that had a rough surface texture. Comparable standard deviation values were obtained in another study conducted by Morris et al. (1996), where different aggregate type was used. A careful selection of aggregate resulting in low penetration of chloride ions and provide high electrical resistivity values is of utmost importance to prevent the detrimental effects of the chloride ions on reinforced concrete structures.

#### **2.3.5.2 Effect of concrete cover**

Concrete cover is defined as the distance from the surface of the concrete to the surface of reinforcing bars embedded in the concrete (Theodosiou, 2009). Its thickness and quality determines the time it takes for aggressive substances such as chloride ions and carbon dioxide to reach the reinforcement embedded in concrete. The greater the cover the longer the period for chloride ions to reach the threshold value (Neville, 1995). Lambert, *et al.*, (1991) conducted an investigation on the corrosion rate using mild steel rods embedded in cement pastes with water/cement ratio of 0.50 using varying cover depths (10, 20, 30 and 40 mm). In their investigation, alternate cycles of wetting and drying with 5% sodium chloride solution (NaCl) were carried out for a period of 2 years. Their results demonstrated the following corrosion rates:

10 mm cover =  $20 \mu\text{A}/\text{cm}^2$

20 mm cover =  $0.2 \mu\text{A}/\text{cm}^2$

30 and 40 mm cover =  $0.04 \mu\text{A}/\text{cm}^2$

At greater cover depths (30 and 40mm) a decrease in corrosion rate was observed compared to a 10 mm cover. As previously mentioned, the corrosion rate is influenced by the presence of oxygen. Greater cover depths result in a decrease in oxygen diffusion. According to Bentur, *et al.*(1997), the concrete cover depth and relative humidity has a significant influence on oxygen diffusion as illustrated in Figure 2.6.

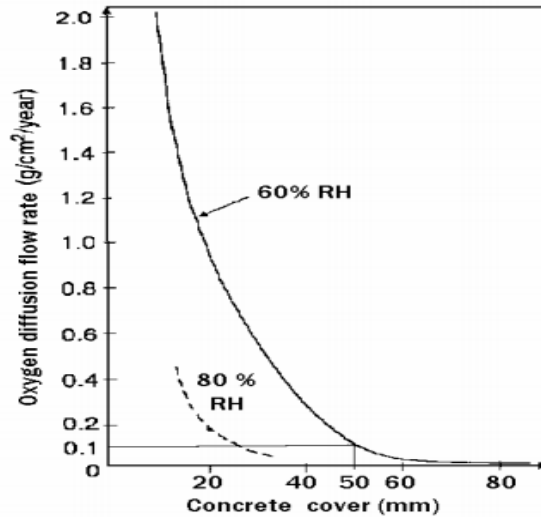


**Figure 2. 6: Effect of concrete cover on the diffusion of oxygen (Bentur *et al.*, 1997)**

A shift in relative humidity from 60 to 80% would lead to a substantial decrease in the availability of oxygen. Cover depth increase is also likely to minimise the influence of any external drying at the level of the steel, thus sustaining a high relative humidity (Scott, 2004).

Moreover, the influence of cover depth was investigated by Yalciner *et al.*, (2012) who studied the effect of corroded steel reinforcement on bond strength. Three different concrete cover depths (15, 30 and 45 mm) were used. The results revealed a higher percentage of bond strength degradation on specimens with low concrete cover due to cover cracking during pull-out tests.

This confirms the importance of ensuring strict quality control during construction to ensure adequate cover to steel reinforcement.

### **2.3.5.3 Effect of temperature and relative humidity**

Temperature is another significant factor influencing the corrosion rate of steel reinforcement. As corrosion is an electrochemical process, temperature plays a significant role in determining the rate of the chemical reaction. In low humidity environments the effects of increasing temperature do not influence the corrosion rate as much as in high relative humidity environments (Theron, 1994). In their research Enevoldsen, Hansson and Hope (1993) found that increasing the relative humidity of concrete results in a

reduction of the resistivity of the concrete thus facilitating corrosion. Their results suggest a relative humidity of 85 % as the threshold level for promoting corrosion.

Corrosion cannot be maintained above a temperature of 40 °C due to the decrease of oxygen solubility in the pore solution at higher temperature and the drying out of concrete (Živica, 2003).

#### **2.3.5.4 Effect of electrical resistivity of concrete**

Electrical resistivity of concrete can be defined as the resistance against the flow of an electrical current. The electrical resistivity of concrete is an important parameter in determination of intensity of the initiated corrosion process. It depends mainly on the relative humidity of the concrete pores, temperature, and binder type as well as the ionic concentration of the pore solution (Ahmad, 2003).

The electrical resistivity of the concrete affects the rate at which corrosion takes place, since an ionic current must pass from the anode to the cathode of the rebar for corrosion to occur (Beushausen & Alexander, 2009). In concrete with high electrical resistivity corrosion process will be slow compared to that in concrete with low resistivity in which the current can easily pass between anode and cathode areas. The electrical resistivity of concrete is affected by many factors including the binder type and content, w/b ratio, curing and the amount of moisture in concrete (Beushausen & Alexander, 2009).

Andrade and Alonso (1996) conducted an assessment on relationship between resistivity and corrosion risk. Their results, shown on Table 2.3 suggest that a resistivity of less than 10 kΩ-cm can result in rapid corrosion of reinforcing steel.

**Table 2.3 : Relationship between resistivity and corrosion risk (Andrade & Alonso, 1996)**

<b>Resistivity (kΩ-cm)</b>	<b>Risk Level</b>
> 100 - 200	Very low Corrosion rate even if chloride contaminated
50 - 100	Low corrosion rate
10 - 50	Moderate to high corrosion rate
< 10	Resistivity is not the controlling parameter

### **2.3.5.5 Effect of cracking**

Despite adherence to concrete specifications, flaws in the concrete are unavoidable even if the finest workmanship and latest techniques are used. It is impossible to completely eliminate concrete cracking as, concrete changes slightly in volume due to fluctuations in moisture content and temperature. During the early stages after concrete is cast, crack occurrence is usually due to thermal effects and plastic shrinkage. The concrete tends to expand when there is a rise in temperature and contract when there is a drop in temperature. If these volume changes in concrete are restrained, cracks start forming when the tensile strength of concrete is exceeded. Also, tension members experience concrete cracking before the tension effect of the steel reinforcement is activated. These concrete cracks may provide easy passage for ingress of various aggressive substances from the environment (chloride ions and oxygen) to reach the embedded reinforcement (Scott, 2004).

Cracks promote localised chloride ingress and result in localised steel corrosion. Cracks can be classified as either active (cracks that undergo continued movement) or inactive (which are dead cracks that do not open, close or extend further). The active cracks can open when the load is applied and close when the load is removed. On the other hand, the inactive cracks can facilitate the ingress of aggressive substances and initiate the corrosion process if they are not repaired. The corrosion rate of the embedded reinforcement is affected by factors such as crack widths, frequency, and orientation (Otieno, 2008).

#### **a. Crack width**

A threshold crack width value of 0.4 mm is generally proposed by various structural design codes of practice. Crack width plays an important role in the corrosion of reinforcement due to rapid penetration of chlorides. With respect to corrosion rates, there has been no agreement on the relationship between corrosion and crack width.

(Beeby, 1983); Arya and Wood (1995) suggests that there is no direct relationship between crack width and corrosion rate. This was in agreement with an investigation conducted by Suzuki *et al.*, (1990), where it was found that crack width has limited effect

on corrosion rate. An experimental study conducted by (Otieno, 2008) illustrated the influence of crack width and concrete quality on corrosion rate. Beam test specimens were made using 100 % Ordinary Portland Cement and 50/50% OPC/Corex slag binders with water/binder (w/b) ratios of 0.40 and 0.55. The crack widths investigated in the study were incipient crack, 0.4 and 0.7 mm. Figure 2.7 shows the results from the experiment conducted during the study:

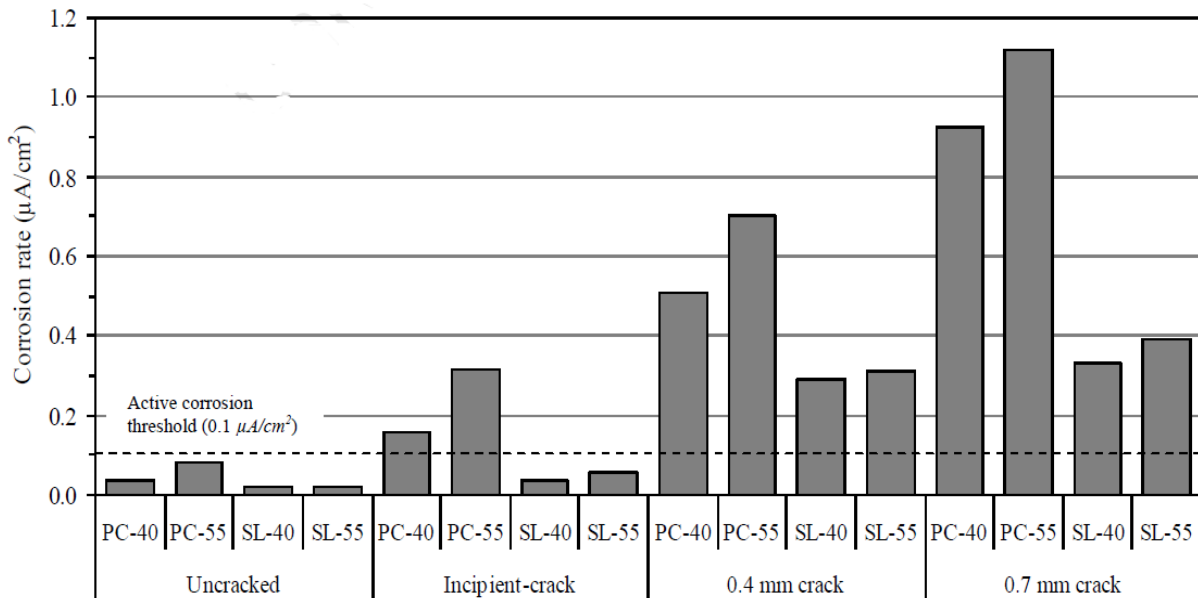


**Figure 2. 7: Average chloride-induced corrosion rates (Otieno, 2008)**

This study has shown that crack width does influence the corrosion rate of steel. A higher corrosion rate was observed for a 0.7 mm crack width compared to 0.4 mm crack width.

The same trend was observed in a study by Scott (2004) where surface crack widths of 0.2 mm and 0.7 mm were introduced in the concrete specimens by the slipping of plain round bars. An increase in corrosion rate was observed with increasing crack width in each binder type.

These observations confirm that aggressive substances (Chlorides and oxygen) can reach the steel reinforcement faster and more abundantly through wider cracks. Therefore, an increase in crack width can result in an increase of chloride penetration and higher corrosion rate due to a greater steel surface area exposed by large cracks.



## **b. Crack frequency**

Crack frequency is the number of cracks present on the concrete surface per unit length. A higher crack frequency may result in significant increase of concrete permeability, thus resulting in increased penetration of aggressive substances (chlorides and oxygen). Arya and Ofori-Darko (1996) conducted a study on the effect of crack frequency on reinforcement corrosion, and suggested that when many surface cracks exist, crack frequency may be more important than crack width.

## **c. Crack orientation**

The orientation of cracks is either longitudinal (parallel to the reinforcement) or transverse (intersecting with the reinforcement). Longitudinal cracks can occur as a result of the plastic settlement and plastic shrinkage, while transverse cracks normally occur as a result of flexural stresses.

Longitudinal cracks can be very dangerous as they expose a large area of steel for aggressive agents. Having a large area of steel exposed can speed up the corrosion process. In the case of transverse cracks, the cathodic site is situated at the uncracked region.

### **2.3.5.6 Effect of tensile stress on reinforcement steel corrosion**

Due to low tensile strength and brittle nature of concrete, it is difficult to avoid flexural cracks in the bending moment zones of reinforced concrete members. These cracks occur in the tension zone when the tensile stresses applied in concrete have exceeded the tensile strength on concrete (Malumbela *et al.*, 2009). As pointed out in Section 2.3.5.5, cracks can locally permit the ingress of aggressive substances (chlorides and oxygen) that lowers the pH of concrete in the vicinity of the crack, thus resulting to pitting corrosion (Zhang *et al.*, 2010). Pitting corrosion can become sites for high-stress concentration and result in the reduction of load carrying capacity of the reinforced concrete member.

Houston *et al.*, (1972) have studied the effect of the level of steel stress by subjecting comparable beam specimens to sustained steel stresses of 138, 207, and 248 MPa. Since stressing is frequently accompanied by flexural cracking in reinforced concrete structures,

the work by Houston *et al.*, (1972) suggested that the effect of stressing or cracking cannot be presented separately. Their results suggested that the combined effect of stressing and cracking result in increase of the corrosion degree by 10 to 15 percent. There is an increase in corrosion level with the increase in stress level. The increased corrosion level for the stressed reinforcement steel was caused by stress in the steel and the presence of flexural cracks in the vicinity of stressed zones.

### **2.3.6 Accelerated corrosion**

Accelerated corrosion techniques are used to induce corrosion in the laboratory so that tests are completed within a reasonable amount of time (El Maaddawy & Soudki, 2003). As already mentioned the alkaline environment of concrete protects the embedded reinforcement from corrosion. This environment can be destroyed by either carbonation or chloride attack. These deleterious substances enter through concrete cover and then lead to reinforcement corrosion by destroying the protective passive oxide layer on the embedded reinforcement (Raja *et al.*, 2015). However, it may take several years for chlorides to reach the steel in sufficient quantities and for steel de-passivation to occur (Malumbela *et al.*, 2012).

Several researchers (Castel *et al.*, 2003; Vidal *et al.*, 2007 and Zhang *et al.*, 2010) who exposed their laboratory test specimens to natural corrosive environment and let them be corroded naturally, waited four years for corrosion to initiate. The structural damage was only obtained after 20 years.

Researchers have and continue to use accelerated corrosion techniques in the laboratory to achieve high corrosion degrees within a reasonable short period of time, while others obtain steel corrosion characteristics by making use of reinforced concrete samples taken from existing structures that have been in use for several years (Wei-liang & Yu-xi, 2001). The following techniques are used to accelerate chloride-induced corrosion.

#### **2.3.6.1 Wet/drying technique**

This method entails exposing the concrete member through alternate cycles of wetting and drying with a chloride solution until the passivating layer is destroyed to activate reinforcement corrosion (ASTM G109, 2007). This method closely resembles the natural

reinforcement corrosion in the case of concrete members exposed to tidal sprays in the marine environment. The advantage of this method is that it closely resembles natural corrosion of reinforced concrete in the case of concrete structures exposed to tidal spray of sea-water. Yuan, *et al.*, (2007) conducted an experiment using this technique to accelerate the corrosion process of the reinforced concrete test beams. In their experiment, the solution used for wetting and drying cycles consisted of salt water with 5% NaCl. Their results revealed that the corrosion process and corrosion characteristics of the steel bar under artificial climate environment are similar to that of corrosion under natural environment. The disadvantage of this technique is that it may take several months for sufficient levels of chloride ions to permeate through the concrete and de-passivate the steel.

#### **2.3.6.2 Admixed chlorides**

This method entails the introduction of a sufficient percentage of chlorides into the fresh concrete mix prior to concrete casting (Ing, 2003). The penetration of chlorides through concrete is a slow process, the introduction of chlorides into the fresh concrete mix can initiate corrosion immediately (Trejo & Weyers, 2013). Several researchers have revealed that the presence of sufficient quantities of chlorides in cementitious materials results in immediate de-passivation of the embedded reinforcing steel. (Lambert *et al.*, 1991 and López *et al.*, 1993) conducted a study to investigate the appropriate quantity of chlorides to admix. The study revealed that additions as low as 1% by weight of cement are considered to pose a high risk of corrosion in good quality concrete. However, the usual quantity of chlorides admixed for accelerated testing is in the range of 2-4% NaCl by weight of cement. Adding greater quantities, such as 4-6% is reported to result in a negligible difference in the corrosion rate in comparison to when only 2% is added (López *et al.*, 1993). The advantage of this technique is that it leads to immediate steel de-passivation as chlorides are added into the concrete mix, while the disadvantages are that it does not allow the steel to first passivate and it leads to uniform corrosion of the steel bar, rather than the localised corrosion dominant in the case of natural chloride-induced corrosion (Malumbela *et al.*, 2012).

### 2.3.6.3 Impressed current technique

The impressed current technique entails applying a direct current (DC) to the steel embedded in concrete to induce significant corrosion within a reasonable amount of time. The positive terminal from a DC power supply is connected to the reinforcement and the negative terminal is connected to a stainless steel bar, while the test specimen is immersed in an electrolyte solution (Ballim & Reid, 2003). The reinforcement becomes an anode while the stainless steel becomes a cathode.

After applying the current for a given period, the degree of induced corrosion can be determined theoretically using Faraday's law, or the percentage of actual mass of steel lost in corrosion can be calculated using a gravimetric test conducted on the extracted bars after subjecting them to accelerated corrosion (Ahmad, 2009). The ASTM G1-90 (1999) specifies that the corroded steel bars shall be properly cleaned to remove corrosion products prior to weighing. Equation 2.8 illustrates Faraday's law for calculating the steel loss:

$$\Delta m = \frac{Mit}{zF} \quad (2.8)$$

where  $\Delta m$  is mass of steel consumed (in grams),  $M$  is the atomic mass of metal (55.847 g for Fe),  $I$  is the current intensity (in ampere),  $t$  is the time (seconds),  $z$  is number of electrons transferred (2) and  $F$  is the Faraday constant (96.500 amp.second).

The limitations of this law is that it does not take into consideration the effect of concrete resistivity when estimating required current to induce a certain degree of corrosion. Due to concrete resistivity, the corrosion current is not equal to the applied current.

## 2.4 Need for lap-splicing of steel reinforcement in concrete

As previously mentioned in Chapter 1, Section 1.2, splicing of steel reinforcement is used to join two reinforcement bars to transfer the force from one bar to the next through the bond between steel and concrete. This is due to reasons such as steel fabrication, transportation limitations, steel workshop fabrication (limited available length) and construction joints. Therefore, splicing of steel reinforcement is unavoidable. Splicing of

steel reinforcement is carried out in three ways including bar lapping, mechanical joints, and welded joints. In this study, the focus is lap splicing on flexural members.

#### 2.4.1 Code stipulations on lap splicing of flexural steel reinforcement

The minimum anchorage length of lap-spliced reinforcement to prevent bond failure under normal conditions (non-corrosion) is stipulated by the various codes of practice. The bond failure may occur when the longitudinal bond stresses have exceeded the shear strength of the concrete keys between ribs and the bar can pull free. With respect to flexural members, splitting cracks tend to propagate from the bar to the surface of the concrete until the cover spalls off. This result in excessive deflection, making beams unable to maintain applied loading until collapse.

As previously mentioned in chapter 1, a comparison between SANS 10100-1 and Eurocode 2 was made in this study.

Table 2.4 illustrates the minimum lap splice length as stipulated by the South African National Standard (SANS) and Eurocode 2.

**Table 2. 4: Stipulated minimum anchorage length**

<b>SANS 10100-1</b>	<b>Eurocode 2</b>
40 × D, where D is the bar diameter	36 × D, where D is the bar diameter
- Calculated based on a high tensile steel bar ( $f_y = 450$ MPa) in tension using 25 MPa concrete and a bond stress of 2.5 MPa.	- Calculated based on a high tensile steel bar ( $f_y = 500$ MPa) in tension using 25 MPa concrete and a bond stress of 2.7 MPa.

Eurocode 2 has a reduced embedded / splice length compared to 10100-1, hence higher bond stress. For the same development length, the bond strength can also be influenced by the choice of bar diameter, as a smaller bar diameter develops a greater bond stress than a larger bar diameter under the same applied force (ACI 408.2R, 2012). This is because the bar diameter inversely influences the bond strength. Therefore, a small bar diameter and embedded length has greater bond strength than that large bar diameter and embedded length.

## 2.5 Summary

In this chapter, transport properties in concrete, mechanism of corrosion, its causes and lap length requirements as well as effect of steel reinforcement corrosion on flexural strength of RC members have been critically discussed.

Steel reinforcement corrosion leads to spalling, cracking of the concrete section, reduction in the cross sectional area of the reinforcing steel, and reduction in the bond strength between the steel and the surrounding concrete. These problems result in deterioration of the RC member, thus affecting the integrity and service life of the structure.

The literature review has revealed that the main factors affecting the corrosion are thickness of cover, concrete penetrability, concrete quality and concrete cracking. Low concrete permeability helps in restricting the corrosion rate by improving the electrical resistivity of concrete, thereby decreasing the flow of hydroxyl ions from anode to cathode. The use of cement replacement materials is becoming more common in concrete structures. This is due to the favourable permeability and good corrosion resistance of the resulting concrete. The literature suggest that the use of low w/c ratio and cement extenders helps to reduce the permeability of concrete through refinement of pore structure and improved characteristics of the interfacial transition zone (ITZ). This result in increased resistivity of concrete.

As steel reinforcement corrosion may take decades to manifest itself in reinforced concrete structures due to protection provided by the high alkaline environment in the concrete, several techniques for corrosion acceleration have been critically discussed. No critical details have been reported on the effect of corroded splice-reinforcement on flexural capacity of concrete members. Experimental studies will be performed in the next chapter to assess the flexural behaviour of lap spliced steel reinforcement affected by corrosion.

## 2.6 References

- Ahmad, S. (2003). Reinforcement corrosion in concrete structures, its monitoring and service life prediction—a review. *Cement and Concrete Composites*, 25(4–5), 459–471.
- Ahmad, S. (2009). Techniques for inducing accelerated corrosion of steel in concrete. *Arabian Journal for Science and Engineering*, 34(2), 95.
- Alexander, M., & Mindess, S. (2005). *Aggregates in concrete* (1st ed.). Taylor & Francis.
- Almusallam, A. A. (2001). Effect of degree of corrosion on the properties of reinforcing steel bars. *Construction and Building Materials*, 15(8), 361–368.
- Al-Sulaimani, G., Kaleemullah, M., & Basunbul, I. (1990). Influence of corrosion and cracking on bond behavior and strength of reinforced concrete members. *Structural Journal*, 87(2), 220–231.
- Andrade, C., & Alonso, C. (1996). Corrosion rate monitoring in the laboratory and on-site. *Construction and Building Materials*, 10(5), 315–328.
- Andrade, C., Alonso, C., Garcia, D., & Rodriguez, J. (1991). Remaining service lifetime of reinforced concrete structures: Effect of corrosion on the mechanical properties of the steel. *International Conference on Life Prediction of Corrodible Structures, Cambridge, UK (1991)*, Pp. 12/1-12/11.
- Arya, C, Buenfeld, N., & Newman, J. (1990). Factors influencing chloride-binding in concrete. *Cement and Concrete Research*, 20(2), 291–300.
- Arya, C, & Ofori-Darko, F. (1996). Influence of crack frequency on reinforcement corrosion in concrete. *Cement and Concrete Research*, 26(3), 345–353.
- Arya, C, & Xu, Y. (1995). Effect of cement type on chloride binding and corrosion of steel in concrete. *Cement and Concrete Research*, 25(4), 893–902.

- Arya, Chanakya, & Wood, L. A. (1995). *The relevance of cracking in concrete to corrosion of reinforcement*. Concrete Society.
- ASTM G1-90. (1999). *Standard Practice for preparing, cleaning and evaluating corrosion test specimens*. American Society for Testing and Materials.
- ASTM G109. (2007). *Standard Test Method for Determining the Effects of Chemical Admixtures on the Corrosion of Embedded Steel Reinforcement in Concrete Exposed to Chloride Environments*. American Society for Testing and Materials.
- Azarsa, P., & Gupta, R. (2017). Electrical resistivity of concrete for durability evaluation: A review. *Advances in Materials Science and Engineering, 2017*.
- Ballim, Y., Alexander, M., & Beushausen, H. (2009). *Durability of concrete*. In G. Owens, ed. *Fulton's Concrete Technology* (9th ed.). Cement and Concrete Institute (CNCI).
- Ballim, Y., & Reid, J. (2003). Reinforcement corrosion and the deflection of RC beams— an experimental critique of current test methods. *Cement and Concrete Composites, 25*(6), 625–632.
- Batis, G., & Rakanta, E. (2005). Corrosion of steel reinforcement due to atmospheric pollution. *Cement and Concrete Composites, 27*(2), 269–275.
- Beeby, A. (1983). Cracking, Cover, and Corrosion of Reinforcement. *Concrete International, 5*(2), 35–40.
- Bentur, A., Berke, N., & Diamond, S. (1997). *Steel corrosion in concrete: Fundamentals and civil engineering practice*. CRC Press.
- Bertolini, L., Elsener, B., Pedferri, P., & Polder, R. B. (2004). *Corrosion of Steel in Concrete: Prevention, Diagnosis, Repair* (1st ed.). Wiley.



- Bertolini, L., & Redaelli, E. (2009). Depassivation of steel reinforcement in case of pitting corrosion: Detection techniques for laboratory studies. *Materials and Corrosion*, 60(8), 608–616.
- Beushausen, H., & Alexander, M. (2009). *Concrete Repair*. In G. Owens, ed. *Fulton's Concrete Technology* (9th ed.). Cement and Concrete Institute (CNCI).
- Boddy, A., Bentz, E., Thomas, M., & Hooton, R. (1999). An overview and sensitivity study of a multimechanistic chloride transport model. *Cement and Concrete Research*, 29(6), 827–837.
- Broomfield, J. P. (2007). *Corrosion of steel in concrete: Understanding, investigation and repair*. CRC Press.
- Cabrera, J. (1996). Deterioration of concrete due to reinforcement steel corrosion. *Cement and Concrete Composites*, 18(1), 47–59.
- Castel, A., François, R., & Arliguie, G. (2000). Mechanical behaviour of corroded reinforced concrete beams—Part 1: Experimental study of corroded beams. *Materials and Structures*, 33(9), 539–544.
- Castel, A., Vidal, T., François, R., & Arliguie, G. (2003). Influence of steel–concrete interface quality on reinforcement corrosion induced by chlorides. *Magazine of Concrete Research*, 55(2), 151–159.
- El Maaddawy, T. A., & Soudki, K. A. (2003). Effectiveness of impressed current technique to simulate corrosion of steel reinforcement in concrete. *Journal of Materials in Civil Engineering*, 15(1), 41–47.
- Elbusaefi, A. A. (2014). The effect of steel bar corrosion on the bond strength of concrete manufactured with cement replacement materials. *PHD Studies, Cardiff University*.

- Enevoldsen, J., Hansson, C., & Hope, B. (1993). *The influence of relative humidity on the corrosion rates of steel embedded in mortar and concrete*. 342–350.
- Fernandez, I., Herrador, M. F., Marí, A. R., & Bairán, J. M. (2016). Structural effects of steel reinforcement corrosion on statically indeterminate reinforced concrete members. *Materials and Structures*, 49(12), 4959–4973.
- Grieve, G. (2009). *Cementitious materials*. In G. Owens, ed. *Fulton's Concrete Technology* (9th ed.). Cement and Concrete Institute (CNCI).
- Hausmann, D. (1967). Steel corrosion in concrete—How does it occur? *Materials Protection*.
- Houston, J. T., Atimtay, E., & Ferguson, P. M. (1972). *Corrosion of reinforcing steel embedded in structural concrete*. Center for Highway Research, University of Texas at Austin.
- Ing, M. J. (2003). *Detection of Reinforcement Corrosion by an Acoustic Technique*. Leicestershire: Loughborough University.
- Kearsley, E. P., & Joyce, A. (2014). Effect of corrosion products on bond strength and flexural behaviour of reinforced concrete slabs. *Journal of the South African Institution of Civil Engineering*, 56(2), 21–29.
- Lambert, P., Page, C., & Vassie, P. (1991). Investigations of reinforcement corrosion. 2. Electrochemical monitoring of steel in chloride-contaminated concrete. *Materials and Structures*, 24(5), 351–358.
- López, W., González, J., & Andrade, C. (1993). Influence of temperature on the service life of rebars. *Cement and Concrete Research*, 23(5), 1130–1140.

- Maage, M., Helland, S., Poulsen, E., Vennesland, O., & Carl, J. E. (1996). Service life prediction of existing concrete structures exposed to marine environment. *Materials Journal*, 93(6), 602–608.
- Malumbela, G., Moyo, P., & Alexander, M. (2009). Behaviour of RC beams corroded under sustained service loads. *Construction and Building Materials*, 23(11), 3346–3351.
- Malumbela, G., Moyo, P., & Alexander, M. (2012). A step towards standardising accelerated corrosion tests on laboratory reinforced concrete specimens. *Journal of the South African Institution of Civil Engineering*, 54(2), 78–85.
- Mangat, P., & Molloy, B. (1992). Factors influencing chloride-induced corrosion of reinforcement in concrete. *Materials and Structures*, 25(7), 404–411.
- Martin-Pérez, B. (1999). *Service life modelling of RC highway structures exposed to chlorides*.
- Neville, A. M. (1995). *Properties of concrete* (4th ed, Vol. 4). Longman.
- Otieno, M. (2008). Corrosion Propagation in Cracked and Un-cracked Concrete. *MSc Dissertation, Department of Civil Engineering, University of Cape Town*.
- Otieno, M., Alexander, M., & Beushausen, H. (2012). Corrosion of Steel in reinforced concrete: Influence of binder type, water/binder ratio, cover and cracking. *Epping: Fingerprint*.
- Raja, P. B., Ghoreishiamiri, S., & Ismail, M. (2015). Natural corrosion inhibitors for steel reinforcement in concrete—A review. *Surface Review and Letters*, 22(03), 1550040.
- Richardson, M. (2002). *Fundamentals of durable concrete, Modern Concrete Technology*. Spon Press.
- Roberge, P. R. (2000). *Handbook of corrosion engineering*. McGraw-Hill,.

- SANS 10100 -2. (2014). *The structural use of concrete: Materials and execution of work*. South African Standard Code of practice.
- Scott, A., & Alexander, M. (2007). The influence of binder type, cracking and cover on corrosion rates of steel in chloride-contaminated concrete. *Magazine of Concrete Research*, 59(7), 495–505.
- Scott, A. N. (2004). The influence of binder type and cracking on reinforcing steel corrosion in concrete. *PhD Thesis, Department of Civil Engineering, University of Cape Town*.
- Sengul, O. (2014). Use of electrical resistivity as an indicator for durability. *Construction and Building Materials*, 73, 434–441.
- Stansbury, E. E., & Buchanan, R. A. (2000). *Fundamentals of electrochemical corrosion*. ASM international.
- Theodosiou, G. (2009). *Reinforcement*. In G. Owens, ed. *Fulton's Concrete Technology* (9th ed.). Cement and Concrete Institute (CNCI).
- Theron, G. D. V. (1994). Effects of reinforcement corrosion on the structural performance of reinforced concrete beams. *MSc Dissertation, Department of Civil Engineering, University of Cape Town*.
- Trejo, D., & Weyers, R. (2013). Admixed Chlorides in Concrete: History, Impacts, and Standardization. *Special Publication*, 291, 1–20.
- Tuutti, K. (1982). *Corrosion of steel in concrete—CBI Research Report*. Swedish Cement and Concrete Research Institute.
- Vidal, T., Castel, A., & Francois, R. (2007). Corrosion process and structural performance of a 17 year old reinforced concrete beam stored in chloride environment. *Cement and Concrete Research*, 37(11), 1551–1561.

- Wei-liang, J., & Yu-xi, Z. (2001). Effect of corrosion on bond behavior and bending strength of reinforced concrete beams. *Journal of Zhejiang University-Science A*, 2(3), 298–308.
- Weyers, R. E. (1998). Service life model for concrete structures in chloride laden environments. *Materials Journal*, 95(4), 445–453.
- Yalciner, H., Eren, O., & Sensoy, S. (2012). An experimental study on the bond strength between reinforcement bars and concrete as a function of concrete cover, strength and corrosion level. *Cement and Concrete Research*, 42(5), 643–655.
- Yuan, Y., Ji, Y., & Shah, S. P. (2007). Comparison of two accelerated corrosion techniques for concrete structures. *ACI Structural Journal*, 104(3), 344.
- Zhang, R, Castel, A., & François, R. (2009). Serviceability limit state criteria based on steel–concrete bond loss for corroded reinforced concrete in chloride environment. *Materials and Structures*, 42(10), 1407.
- Zhang, Ruijin, Castel, A., & François, R. (2010). Concrete cover cracking with reinforcement corrosion of RC beam during chloride-induced corrosion process. *Cement and Concrete Research*, 40(3), 415–425.
- Živica, V. (2003). Influence of w/c ratio on rate of chloride induced corrosion of steel reinforcement and its dependence on ambient temperature. *Bulletin of Materials Science*, 26(5), 471–475.

## CHAPTER 3: EXPERIMENTAL METHODOLOGY

### 3.1 Introduction

This chapter presents the experimental details and methodology that was employed in this study to achieve the research objectives. It covers the specimen type, concrete mix design, casting and curing. The tests that were carried out include concrete cube testing, accelerated corrosion and flexural strength. Accelerated corrosion testing was used to induce steel reinforcement corrosion to achieve the desired level of corrosion within a short period of time. This was achieved by making use of the impressed current technique. Concrete cube testing was used to evaluate the strength of concrete cubes at 28 days. The flexural strength test was used to determine the strength of corroded test specimens and compared these with un-corroded test specimens.

### 3.2 Materials

#### 3.2.1 Cement

For this study, plain Portland cement (PC), CEM I 52.5R complying with SANS 50197-1 was used. This study did not seek to investigate the effect of cement type. Typical oxide composition of the PC is given in Table 3.1.

**Table 3. 1: Typical oxide composition of Plain Portland Cement (Afrisam datasheet, 2017)**

Oxide	SiO <sub>2</sub>	CaO	Al <sub>2</sub> O <sub>3</sub>	Fe <sub>2</sub> O <sub>3</sub>	Mn <sub>2</sub> O <sub>3</sub>	TiO <sub>2</sub>	MgO	SO <sub>3</sub>	K <sub>2</sub> O	Na <sub>2</sub> O
Composition %	20.7	65.0	4.6	2.6	0.1	0.3	1.7	2.9	0.4	0.1

#### 3.2.2 Aggregates

##### a. Fine and coarse aggregates

The fine and coarse aggregates used in concrete mixing should comply with SANS 1083: 2014 standard. Fine aggregates are defined as the material with 90% of its mass passes through the 4.75 mm sieve (SANS 1083, 2014). The fine aggregates have a significant

effect on concrete properties due to the fact that the fine aggregates with a fineness modulus greater than 3.5 lead to a harsh mix which is prone to bleeding and segregation. While aggregates with a fineness modulus that is less than 1 have a large surface area and subsequently, high water demand (Alexander & Mindess, 2005). Coarse aggregates are defined as the material retained on the 4.75 mm sieve (SANS 1083, 2014). A study by Alexander and Mindess (2005) suggests that the larger the maximum stone size, the less aggregate surface area there is. This results in less paste required to cover all aggregates. The reduction in paste result in less shrinkage, creep and more economical concrete due to less cement used.

For this study crushed Eikenhof andesite supplied by AfriSam was be used for both fine and coarse aggregates with a nominal maximum stone size of 13.2 mm. The sieve analysis for both fine and coarse aggregates was carried out according to SANS 1083:2014. Standard sieve apertures were placed in decreasing size from top to bottom and the measured grading curves of fine aggregate is given in Figures 3.1. All calculations and grading curve for coarse aggregates are given in appendix B.

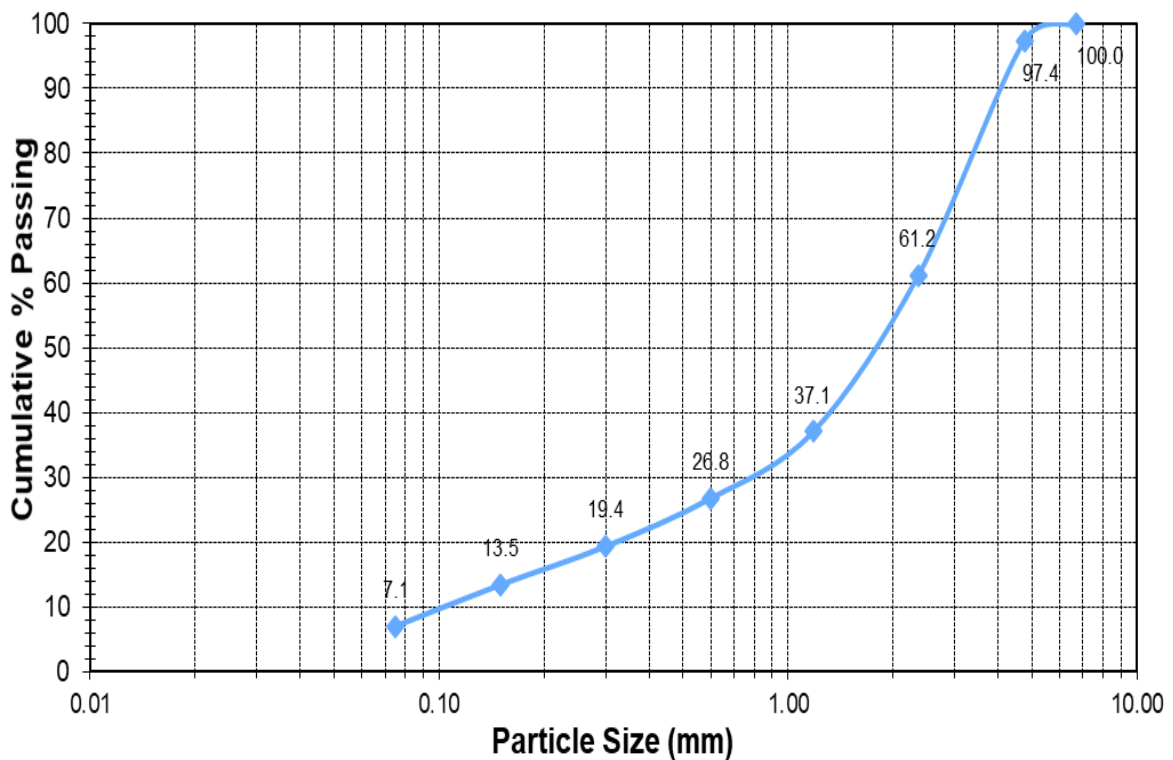


**Figure 3. 1: Grading curve of fine aggregate**

The grading curve shows that 97.4% of the crushed sand passes through the 4.75 mm sieve. The sand had a continuous grading and a fineness modulus of 3.45. The typical characteristics of andesite aggregates are given in Table 3.2.

**Table 3. 2: Typical characteristics of Andesite (Alexander & Mindess, 2005)**

<b>Andesite property</b>	<b>Value</b>
Relative density	2.6 – 2.8
Water absorption (%)	3.0
Unconfined compressive strength (MPa)	516 – 538
10% Fines Aggregate Crushing Value (kN)	458
Elastic Modulus (GPa)	101

### **3.2.3 Reinforcing steel**

The steel reinforcement complying with the requirements of SANS 920, consisted of high yield (ribbed) bars with a minimum characteristic yield strength of 450 MPa and plain round mild steel bars with a minimum characteristic yield strength of 250 MPa. 10 mm diameter steel bars were used on beam specimens designed for SANS 10100 -1 and 8 mm diameter steel bars were used on beam specimens designed for Eurocode 2.

All specimens were designed for flexural failure by providing 6 mm diameter plain round mild steel links at a spacing of 50 mm centres. The spacing of shear links was decreased from 100 mm centres obtained in the design of RC beams. The aim of reducing the spacing of shear links was to prevent shear failure during flexural tests, as the experimental failure load was anticipated to be higher than the theoretical failure load. The hanger bars for the links were two 8 mm diameter longitudinal steel bars with a minimum characteristic yield strength of 450 MPa. The steel reinforcement details are presented in section 3.4.

### **3.2.4 Formwork**

Formwork consisted of three steel moulds and three 19 mm plywood boards which were fabricated and connected with screws to ensure they are sufficiently tight to prevent loss



of cement paste. Shutter release oil was applied on the internal surfaces of the formwork to ensure easy demolding of the beam specimens. Prior to reuse of formwork, the internal surfaces in contact with concrete were cleaned thoroughly. The formwork prior to concrete casting and after concrete casting is shown in Figures 3.2 and 3.3, respectively.



**Figure 3. 2: Photograph of moulds prior to concrete casting**

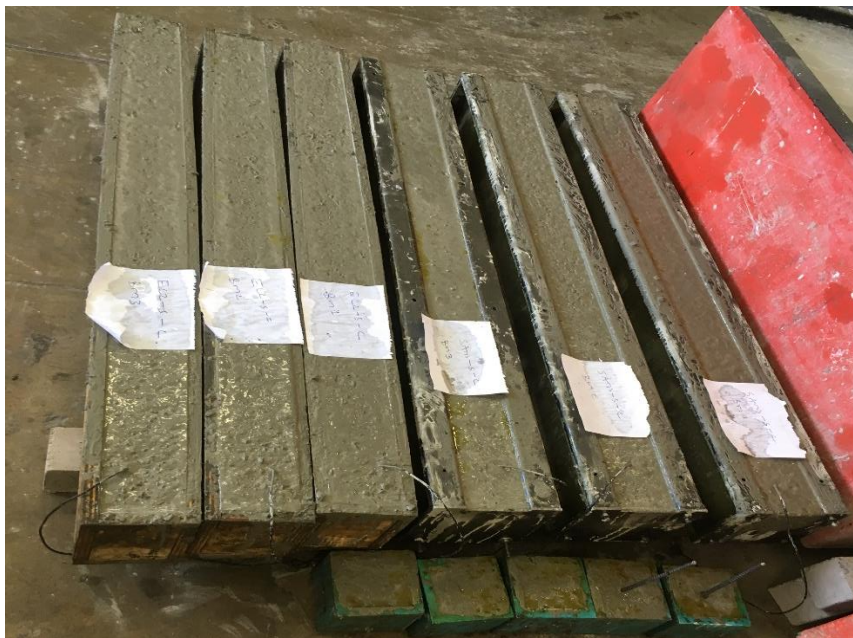


**Figure 3. 3: Photograph of moulds post concrete casting**

### 3.3 Concrete mix proportions

One concrete mix design was used for all the test specimens and was based on the Cement and Concrete Institute (C&CI) volumetric mix design method which is derived from the ACI 211.1-91 method and modified to suit South African practice (Addis & Goodman, 2009).

Table 3.3 shows a summary of the concrete mix proportions (per cubic meter) used in this study.

**Table 3. 3: Concrete mix proportions**

<b>Concrete ingredients</b>	<b>Quantity</b>
Water content	195 kg/m <sup>3</sup>
CEM I 52.5R	390 kg/m <sup>3</sup>
Fine aggregate (Crusher sand) – Eikenhof Andesite	368 kg/m <sup>3</sup>
Coarse aggregate (13.2 mm Eikenhof Andesite stone)	1005 kg/m <sup>3</sup>
Water/Cement ratio	0.50
28 day Compressive strength	52.5 MPa

### 3.4 Specimen type and sample size

A total number of 24 reinforced concrete beam specimens were made for the experimental work. For test specimens with lap spliced reinforcement, the lap splicing was located within the maximum moment section of the span to determine the flexural strength of RC beam. Test specimens were divided into two groups (Type A and Type B). The reinforcement design for Type A and Type B was carried out according to relevant requirements of SANS 10100-1 and Eurocode 2, respectively. The design parameters are presented in Table 3.4.

**Table 3. 4: Design Parameters**

Parameter	SANS 10100-1	Eurocode 2
Concrete unit weight	24 kN/m <sup>3</sup>	25 kN/m <sup>3</sup>
Ultimate design load	1.2 × DL + 1.6 × DL	1.35 × DL + 1.5 × DL
Hot-rolled mild steel reinforcement	250 MPa	250 MPa
Hot-rolled high-yield reinforcement	450 MPa	500 MPa

Due to the varied loading parameters as shown in Table 3.4, different values were obtained for bending moments and shear forces. The required tension reinforcing steel area was 154 mm<sup>2</sup> for SANS standard and 129 mm<sup>2</sup> for Eurocode standard; therefore 2Y10 bars were adopted for Type A beams and 3Y8 bars for Type B beams. Detailed calculations are presented in Appendix A. Table 3.5 summarises the number and type of test specimens used in the study.

**Table 3. 5: Specimens details**

Beam Type	Guidelines used for splicing of flexural steel	Splice length	Number of specimens	Specimen treatment	Specimen label
A	SANS 10100-1	40 × Ø = 400 mm	3	Steel corroded	SANS-S-C
		40 × Ø = 400 mm	3	Steel not corroded	SANS-S-NC
		Flexural steel not spliced	3	Steel corroded	SANS-NS-C
		Flexural steel not spliced	3	Steel not corroded	SANS-NS-NC
B	Eurocode 2	36 × Ø = 288 mm	3	Steel corroded	EC2-S-C
		36 × Ø = 288 mm	3	Steel not corroded	EC2 -S-NC
		Flexural steel not spliced	3	Steel corroded	EC2 -NS-C
		Flexural steel not spliced	3	Steel not corroded	EC2 -NS-NC

**Note:** S: Spliced; NS: Not spliced; C: Corroded; NC: Not corroded

As shown in Figures 3.4 and 3.5, the beam sizes were  $100 \times 165 \times 1500$  mm long for ease of handling during casting and testing.

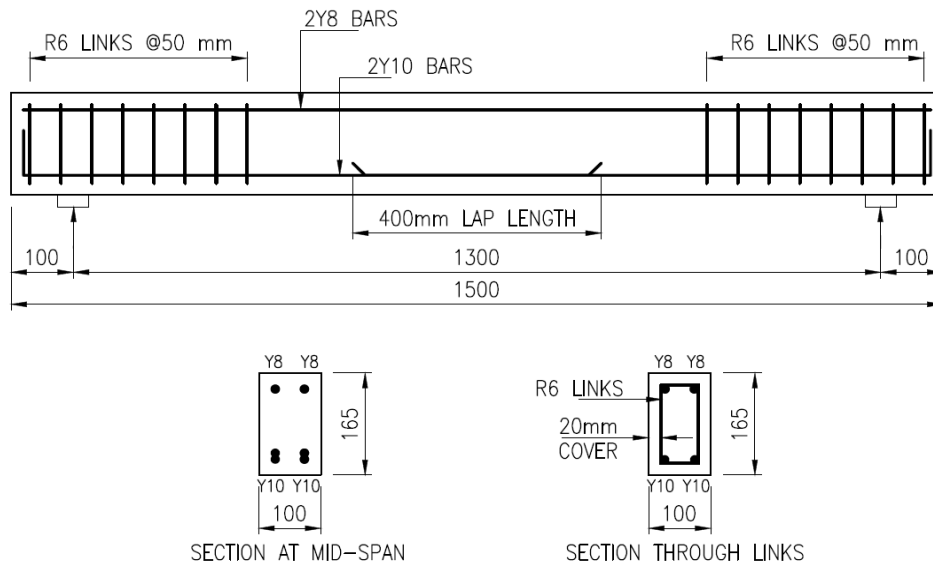


**Figure 3. 4: Type A RC beams geometry and reinforcement details (according to SANS10100-1)**

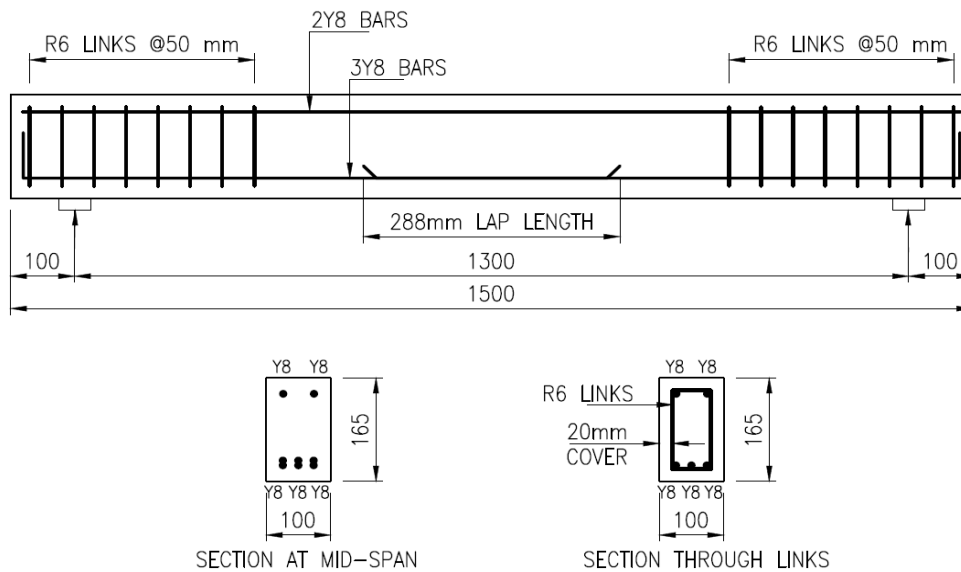


**Figure 3. 5: Type B RC beams geometry and reinforcement details (according to Eurocode 2)**

### 3.5 Mixing, casting and curing of specimens

Prior to concrete casting, the steel reinforcement bars cut into appropriate length (as shown on Figures 3.4 and 3.5) were cleaned using a wire brush to remove any rust on the

steel surface. Once cleaning was complete, the steel reinforcement bars were weighed individually, to determine their mass before corrosion. The purpose of this was to enable the determination of the degree of corrosion once corrosion acceleration is complete. A 1.5 mm<sup>2</sup> multi-strand copper wire was connected to the tension reinforcement. This copper wire was used to apply the voltage during corrosion acceleration. The cover to steel reinforcement was maintained using 20 mm plastic cover blocks connected to stirrups.

A corrosion protective coating was applied to all stirrups on corroded beam specimens. The purpose of this was to electrically isolate the shear reinforcement from the tensile reinforcement and prevent current flow to the stirrups in-order for the impressed current to induce corrosion only on the tension reinforcement (Ballim & Reid, 2003).

The concrete material was mixed using a drum mixer with the capacity of 175 litres. All six beams cast in one day, along with six 100 mm cubes for compressive strength test were mixed in one batch. After concrete mixing was complete, fresh concrete was cast into moulds in two layers and each layer was compacted using a mechanical vibration table. Once casting and compaction was complete, the top surface was floated to make it smooth.

After casting, beams and cubes were left in the moulds for 24 hours in the laboratory (at room temperature), covered with a polyethene sheeting to prevent excessive moisture loss. After 24 hours, the formwork was removed and the RC beams and cubes were cured in a water tank at 23 °C ( $\pm 2$  °C). RC beams were cured for a period of 21 days while cubes for concrete compressive strength test were cured for 28 days. The curing of beams and cubes was carried out according to requirements of the South African standard code of practice SANS 5861-3 (2006).

### **3.6 Corrosion acceleration experimental set-up**

Impressed current technique was used to accelerate corrosion. This technique has previously been used by several researchers (Austin et al., 2004; Ballim & Reid, 2003; El Maaddawy & Soudki, 2003; Malumbela *et al.*, 2009b) to accelerate the corrosion of reinforcement steel in concrete. Although corrosion can occur along the entire beam

length, in this study the tensile steel reinforcement was corroded in the region corresponding to lapped splices. The tension reinforcement was connected to the positive terminal of the applied external direct current, while the stainless steel bar was connected to the negative terminal of the external power supply.

The set-up consisted of a Direct Current (DC) power supply, a counter electrode, working electrode, and an electrolyte solution (Ahmad, 2009). The cured RC test specimen were turned upside down and saturated (in the region corresponding to lap-spliced steel reinforcement) with a 5% solution of sodium chloride to supply chlorides required to accelerate steel de-passivation and function as an electrolyte solution in the corrosion cell. This was achieved by building reservoir on the surface of RC specimens in accordance with the previous work carried out by Yoon, *et al.*, (2000) & Malumbela *et al.*, (2009).

The positive terminal from a DC power supply was connected to the tension reinforcement (anode) and the negative terminal was connected to the stainless steel bar (cathode) that was placed inside the sodium chloride solution reservoir pond. The arrangement of the accelerated corrosion set-up is shown in figures 3.6 and 3.7.

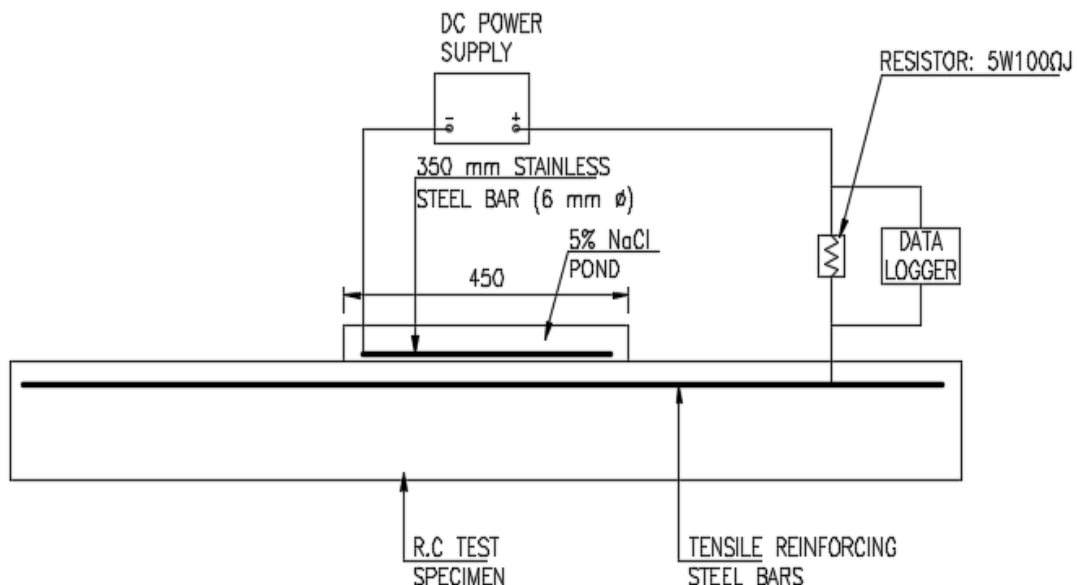


**Figure 3. 6: Accelerated corrosion set-up of beam specimens**

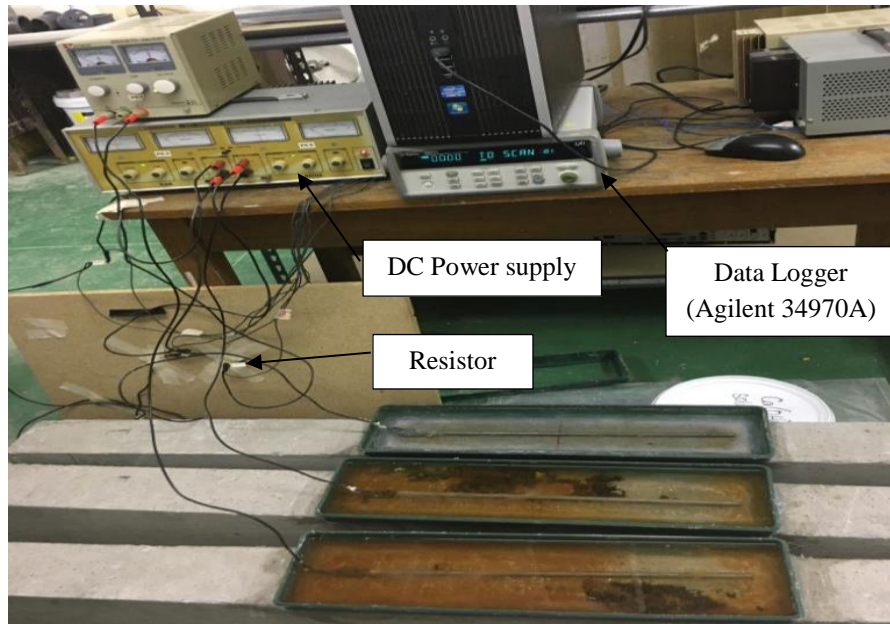


**Figure 3. 7: Photograph showing accelerated corrosion set-up**

A 20% loss of cross sectional area was chosen as the desired degree of corrosion. The reason for choosing this corrosion degree was to ensure that significant effect of corrosion is observed. A lower corrosion degree, in the case of non-lap spliced beams would not have shown a significant effect of corrosion due to partial load factors used by South African standard code of practice SANS 10100-1 (2000) and European standard code of practice (EN 1992-1-1, 2004). To achieve a 20% loss of cross sectional area of the tension steel, the DC power supply was set to maximum current of 0.48 A for specimens designed according to SANS 10100 – 1 and a maximum current of 0.31 A for specimens designed according to Eurocode 2. The required current was calculated as shown in appendix C, using the Faraday’s law equation 2.8 (section 2.3.6.3).

As the Faraday’s law equation does not take into account the resistivity of the concrete where some current will be taken by concrete, each RC beam specimen was connected to its own DC power supply unit with a voltage limit of 30 *Volts* and a maximum current output of 2 *Ampere*. A constant voltage was supplied to steel reinforcement through a resistor of known resistance. This was delivered through 1.5 mm<sup>2</sup> insulated copper wire fixed by means of electrical insulation tape. The sealing for the insulation tape is provided by silicone. The Agilent 34970A data logger was connected to the circuit to record the voltage across the resistor. The voltage readings were set to be recorded every five



seconds. The applied voltage was monitored regularly and the corrosion acceleration test was stopped once the required current was achieved. The duration of corrosion acceleration for each beam specimen is presented in Appendix C. The current flowing through the resistor was determined using Ohm's law, shown in equation 3.1.

$$V = IR \tag{3.1}$$

where:

V = voltage in volts

I = current in amps

R = resistance in ohms ( $\Omega$ )

At the end of the corrosion acceleration tests, longitudinal cracks were formed on the concrete surface during corrosion acceleration. Corrosion products were also visible on the concrete surface. The longitudinal cracking and corrosion products are presented in Figures 3.8 and 3.9 respectively.



**Figure 3. 8: Photograph showing longitudinal cracks on concrete surface**





**Figure 3. 9: Photograph showing corrosion products**

### **3.7 Specimen testing**

#### **3.7.1 Compressive strength tests**

As previously mentioned, six 100 mm cubes were cast for each concrete batch. The cubes were tested at 7 and 28 days for compressive strength in accordance with SANS 5863 (2006).

SANS 5863 (2006) recommends the application of compression load at a uniform rate of between 0.3 MPa/sec  $\pm$  0.1 MPa/sec until the specimens fails. For this study, the compressive strength tests were performed using a hydraulic compression machine at a loading rate of 0.25 MPa/sec until failure. The maximum load resulting to failure was recorded for the calculation of the compressive strength using equation 3.2. The results for compressive strength tests are presented in Appendix C.

$$f_{cc} = \frac{F}{A_c} \quad (3.2)$$

where:

$f_{cc}$  = compressive strength, in megapascals;

$F$  = maximum load at failure, in newtons;

$A_c$  = cross-sectional area of the specimen on which the compressive force acts, in square millimetres.

### 3.7.2 Flexural strength tests

The control beam specimens were tested at 28 days after casting to determine their respective ultimate flexural load while the corroded beams were tested once the desired corrosion level was reached. As shown in Figure 3.10, beams were simply supported, with a span of 1300 mm between the supports and loaded with two equal point loads placed symmetrically between the supports to produce a four point bending.



**Figure 3. 10: Photograph showing support conditions and loading arrangement**

This type of loading produced a zero shear force between the loading points, thus resulting in pure bending. SANS 5864 (2006) recommends loading to be kept at a constant rate of between 0.03 MPa/s + 0.01 MPa/s until failure. For this study the applied load was kept at a constant loading rate of 2 kN per minute and increased progressively until failure. The adopted loading rate is similar to that used by Theron (1994). The structural behaviour of beam specimens was examined through measurements of loads and mid-span deflection using a dial gauge. The results obtained from corroded beam specimens were compared with those obtained from non-corroded RC beams. Beam failure modes were examined and are reported in chapter 4.

The maximum load at failure was recorded for calculation of flexural strength using equation 3.3.

$$f_{cf} = \frac{Fl}{bd^2} \quad (3.3)$$

where:

$f_{cf}$  = Flexural strength, in megapascals;

$F$  = Maximum load at failure, in newtons;

$l$  = Distance between axes of supporting rollers, in mm;

$b$  = Width of specimen, in millimetres; and

$d$  = Depth of specimen, in millimetres.

### 3.8 Assessment of corrosion in corroded RC beams

Upon completion of flexural tests, the tensile reinforcements were extracted from corroded beams and cleaned with a wire brush to remove the corrosion products and residues of concrete adhered to the surface of the bars as outlined in ASTM G1-90 (1999) for determination of corrosion level. After cleaning, the bars were physically measured using a Vernier Caliper and the bar diameter loss was determined using equation 3.4.

$$D_{loss} = D_i - D_f \quad (3.4)$$

where:

$D_{loss}$  = Diameter loss;

$D_i$  = initial steel diameter before corrosion;

$D_f$  = final steel diameter after the removal of corrosion products.

From equation 3.4, the initial and final areas of steel bars were calculated. The total corrosion degree of steel bars was calculated using equation 3.5.

$$\text{Cross sectional area loss} = 100 - \left( \frac{\text{Final area}}{\text{Initial area}} \right) \times 100 \quad (3.5)$$

### 3.9 Conclusion

A brief schematic of the experimental detail set-up is presented in Figure 3.11:

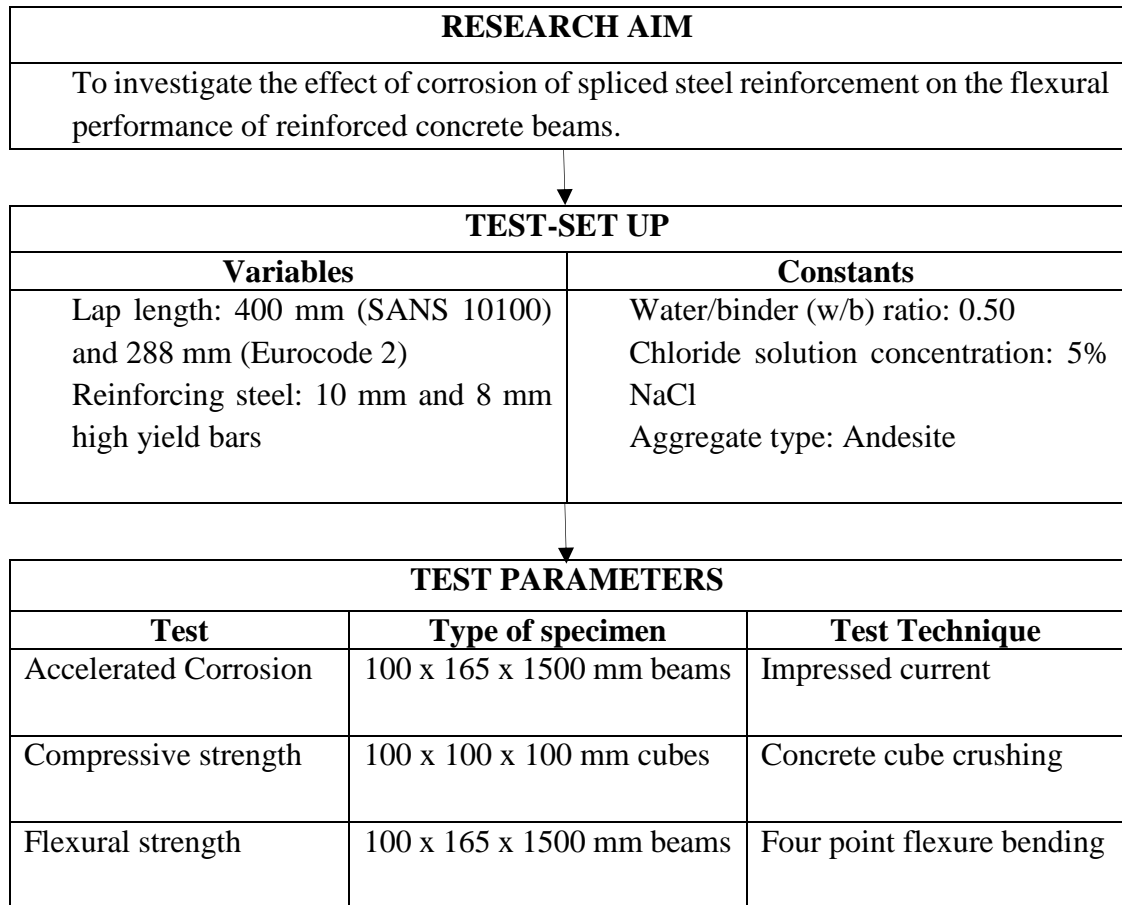


**Figure 3. 11: Flow chart showing experimental details**

The next chapter will present the analysis and discussion of the results obtained from the experiments conducted in this study.

### 3.10 References

Addis, B., & Goodman, J. (2009). *Concrete mix design*. In G. Owens, ed. *Fulton's Concrete Technology* (9th ed.). Cement and Concrete Institute (CNCI).

Afrisam datasheet. (2017). *Afrisam Technical Reference Guide* (8th ed.). Afrisam.

Ahmad, S. (2009). Techniques for inducing accelerated corrosion of steel in concrete. *Arabian Journal for Science and Engineering*, 34(2), 95.

Alexander, M., Beushausen, H., & Otieno, M. (2012). Corrosion of Steel in reinforced concrete: Influence of binder type, water/binder ratio, cover and cracking. *CoMSIRU, University of Cape Town*.

- Alexander, M., & Mindess, S. (2005). *Aggregates in concrete* (1st ed.). Taylor & Francis.
- ASTM G1-90. (1999). *Standard Practice for preparing, cleaning and evaluating corrosion test specimens*. American Society for Testing and Materials.
- Austin, S. A., Lyons, R., & Ing, M. (2004). Electrochemical behavior of steel-reinforced concrete during accelerated corrosion testing. *Corrosion*, 60(2), 203–212.
- Ballim, Y., & Reid, J. (2003). Reinforcement corrosion and the deflection of RC beams—  
—an experimental critique of current test methods. *Cement and Concrete Composites*, 25(6), 625–632.
- El Maaddawy, T. A., & Soudki, K. A. (2003). Effectiveness of impressed current technique to simulate corrosion of steel reinforcement in concrete. *Journal of Materials in Civil Engineering*, 15(1), 41–47.
- EN 1992-1-1. (2004). Eurocode 2: Design of concrete structures—Part 1-1: General rules and rules for buildings. *European Committee for Standardization (CEN)*.
- Malumbela, G., Moyo, P., & Alexander, M. (2009). Behaviour of RC beams corroded under sustained service loads. *Construction and Building Materials*, 23(11), 3346–3351.
- SANS 1083. (2014). *Aggregates from natural sources—Aggregates for concrete*. South African Standard Code of practice.
- SANS 5861-3. (2006). *Making and curing of test specimens*. South African Standard Code of practice.
- SANS 5864. (2006). *Concrete tests—Flexural strength of hardened concrete*. South African Standard Code of practice.
- SANS 10100 -1. (2000). *The Structural Use of Concrete. Part 1: Design*. South African Standard Code of practice.

Theron, G. D. V. (1994). Effects of reinforcement corrosion on the structural performance of reinforced concrete beams. *MSc Dissertation, Department of Civil Engineering, University of Cape Town.*

## CHAPTER 4: RESULTS AND DISCUSSION

### 4.1 Introduction

This chapter presents the analysis and discussion of test results carried out on the reference and corroded beams. Tests performed during the experimental testing phase of this research include concrete compressive strength, accelerated corrosion tests, and flexural tests. After flexural tests, the load-carrying capacity of the corroded beams is compared with that of reference beams, then the reduction in the load-carrying capacity of corroded beams is analysed and discussed. As previously given in Chapter 3, the RC beam specimens labels are summarised in Table 4.1 for ease of reference.

**Table 4. 1: Presentation of RC beam specimens**

Beam Type	Guidelines used for splicing of flexural steel	Steel treatment	Specimen label range
A	SANS 10100-1	Corroded	SANS-NS-C B1 to SANS-NS-C B3
			SANS-S-C B1 to SANS-S-C B3
		Non-corroded	SANS-NS-NC B1 to SANS-NS-NC B3
			SANS-S-NC B1 to SANS-S-NC B3
B	Eurocode 2	Corroded	EC2-NS-C B1 to EC2-NS-C B3
			EC2-S-C B1 to EC2-S-C B3
		Non-corroded	EC2-NS-NC B1 to EC2-NS-NC B3
			EC2-S-NC B1 to EC2-S-NC B3

**Note:** S: Spliced; NS: Not spliced; C: Corroded; NC: Not corroded

### 4.2 General observations

#### 4.2.1 Corrosion induced cracking

During the accelerated corrosion tests, each RC beam was closely monitored on a regular basis. A longitudinal surface crack through the concrete cover on the ponding surface was first observed after 6 days, except in beam SANS-S-C B3 where the first visible crack only appeared after 18 days. Surface cracks were followed by the formation of two side cracks at the interface between tensile steel reinforcement and concrete cover. Rust stains were then observed on the ponded surface, followed by corrosion products exuding

through the surface crack. Once these corrosion products were on the concrete surface, it became difficult to monitor further development of cracks on the concrete surface ponded with NaCl solution.

Concrete cracking provided an easy passage for NaCl solution to reach the embedded steel reinforcement. Cracking also increased the ingress of chloride ions at the crack location. This cracking occurred along the line of the reinforcement in the NaCl pond and on both sides of the RC beams at the level of concrete cover.

The schematic diagram of RC beam specimens is given in Figure 4.1 and the visible damage due to corrosion in SANS 10100-1 and Eurocode 2 beams is presented in Figures 4.2 and 4.3.

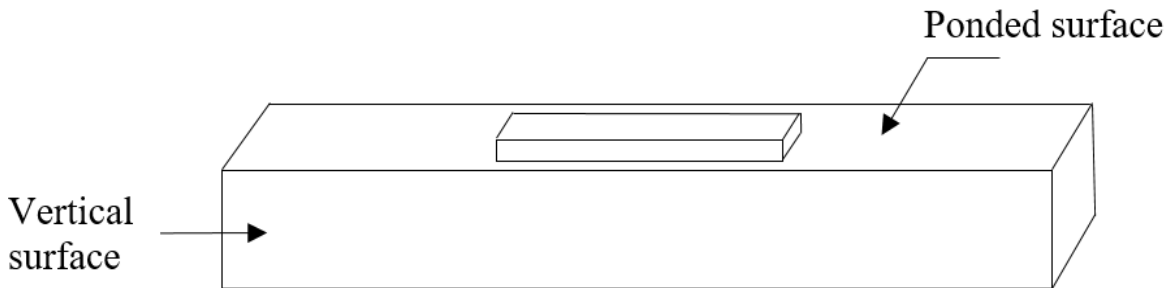


**Figure 4. 1: Schematic diagram of RC beam specimens**

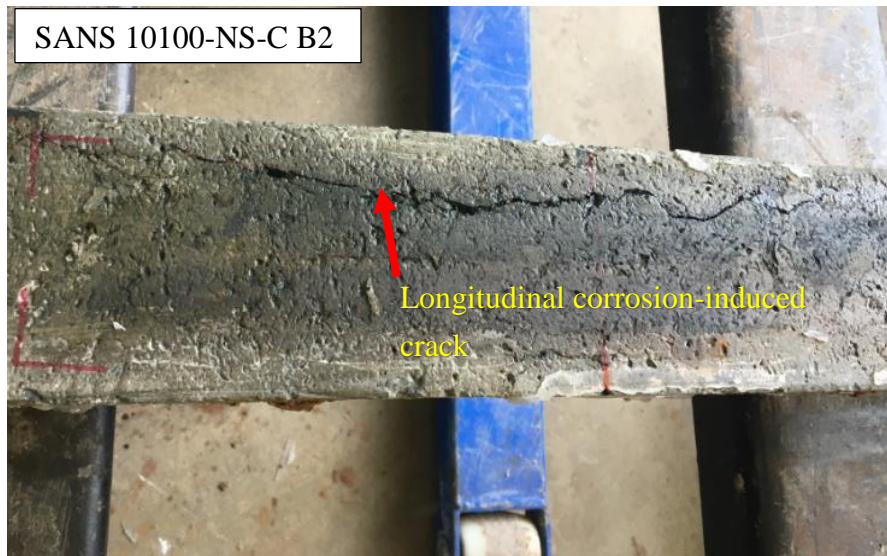


**Figure 4. 2: Cracking on the ponded surface**



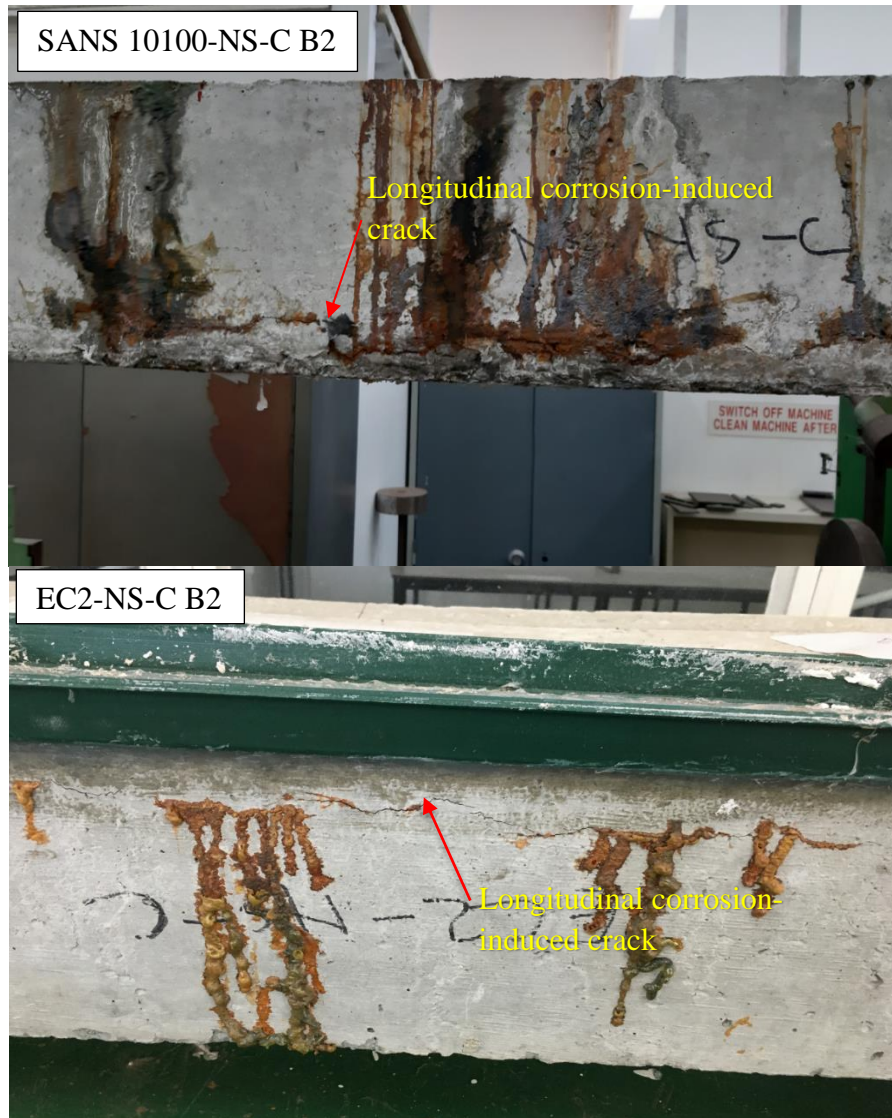


**Figure 4. 3: Cracking on the vertical side of beam**

As presented in Figures 4.2 and 4.3, the corrosion cracking in all corroded beams had similar patterns. Although no detailed analysis was carried out with respect to crack widths, the general observations were wider cracks on beams reinforced with Y10 bars and smaller cracks on beams reinforced with Y8 bars. This may be attributed to the greater surface area of steel of larger diameter bars compared to that of smaller diameter bars.

#### **4.2.2 Steel corrosion morphology**

The steel corrosion damage was generally spread along the corroded region with severe corrosion occurring in the direction of ingress of the NaCl solution (see Figure 4.4). In the case of lap-spliced bars, severe steel reinforcement corrosion occurred on steel bars closest to the concrete cover/ NaCl solution (see Figure 4.5).

The morphology of corrosion on steel reinforcement resembled a combination of general and some pitting corrosion. The occurrence of pitting corrosion can be attributed to the variation in concrete penetrability due to cracking. As presented in Figure 4.4, serious cross-section loss occurred in areas affected by pitting corrosion but varied across the corroded zone. The variation of cross-section loss may be attributed to the electrical resistivity of concrete which can reduce the amount of current reaching the steel bars in the case of higher resistivity.

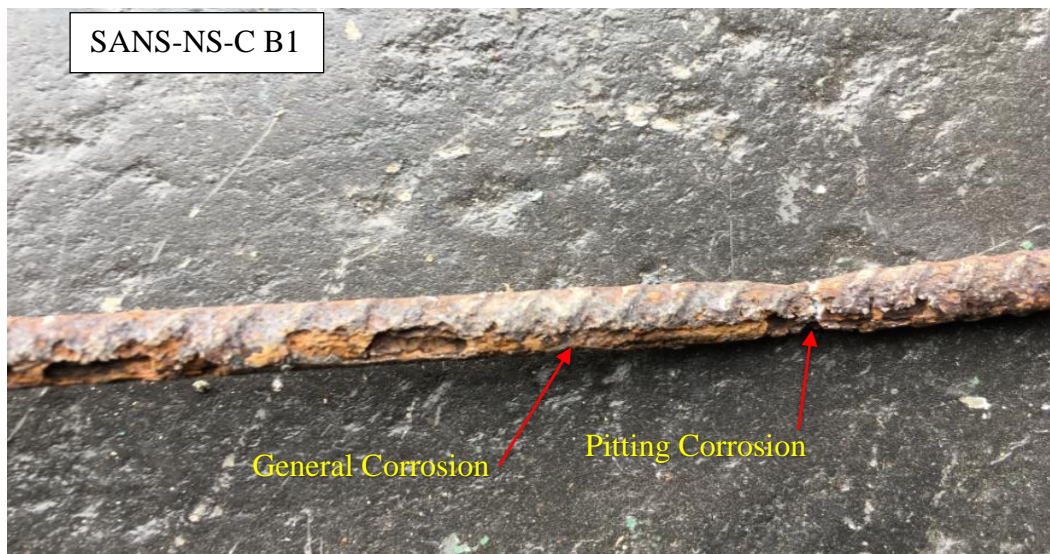


**Figure 4. 4: Corrosion distribution on non-lap steel bars**



**Figure 4. 5: Corrosion distribution on lap-spliced bars**

### 4.3 Determination of corrosion-inducing current

A constant voltage was used to apply current to embedded steel reinforcement. The voltage was induced across 100-Ohm resistors and the Agilent data logger was used to record the voltage across each resistor connected to the system. This was recorded at a 5-second interval.

The voltage and time readings recorded by the data logger were used to plot voltage versus time (V-T) curve, presented in Figure 4.6, with complete curves presented in Appendix C. A voltage variation can be noted in all voltage-time curves. This can be attributed to variation in concrete resistivity and penetrability which can result in lower current reaching embedded tensile steel bars.

The total area under the (V-T) curve was then calculated for determination of corrosion-inducing current by subdividing elements under the curve into trapezoidal segments and using the trapezoidal area method. The corrosion-inducing current was calculated using Ohm's Law previously presented in Chapter 3. The voltage logged per RC beam is presented graphically in Appendix C.

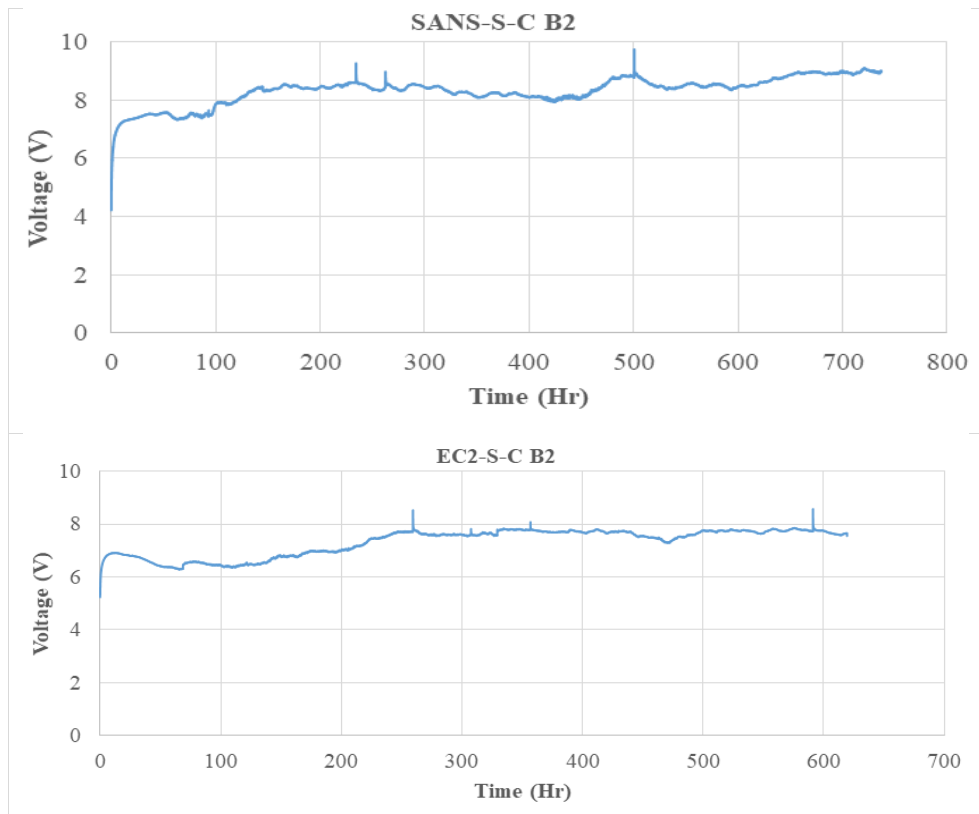


**Figure 4. 6: Voltage-Time curve for lap-spliced RC beams**

As previously discussed in Chapter 3, the theoretical steel diameter loss was estimated using Faraday’s Law. This was to ensure that the corrosion acceleration test is only terminated once steel bars were corroded to produce a level of corrosion as close as possible to the target corrosion.

#### 4.4 Compressive strength tests

The compressive strength test was carried out on an automatic compression machine at the loading rate of 0.25 MPa/s. The concrete cubes were tested for compressive strength after 7 and 28 days of curing. The results of compressive strength tests are presented in Figure 4.7 with detailed results presented in a table format in Appendix C. The 95% Confidence Interval (CI) indicate no overlapping of error bars for both 7 day and 28 compressive strength results, therefore the results are not scattered from one another.

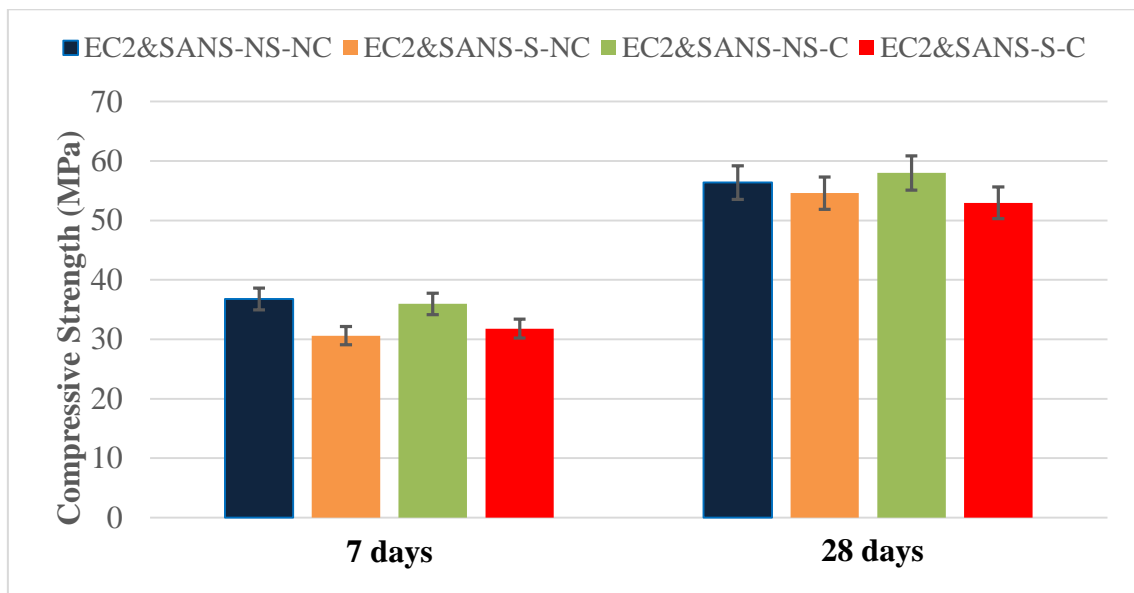


Figure 4. 7: Compressive Strength Test Results

#### 4.5 Flexural strength tests

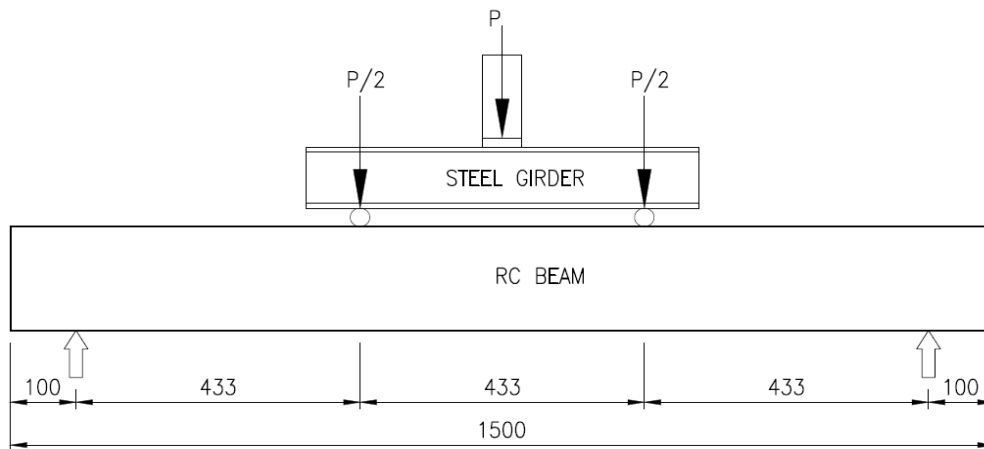
##### 4.5.1 Testing set-up

The reference beam specimens were tested 28 days after casting to determine their respective ultimate flexural strength while the corroded beams were tested once the desired corrosion level was reached. The beams were designed to fail in flexure, reinforced with longitudinal reinforcement and shear reinforcement near the supports. No



shear reinforcement was provided in the constant bending moment span. All beam specimens (corroded and non-corroded) were tested to failure in four-point bending using an Amsler testing machine. As previously discussed in Chapter 3, the reason for selecting this type of loading was to ensure that the middle span (between loading points) has a zero shear force, thus ensuring that the failure (flexure) desired in this research is achieved. A three-point bending test would have produced a shear force in the moment span, except at the point (center) of maximum bending moment.

The loading test arrangement is presented in Figure 4.8.



a) Schematic diagram (Dimensions in millimetres)



b) Laboratory loading test

**Figure 4. 8: Loading test arrangement**

#### 4.5.2 Load-midspan deflection behaviour of reference beams

As previously discussed in Chapter 3, test specimens consist of twelve (12) RC beams, of which six (6) of these beams were designed according to the requirements of South African standard code of practice SANS 10100-1 (2000) and the remaining six (6)

designed according to the requirements of the European standard code of practice (EN 1992-1-1, 2004).

During flexural tests, the load and mid-span deflection were recorded throughout the loading process until failure load was reached. Detailed information (see Table 4.2) such as yield and failure loads was recorded for each beam. The load-mid-span deflection curves are presented in Figure 4.9.

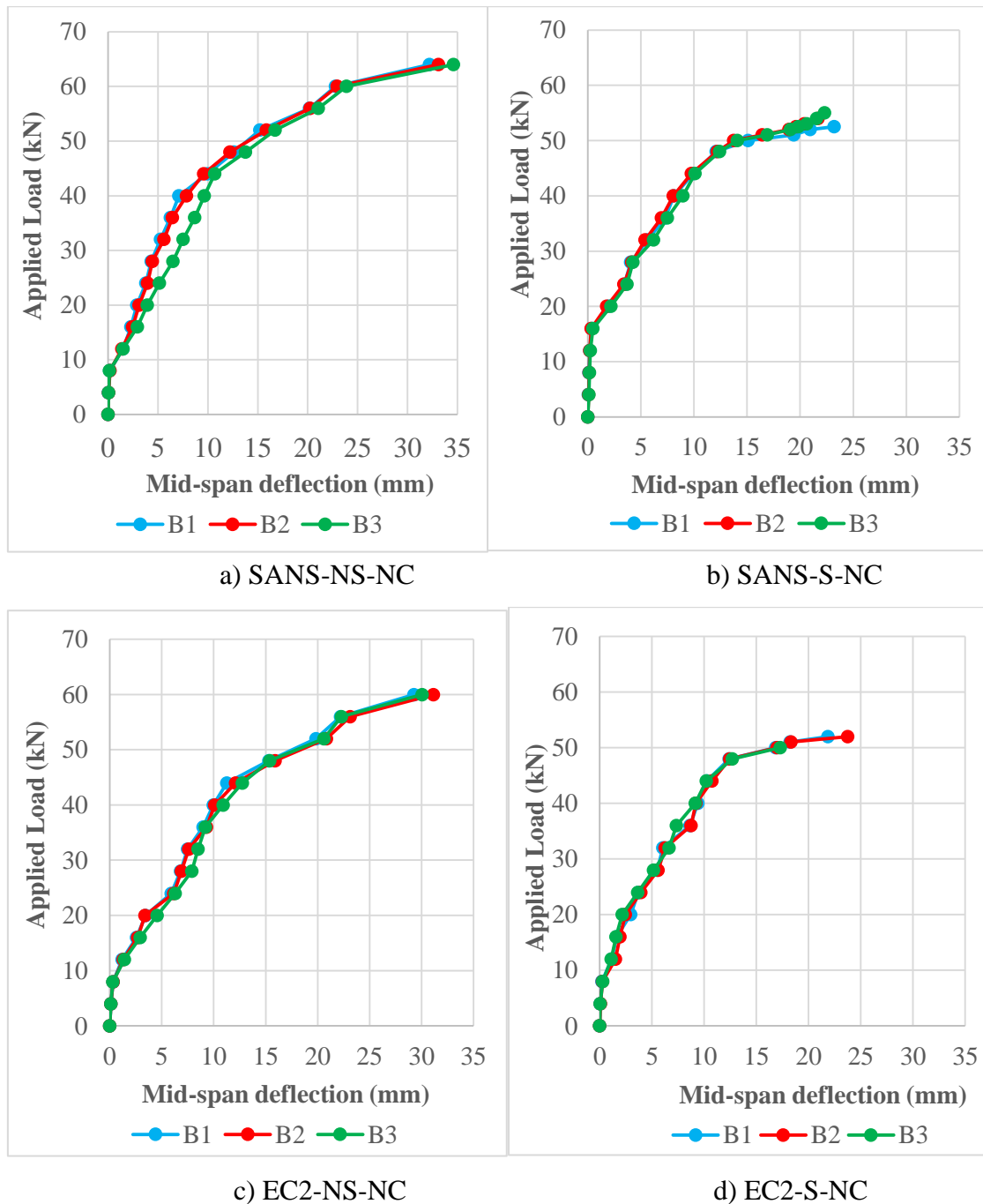


**Figure 4. 9: Load-midspan deflection curves of non-corroded beams**

**Table 4. 2: Applied loads vs mid-span deflections of non-corroded beams**

Non-corroded beams				
Beam Number	Applied Load at yield point (kN)	Deflection at yield point (mm)	Applied Load at failure (kN)	Deflection at failure (mm)
SANS-NS-NC B1	48.0	12.60	64.0	32.20
SANS-NS-NC B2	48.0	12.22	64.0	33.10
SANS-NS-NC B3	44.0	10.70	64.0	34.60
SANS-S-NC B1	50.0	15.10	52.5	23.20
SANS-S-NC B2	50.0	13.75	54.0	21.70
SANS-S-NC B3	50.0	14.10	55.0	22.30
EC2-NS-NC B1	44.0	11.26	60.0	29.26
EC2-NS-NC B2	44.0	12.10	60.0	31.15
EC2-NS-NC B3	44.0	12.75	60.0	30.05
EC2-S-NC B1	48.0	12.40	52.0	21.85
EC2-S-NC B2	48.0	12.44	52.0	23.75
EC2-S-NC B3	48.0	12.70	50.0	17.30

**a) SANS 10100-1 non-spliced beams**

As shown in the load-midspan deflection curves presented in Figure 4.9 (a) and Table 4.2, all three non-spliced reference beams represented a good ductile behaviour as they showed a good plastic behaviour after yield points, with an ample amount of load increase before the maximum failure loads were reached.

All non-spliced reference beams failed in flexure, with closely spaced flexural cracks, mainly located in the constant bending moment span. The typical cracking pattern of non-spliced RC beam specimens is represented in Figure 4.10.



**Figure 4. 10: Flexural crack pattern developed on SANS 10100-NS-NC beams**

### b) SANS 10100-1 lap-spliced beams

As shown in the load-midspan deflection curves presented in Figure 4.9 (b) and Table 4.2, the steel reinforcement on lap-spliced reference beams yielded at a load greater than that of non-spliced beams, however a decrease in flexural stiffness was observed in lap-spliced beams. As a result, the average failure load on lap-spliced beams was 16% less than that of non-spliced reference beams. Therefore these beams had less load carrying capacity compared to non-spliced control beams.

Flexural cracks on lap-spliced reference beams were observed to be fewer and spaced further apart compared to SANS non-spliced reference beams. There were two vertical cracks at both ends of lapped bars. When the failure load was reached, there was a slip of steel bars and development of a side longitudinal splitting crack within the spliced zone. The typical cracking pattern of lap-spliced RC beam specimens is represented in Figure 4.11.

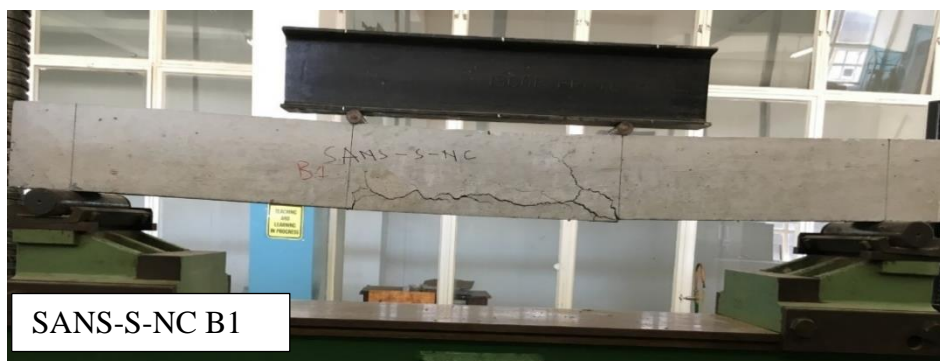


**Figure 4. 11: Cracking pattern developed on SANS 10100-S-NC beams**

### c) Eurocode 2 non-spliced beams

As shown in the load-midspan deflection curves presented in Figure 4.9 (c) and Table 4.2, all three Eurocode 2 non-spliced reference beams represented a good ductile behaviour as they showed a good plastic behaviour after yield points, with an ample amount of load increase before the maximum failure loads were reached. A similar behaviour was observed in SANS non-spliced beams.

Flexural cracks of Eurocode 2 non-spliced reference beams were observed to resemble those of SANS non-spliced reference beams. Typical cracking pattern of Eurocode 2 non-spliced reference beams is represented in Figure 4.12.





**Figure 4. 12: Flexural crack pattern developed on EC2-NS-NC beams**

#### **d) Eurocode 2 lap-spliced beams**

The behaviour of Eurocode 2 lap-spliced beams was observed to resemble that of SANS 10100-1 lap-spliced beams. As presented in Figure 4.9 (d) and Table 4.2, the failure load was 3.9% lower than that of SANS 10100-1 beams.

When the failure load was reached, there was a slip of steel bars and development of a side longitudinal splitting crack within the spliced zone. The cracking pattern (given in Figure 4.13) of Eurocode 2 lap-spliced beams was similar to that observed in SANS 10100-1 lap-spliced beams.



**Figure 4. 13: Flexural crack pattern developed on EC2-S-NC beams**

#### **4.5.3 Load-midspan deflection behaviour of corroded beams**

As previously discussed in the section (4.5.2) for reference beams, the corroded beams had the same design as control beams. The only difference, they were cast with 1.5 mm<sup>2</sup> insulated copper wire aimed to deliver voltage for corrosion acceleration of steel reinforcement.

The load-midspan deflection curves for all corroded beams are presented in Figure 4.14. The general observation was that an increase in degree of steel reinforcement corrosion results in excessive deflections and a reduction in the load-carrying capacity of RC beams. When the load-deflection results of corroded beams were compared with those of control beams, a reduction in stiffness was observed as applied loading and corresponding deflections of corroded RC beams were much less than those obtained in control beams. The cracking pattern of corroded beams resembled that of reference beams, with corroded beams having fewer and wider cracks.

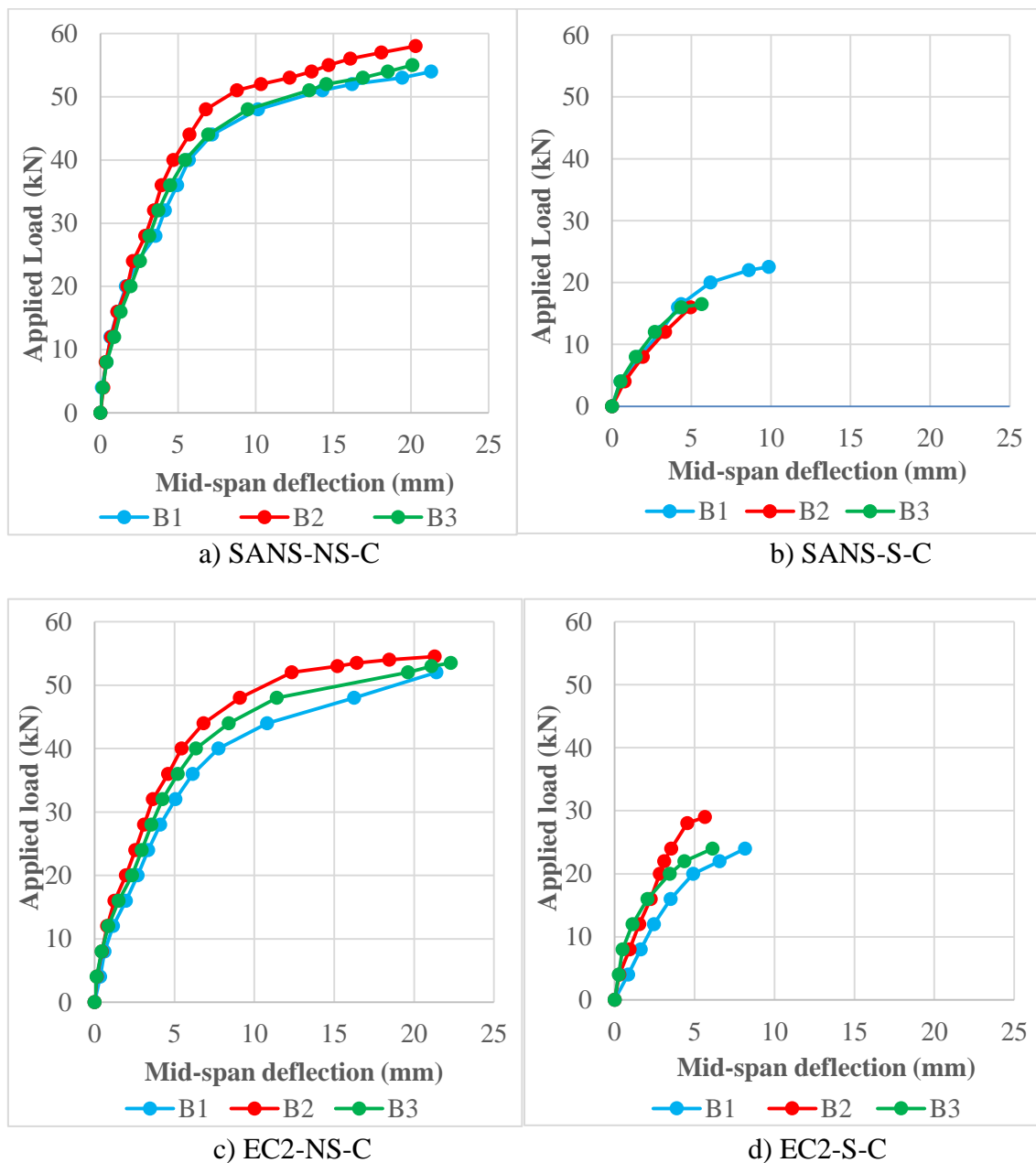


**Figure 4. 14: Load-midspan deflection curves of corroded beams**

**Table 4. 3: Applied loads vs mid-span deflections of corroded beams**

<b>Beam Number</b>	<b>Applied Load at estimated yield point (kN)</b>	<b>Deflection at estimated yield point (mm)</b>	<b>Applied Load at failure (kN)</b>	<b>Deflection at failure (mm)</b>
SANS-NS-C B1	48.0	10.15	54.0	21.30
SANS-NS-C B2	51.0	8.80	58.0	20.30
SANS-NS-C B3	48.0	9.50	55.0	20.10
SANS-S-C B1	20.0	6.20	22.5	9.85
SANS-S-C B2	16.0	4.95	16.0	4.95
SANS-S-C B3	16.0	4.35	16.5	5.64
EC2-NS-C B1	44.0	10.80	52.0	21.40
EC2-NS-C B2	52.0	12.35	54.5	21.30
EC2-NS-C B3	48.0	11.40	53.5	22.30
EC2-S-C B1	20.0	4.92	24.0	8.15
EC2-S-C B2	28.0	4.54	29.0	5.65
EC2-S-C B3	22.0	4.36	24.0	6.12

**a) SANS 10100-1 non-spliced beams**

As shown in the load-midspan deflection curves presented in Figure 4.14 (a) and Table 4.3, all three non-spliced corroded beams indicated a good ductile behaviour as they showed a plastic behaviour after yield points, with an ample amount of load increase before the maximum failure loads were reached.

When comparing load-midspan deflection results of SANS 10100-1 non-spliced corroded beams with SANS 10100-1 non-spliced reference beams, the failure load and corresponding midspan deflection of corroded RC beams was observed to be less than those obtained in reference beams. A reduction in failure load and midspan deflection was observed to be 13% and 38% respectively.

**b) SANS 10100-1 lap-spliced beams**

Figure 4.14 (b) and Table 4.3 shows the results of the load-midspan deflection curve for SANS 10100-1 lap-spliced corroded beams. When comparing load-midspan deflection results of lap-spliced corroded beams with lap-spliced reference beams, the failure of all three beams occurred suddenly and was reached immediately after the widening of the side longitudinal crack, followed by the spalling of concrete cover in the lapped zone and

slipping of longitudinal bars. A reduction in failure load and midspan deflection was observed to be 65% and 70% respectively.

#### **c) Eurocode 2 non-spliced beams**

As shown in the load-midspan deflection curves presented in Figure 4.14 (c) and Table 4.3, all three non-spliced corroded beams indicated a good ductile behaviour which was observed to resemble that of Eurocode 2 lap-spliced reference beams.

When comparing load-midspan deflection results of Eurocode 2 non-spliced corroded beams with Eurocode 2 non-spliced reference beams, a reduction in failure load and midspan deflection was observed to be 11% and 28% respectively.

#### **d) Eurocode 2 lap-spliced beams**

Figure 4.14 (d) and Table 4.3 shows the results of the load-midspan deflection curve for Eurocode 2 lap-spliced corroded beams. When comparing load-midspan deflection results of lap-spliced corroded beams with lap-spliced reference beams, the failure of all three corroded beams occurred suddenly and was reached immediately after the widening of the side longitudinal crack, followed by the spalling of concrete cover in the lapped zone and slipping of longitudinal bars.

A reduction in failure load and midspan deflection was observed to be 50% and 68% respectively. The Eurocode 2 lap-spliced corroded beams behaved in a similar manner as SANS 10100-1 lap-spliced corroded beams.

#### **4.5.4 Mode of failure**

The design failure mode of SANS 10100-1 beams is flexure as they were under-reinforced with longitudinal steel bars. Shear reinforcement was provided up-to a length of 300 mm from the supports by means of 6 mm diameter plain round mild steel bars at a spacing of 50 mm centres. The aim of providing shear reinforcement was to prevent shear failure. The description of the mode of failure observed in each RC beam is given in Table 4.4.

**Table 4. 4: Observed failure modes for each beam.**

<b>Beam</b>	<b>Description of failure mode</b>
SANS Reference beams (non-spliced)	<b>Ductile flexural failure.</b> During the flexural test, a number of vertical flexural cracks formed within the constant moment region. These cracks widened and grew vertically until the failure load was reached. There was no evidence of shear failure (see Figure 4.15 (a)).
SANS Reference beams (lap-spliced)	<b>Ductile flexural failure.</b> The failure was by a bond splitting failure between the concrete and steel bars. There was a longitudinal splitting crack between the two flexural cracks that appeared at the end of lap-spliced bars (see Figure 4.16 (a)).
EC2 Reference beams (non-spliced)	<b>Ductile flexural failure.</b> During the flexural test, a number of vertical flexural cracks formed within the constant moment region. These cracks widened and grew vertically until the failure load was reached. There was no evidence of shear failure (see Figure 4.15 (b)).
EC2 Reference beams (lap-spliced)	<b>Ductile flexural failure.</b> The failure was by a bond splitting failure between the concrete and steel bars. There was a longitudinal splitting crack between the two flexural cracks that appeared at the end of lap-spliced bars (see Figure 4.16 (b)).
SANS Corroded beams (non-spliced)	<b>Ductile flexural failure</b> with no evidence of shear failure. During the flexural test, there was a formation of flexural cracks and a widening of the longitudinal splitting crack through the whole concrete cover formed. The longitudinal crack had initially formed during corrosion acceleration. These cracks were within the constant moment region (see Figure 4.17 (a)).
SANS Corroded beams (lap-spliced)	<b>Brittle flexural failure</b> with evidence of bond splitting between the concrete and steel bars. The side corrosion-induced cracking cracks widened and grew until slipping of bars occurred at failure load. Four flexural cracks were observed at the lap-spliced zone (see Figure 4.17 (b)).
EC2 Corroded beams (non-spliced)	<b>Ductile flexural failure</b> with no evidence of shear failure. During the flexural test, a combination of flexural cracks with a horizontal

	splitting crack formed within the constant moment region. These cracks widened and grew until the failure load was reached (see Figure 4.18).
EC2 Corroded beams (lap-spliced)	<b>Brittle flexural failure</b> with evidence of bond splitting between the concrete and steel bars. The side corrosion-induced cracking cracks widened and grew until slipping of bars occurred at failure load. Four flexural cracks were observed at the lap-spliced zone (see Figure 4.19).

The typical failure modes observed in both control and corroded RC beams are given in Figure 4.15 to Figure 4.19.

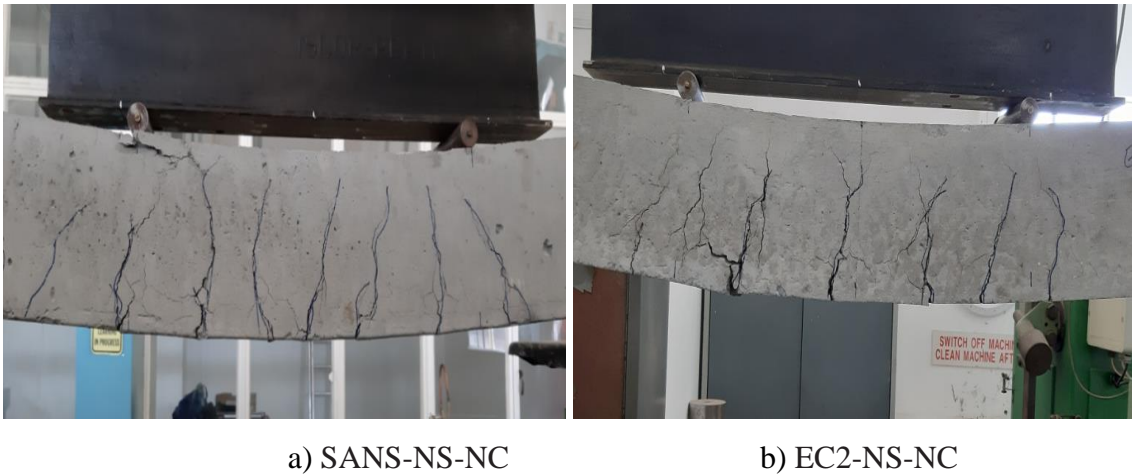


**Figure 4. 15: Flexural and splitting bond failure on non-spliced control beams**

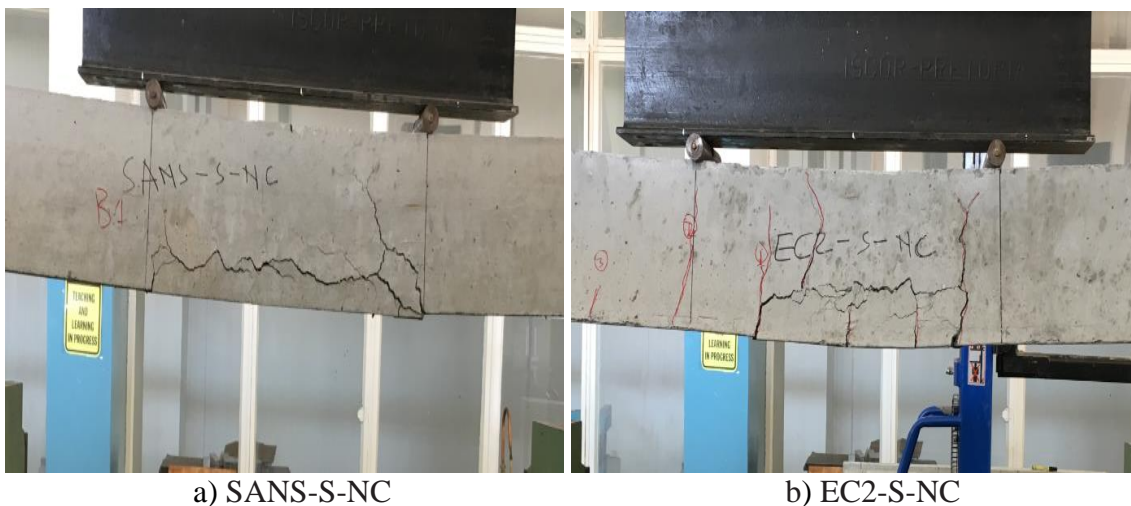


**Figure 4. 16: Flexural and splitting bond failure on lap-spliced control beams**



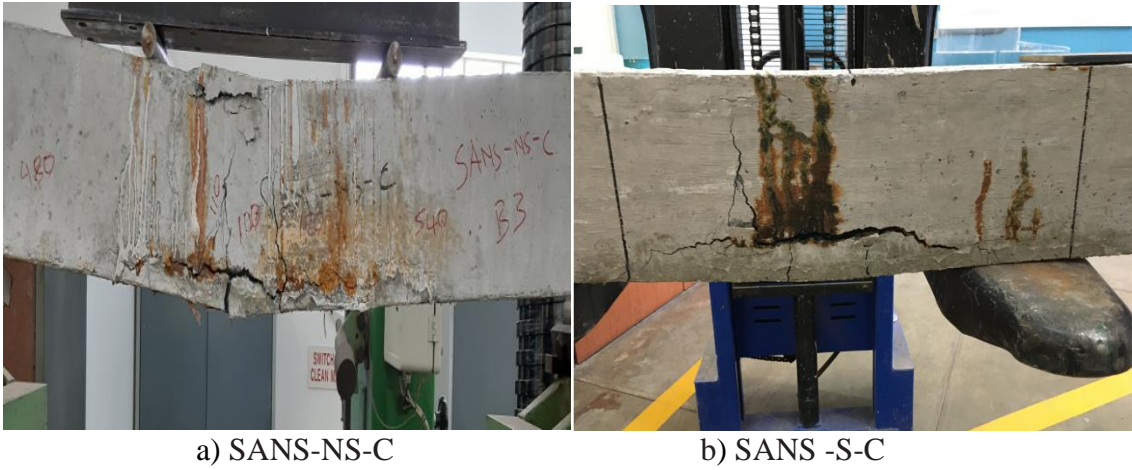


**Figure 4.17: Flexural and splitting bond failure on SANS non-spliced and lap-spliced beams**

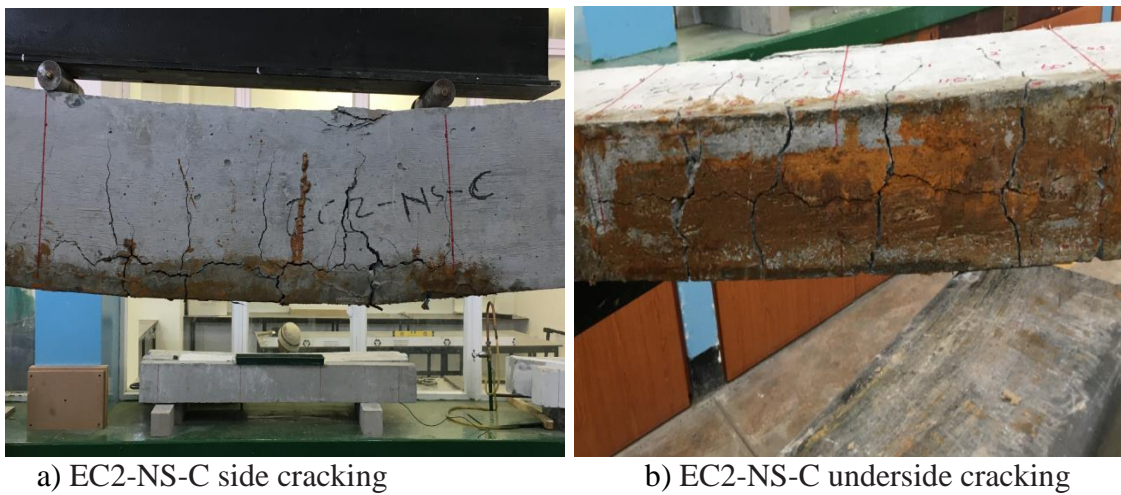


**Figure 4.18: Flexural and splitting bond failure on EC2 non-spliced corroded beams**

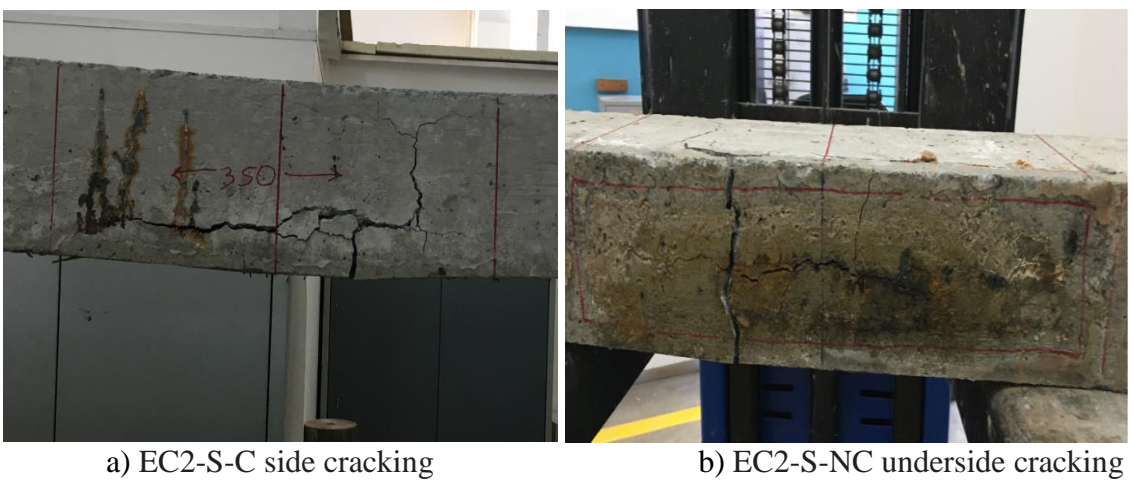


**Figure 4.19: Flexural and splitting bond failure on EC2 lap-spliced corroded beams**

For corroded beams, a combination of vertical flexural cracks and a longitudinal splitting crack through the whole concrete cover formed during flexural tests. This concrete splitting and sudden failure mode was a predominant type of failure for corroded RC beams containing lap-spliced bars.

#### **4.2.3 Determination of corrosion level / Actual degrees of corrosion**

After the completion of flexural tests, corroded beam specimens were split open and the steel bars carefully extracted from the beams. The bars were cleaned mechanically by lightly brushing using a steel wire brush and washed in tap water to remove the corrosion products and residues of concrete adhering to the surface of the steel bars.

After the removal of corrosion products and concrete residues, the steel bars were dried in the natural environment. Once dried, the extent of steel reinforcement corrosion was assessed. This can either be estimated using a formula derived from Faraday's equation in Chapter 3 or can be physically measured. In this study, the bar diameter loss was measured using a Vernier Caliper. The diameters of all corroded steel bars were measured along the length affected by corrosion and sections affected by pitting corrosion were considered for the purpose of calculating the percentage loss of steel diameter. The reason for considering these areas is that pitting corrosion is likely to result in severe steel cross-section loss than general corrosion, thus becoming the weakest point and leading to a great reduction of load-carrying capacity.

A general trend observed was a high degree of corrosion in the central bar, in the case of Eurocode 2 RC beams. The greater degree of corrosion in the centre bar can be attributed to the corrosion crack pattern which causes the corrosion agents to reach the centre bar much faster than the exterior bars (Malumbela *et al.*, 2010).

With regard to SANS specimens, the corrosion degree was almost the same for both steel bars. The average cross sectional loss of steel embedded in each RC beam specimen was used in the calculation of the total corrosion degree.

The corrosion degree results for SANS 10100-1 and Eurocode 2 beams are presented in Table 4.5.



**Table 4. 5: Corrosion degree in SANS 10100-1 and Eurocode 2 beams**

Element	Bar Number	Initial dia. (mm)	Final dia. (mm)	Cross sect. area loss (%)	Average corr. Degree (%)
SANS-NS-C B1	1	10	5.3	71.9	47.8
	2	10	8.74	23.6	
SANS-NS-C B2	1	10	9.22	15.0	14.6
	2	10	9.26	14.3	
SANS-NS-C B3	1	10	8.74	23.6	31.2
	2	10	7.82	38.8	
SANS-S-C B1	1	10	8.9	20.8	14.5
	2	10	8.71	24.1	
	3	10	9.42	11.3	
	4	10	9.9	2.0	
SANS-S-C B2	1	10	7.8	39.2	21.9
	2	10	8.56	26.7	
	3	10	9.76	4.7	
	4	10	9.12	16.8	
SANS-S-C B3	1	10	9.46	10.5	17.4
	2	10	9.18	15.7	
	3	10	8.84	21.9	
	4	10	8.86	21.5	
EC2-NS-C B1	1	8	7.20	19.0	37.7
	2	8	4.10	73.7	
	3	8	7.14	20.3	
EC2-NS-C B2	1	8	7.24	18.1	25.5
	2	8	6.90	25.6	
	3	8	6.56	32.8	
EC2-NS-C B3	1	8	6.44	35.2	34.5
	2	8	6.76	28.6	
	3	8	6.21	39.7	
EC2-S-C B1	1	8	6.78	28.2	27.9
	2	8	6.84	26.9	
	3	8	6.84	26.9	
	4	8	6.48	34.4	
	5	8	7.44	13.5	
	6	8	6.32	37.6	
EC2-S-C B2	1	8	6.90	25.6	27.0
	2	8	6.84	26.9	
	3	8	7.30	16.7	
	4	8	7.20	19.0	
	5	8	6.02	43.4	
	6	8	6.68	30.3	
EC2-S-C B3	1	8	6.48	34.4	29.0
	2	8	6.12	41.5	
	3	8	7.24	18.1	
	4	8	7.14	20.3	
	5	8	6.58	32.3	
	6	8	6.82	27.3	

#### 4.5.5 Effect of degree of corrosion on flexural capacity of RC beams

Although the current was applied such that the same degree of corrosion was expected to be produced on all beam specimens, this was not the case in this study as the steel diameter loss was not the same (see Table 8). The varied steel diameter loss can be attributed to variation in penetrability due to cracking and concrete resistivity. All corroded beam specimens were compared with reference beams to determine the effect of corrosion on the flexural capacity of beams. The reference beams were tested at 28 days while the corroded beams were tested after the desired corrosion current was passed.

Generally, all corroded beams were observed to have less flexural capacity compared to reference beams (see Figure 4.20). This was attributed to the increase in steel reinforcement corrosion that resulted in the loss of a bond between steel reinforcement and surrounding concrete. Detailed results analysis is presented in Table 4.6 to 4.9.

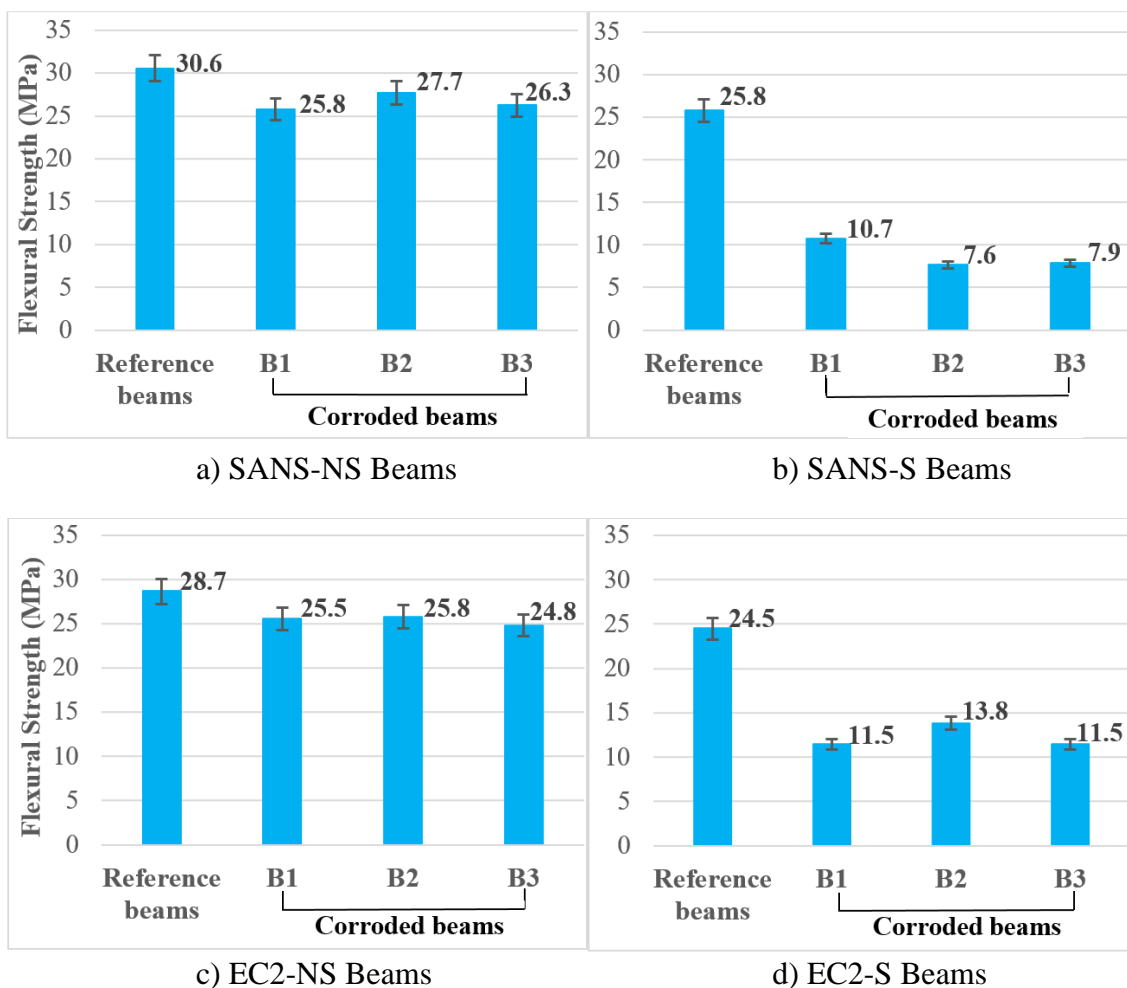


**Figure 4. 20: Flexural Strength results for SANS 10100-1 and Eurocode 2 beams**

**a) SANS 10100-1 Beams**

The effect of corrosion on the flexural capacity of non-spliced beams obtained for each corroded beam is given in Table 4.6. As expected, the corroded RC beams when compared to flexural test results obtained in reference beams were found to have a reduced load-carrying capacity.

**Table 4. 6: Corrosion and flexure capacity of SANS-NS-C beams**

<b>Beam</b>	<b>Steel cross-sectional area loss (%)</b>	<b>Failure Load (kN)</b>	<b>Reduction in flexural capacity (%)</b>
Reference beams	Not Applicable	64.0	Not Applicable
B1	47.8	54.0	15.6
B2	14.6	58.0	9.4
B3	31.2	55.0	14.1

The results for lap-spliced beams are given in Table 4.7. The reduction in steel cross-sectional area in lap-spliced beams was less than that obtained in non-spliced beams, but lap-spliced beams reached a much lower moment capacity than that of corroded non-spliced beams. The behaviour of corroded beams was different from that of the reference beams as there were no warnings before failure load was reached, the type of failure was sudden and a brittle bond failure was displayed. This behaviour may be attributed to the loss of bond between the concrete and steel reinforcement which led to a drop in anchorage capacity at the splice zone and thus, slipping of steel reinforcement. When the entire concrete cover was removed in the corroded region, the slippage of steel reinforcement was measured to range between 3 to 8 mm.

**Table 4. 7: Corrosion and flexure capacity of SANS-S-C beams**

<b>Beam</b>	<b>Steel cross-sectional area loss (%)</b>	<b>Failure Load (kN)</b>	<b>Reduction in flexural capacity (%)</b>
Reference beams	Not Applicable	53.8	Not Applicable
B1	14.5	22.5	58.2
B2	21.9	16.0	70.3
B3	17.4	16.5	69.3

### b) Eurocode 2 Beams

The effect of corrosion on the flexural capacity of non-spliced beams obtained for each corroded beam is given in Table 4.8. The corroded RC beams, when compared to flexural test results obtained in reference beams, were found to have a reduced load-carrying capacity. The Eurocode 2 non-spliced beams behaved in a similar manner as the SANS 10100-1 non-spliced beams, but attained less load carrying capacity.

**Table 4. 8: Corrosion and flexure capacity of EC2-NS-C beams**

<b>Beam</b>	<b>Steel cross-sectional area loss (%)</b>	<b>Failure Load (kN)</b>	<b>Reduction in flexural capacity (%)</b>
Reference beams	Not Applicable	60.0	Not Applicable
B1	37.7	52.0	13.3
B2	25.5	54.5	9.2
B3	34.5	53.5	10.8

The results for lap-spliced beams are given in Table 4.9. The reduction in steel cross-sectional area in lap-spliced beams was less than that obtained in non-spliced beams, but lap-spliced beams reached a much lower moment capacity than that of corroded non-spliced beams. These beams (lap-spliced) behaved in a similar manner as the SANS corroded lap-spliced beams as they provided no warnings before failure load was reached, the type of failure was sudden and a brittle failure was displayed. The reason for this could be attributed to the loss of bond between the concrete and steel reinforcement which led to a drop in anchorage capacity at the splice zone and thus, slipping of steel reinforcement. The steel slipping was measured to range between 2 and 7 mm.

**Table 4. 9: Corrosion and flexure capacity of EC2-S-C beams**

<b>Beam</b>	<b>Steel cross-sectional area loss (%)</b>	<b>Failure Load (kN)</b>	<b>Reduction in flexural capacity (%)</b>
Reference beams	Not Applicable	51.3	Not Applicable
B1	27.9	24.0	53.2
B2	27.0	29.0	43.5
B3	29.0	24.0	53.2

#### 4.5.6 Effect of corrosion on ductility of RC beams

Ductility is defined as the ability of a material or structure to sustain post elastic deformations (inelastic deformations) without significant loss of resistance capacity (Theron, 1994).

In this study, control beams exhibited a ductile flexural failure mechanism. The yielding of steel reinforcement and excessive mid-span deflections measured in these beams demonstrated high ductility

Equation 4.1 was used to determine the ductility factors of both non-corroded beams and corroded beams. This equation has been well documented in the literature (Theron, 1994).

$$u = \frac{df}{dy} \quad (4.1)$$

where:

u is the ductility factor;

df is the measured mid-span deflection at failure;

dy is the measured mid-span deflection at yielding.

The sample results of ductility factors are given in Figure 4.21. The full results showing the effect of corrosion are provided in Appendix C.

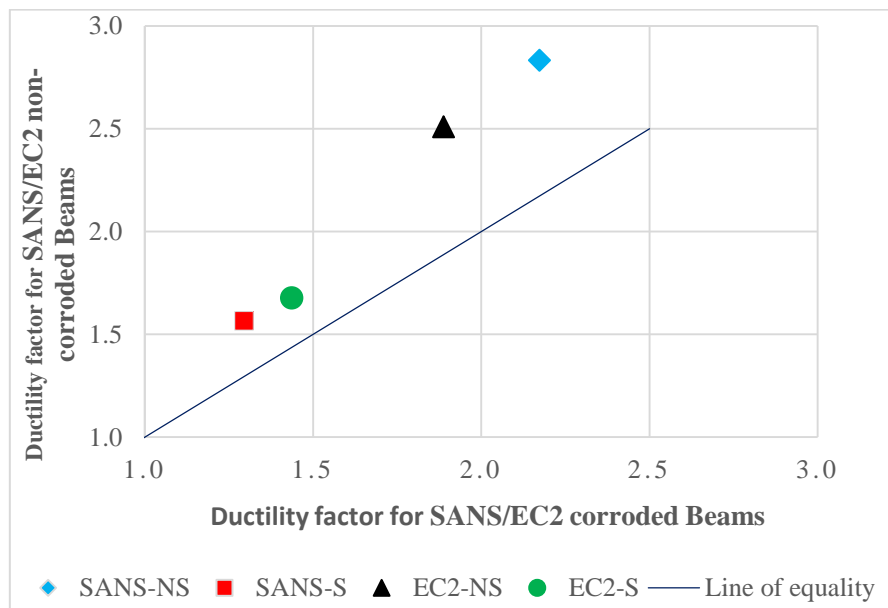


**Figure 4. 21: Mid-span deflection ductility factors for SANS 10100-NS beams**

Figure 4.21 shows a scatter plot graph of mid-span deflection ductility factors for non-corroded beams and corroded beams. The reference line of equality represents the points on the graph where the ductility of corroded beams is equal to that of non-corroded beams. As shown in Figure 4.21, all data points are scattered above the line of equality. This indicates that the mid-span deflection ductility factors for non-corroded beams were greater than those of corroded beams. Therefore the corroded beams are less ductile than non-corroded beams. This can be attributed to the deterioration of steel ribs in the corroded zone which resulted in a reduction of the steel surface area and loss of steel cross-sectional area, thus reducing the bond at the concrete-steel interface.

All lap-spliced beams, when compared to non-corroded lap-spliced beams indicated no ductile response. The lap-spliced beams failed at the loading that is much less than that applied in non-lap-spliced beams. The ductile failure observed in non-corroded beams was replaced by brittle failure.

#### **4.5.7 General findings and comparison of SANS 10100-1 and Eurocode 2 on the performance of lap-spliced RC beams**

All RC beams experienced some variation between target and actual corrosion. As previously discussed, this can be attributed to the variation in concrete resistivity and penetrability due to cracking. For the purpose of this study, the actual bar diameter loss was used to determine the effect of corrosion on flexural capacity. When corroded beams were tested to determine their flexural capacity, they all failed in flexure with signs of bond failure but no evidence of shear failure. The bond failure was observed through the splitting horizontal crack that occurred between the concrete cover and steel bars on the side of the beams. The splitting crack had initially formed during corrosion acceleration tests.

As previously discussed in section 4.2.1, corrosion cracking was observed to be more severe in beams designed according to SANS 10100-1 than in beams designed according to Eurocode 2. This is due to the greater surface area of steel on beams reinforced with larger diameter bars. As a result, the accumulation of corrosion products at the concrete-steel interface led to wider cracks.

As shown in Tables 4.7 to 4.10, there was a severe reduction in flexural capacity in RC beams designed according to SANS 10100-1 than in beams designed according to Eurocode 2 even though the SANS 10100-1 beams experienced lower degrees of steel corrosion than Eurocode 2 beams. The test results of SANS 10100-1 non-spliced beams, indicated a reduction in flexural capacity of up to 16%, while in Eurocode 2 beams the reduction was up to 13%. In the case of lap-spliced beams, the flexural test results of SANS 10100-1 beams indicated a reduction in flexural capacity of up to 70%, while in Eurocode 2 beams the reduction in flexural capacity was up to 53%.

RC beams with no steel lapping were observed to have a larger load carrying capacity than RC beams containing lap-spliced bars. This is despite the higher steel cross-sectional area loss experienced by beams containing steel with no lapping. This may be attributed to steel reinforcement corrosion in anchorage zone of lap-spliced beams which result in bond reduction at concrete-steel interface, while non-spliced steel reinforcement is anchored at the supports where there was no corrosion, thus no reduction of the bond strength.

It is evident from the results presented previously in Tables 4.7 to 4.10 that SANS 10100-1 corroded beams had a severe reduction in flexural capacity when compared to non-corroded beams, however, the corroded non-lapped beams carried larger loads and attained smaller mid-span deflections when compared to Eurocode 2 beams. Therefore the design of non-lapped beams using SANS 10100-1 was observed to be much more conservative than that of Eurocode 2. This may be attributed to different design values of material characteristic strength recommended by the two standards. The SANS design code accept a value of 87% of material characteristic strength, while the Eurocode 2 accept a higher design value at 100% of the characteristic material strength. It can also be noted that partial load factors used by South African loading code and European loading code are different.

#### **4.6 Comparison with results from other researcher's**

There is very limited literature on flexural strength of corroded lap-spliced bars. The available studies to the author's knowledge on flexural members (beams and slabs)

containing non-spliced steel bars. Given this, the results from this study were compared with the previous work based on non-spliced steel reinforcement.

Previous studies conducted by several researchers (Al-Sulaimani *et al.* 1990; Cabrera & Ghoddoussi, 1992; Castel *et al.* 2000a and 2000b and Kearsley & Joyce 2014) to investigate the effect of steel reinforcement corrosion on flexural strength were selected to compare results obtained in this study.

After conducting flexural tests, the authors reported that the increase in corrosion of steel reinforcement results in mid-span deflection increase, thus reducing the stiffness of the structure and load-carrying capacity. They also reported that the load-carrying capacity of RC beams is affected by a bond reduction in the steel-concrete interface due to steel reinforcement corrosion.

The experimental results obtained in this study showed trends similar to those observed in the previous studies mentioned above, where increase in the degree of steel reinforcement corrosion or reduction in steel cross-sectional area results in mid-span deflection increase, thus reducing the stiffness of the structure and load-carrying capacity.

#### **4.7 General discussion of results**

This study aimed to investigate the effect of corrosion of spliced steel reinforcement on the flexural performance of reinforced concrete beams. Flexural test results of corroded RC beams containing lap-splice were used and compared with corroded RC beams containing no steel lapping. The summary of results obtained during experiments for SANS 10100-1 beams and Eurocode 2 beams are presented in Tables 4.10 and 4.11 respectively.



**Table 4. 10: Summary of flexural test results for SANS 10100-1 beams**

<b>Beam</b>	<b>Degree of Corrosion (%)</b>	<b>Ultimate Flexural Strength (MPa)</b>	<b>Max. mid-span deflection (mm)</b>	<b>Ductility Factor</b>	<b>Failure Mode</b>
SANS-NS-NC B1	0	30.56	2.56	2.56	Ductile flexural failure
SANS-NS-NC B2	0	30.56	2.71	2.71	Ductile flexural failure
SANS-NS-NC B3	0	30.56	3.23	3.23	Ductile flexural failure
SANS-S-NC B1	0	25.31	1.58	1.54	Ductile flexural failure
SANS-S-NC B2	0	25.79	1.58	1.58	Ductile flexural failure
SANS-S-NC B3	0	26.26	1.58	1.58	Ductile flexural failure
SANS-NS-C B1	47.8	25.79	21.30	2.10	Ductile flexural failure
SANS-NS-C B2	14.6	27.70	20.30	2.31	Ductile flexural failure
SANS-NS-C B3	31.2	26.26	20.10	2.12	Ductile flexural failure
SANS-S-C B1	14.5	10.74	9.85	1.59	Brittle flexural failure
SANS-S-C B2	21.9	7.64	4.95	1.00	Brittle flexural failure
SANS-S-C B3	17.4	24.83	5.64	1.30	Brittle flexural failure

**Table 4. 11: Summary of flexural test results for Eurocode 2 beams**

<b>Beam</b>	<b>Degree of Corrosion (%)</b>	<b>Ultimate Flexural Strength (MPa)</b>	<b>Max. mid-span deflection (mm)</b>	<b>Ductility Factor</b>	<b>Failure Mode</b>
EC2-NS-NC B1	0	28.65	2.60	2.60	Ductile flexural failure
EC2-NS-NC B2	0	28.65	2.57	2.57	Ductile flexural failure
EC2-NS-NC B3	0	28.65	2.36	2.36	Ductile flexural failure
EC2-S-NC B1	0	24.83	1.76	1.76	Ductile flexural failure
EC2-S-NC B2	0	24.83	1.91	1.91	Ductile flexural failure
EC2-S-NC B3	0	23.88	1.36	1.36	Ductile flexural failure
EC2-NS-C B1	37.7	25.55	21.40	1.98	Ductile flexural failure
EC2-NS-C B2	25.5	25.79	21.30	1.72	Ductile flexural failure
EC2-NS-C B3	34.5	24.83	22.30	1.96	Ductile flexural failure
EC2-S-C B1	27.9	11.46	8.15	1.66	Brittle flexural failure
EC2-S-C B2	27.0	13.85	5.65	1.24	Brittle flexural failure
EC2-S-C B3	29.0	11.46	6.12	1.40	Brittle flexural failure

A great reduction in flexural capacity was observed in both beam types designed according to the requirements of South African standard code of practice SANS 10100-1 (2000) and European standard code of practice (EN 1992-1-1, 2004).

When comparing results obtained in reference beams with results obtained in corroded beams, the consequences of steel reinforcement corrosion (i.e. reduction of steel cross-sectional area, bond loss at the steel-concrete interface and longitudinal cracking a steel-cover interface) resulted in a significant reduction of RC beam stiffness and thereby reducing the load-carrying capacity of the structure. The general trend of decreasing load carrying capacity and increasing deflections with increasing amounts of corrosion is expected and has been reported in literature by various researchers such as Al-Sulaimani *et al.*, (1990); Cabrera & Ghoddoussi, (1992); Castel *et al.*, (2000a and 2000b) and Kearsley & Joyce (2014).

The mid-span deflections in corroded beams during flexural tests were observed to be much larger than those carried by reference beams at the same loading. This behaviour can be attributed to reduced steel cross-sectional area due to corrosion, and also to the reduced bond between concrete and steel reinforcement.

The mid-span deflection ductility in corroded beams containing lap-spliced steel reinforcement was significantly reduced, as a result the failure of these beams changed from ductile response (observed in reference beams) to brittle response.

#### **4.8 References**

Al-Sulaimani, G., Kaleemullah, M., & Basunbul, I. (1990). Influence of corrosion and cracking on bond behavior and strength of reinforced concrete members. *Structural Journal*, 87(2), 220–231.

Cabrera, J., & Ghoddoussi, P. (1992). *The effect of reinforcement corrosion on the strength of the steel/concrete bond*. 10.

Castel, A., François, R., & Arliguie, G. (2000). Mechanical behaviour of corroded reinforced concrete beams—Part 2: Bond and notch effects. *Materials and Structures*, 33(9), 545.

EN 1992-1-1. (2004). Eurocode 2: Design of concrete structures—Part 1-1: General rules and rules for buildings. *European Committee for Standardization (CEN)*.

Kearsley, E. P., & Joyce, A. (2014). Effect of corrosion products on bond strength and flexural behaviour of reinforced concrete slabs. *Journal of the South African Institution of Civil Engineering*, 56(2), 21–29.

Malumbela, G., Alexander, M., & Moyo, P. (2010). Variation of steel loss and its effect on the ultimate flexural capacity of RC beams corroded and repaired under load. *Construction and Building Materials*, 24(6), 1051–1059.

SANS 10100 -1. (2000). *The Structural Use of Concrete. Part 1: Design*. South African Standard Code of practice.

Theron, G. D. V. (1994). Effects of reinforcement corrosion on the structural performance of reinforced concrete beams. *MSc Dissertation, Department of Civil Engineering, University of Cape Town*.

## **CHAPTER 5: CONCLUSIONS AND RECOMMENDATIONS**

### **5.1 Introduction**

This chapter presents the conclusions on findings presented in Chapter 4, as well as providing recommendations for future studies. This study aimed to investigate the effect of corrosion on the flexural strength of reinforced concrete (RC) beams with steel lap-splicing in the central constant moment region.

A total of twenty-four RC beams were designed and cast based on the SANS10100-1 and Eurocode 2 structural design codes. Out of the twenty-four RC beams, twelve RC beams were cast for each design code (six with lap-splicing and six without spliced flexural reinforcement). The RC beams were 1500 mm in length with a rectangular cross-section of 100 mm in width and 165 mm in depth. The steel reinforcement corrosion was induced in the central constant moment region using a 5% solution of NaCl and an impressed current technique. Only six RC beams were corroded for each design code, the remaining six beams were used for reference purposes. All beams were tested for ultimate strength using a four-point bending configuration. The applied load and mid-span deflection were recorded until the ultimate failure load was reached. The following conclusions were drawn from the observations and analysis of test results:

### **5.2 Conclusions**

Based on the findings presented in Chapter 4, the conclusions from this study are presented in the following sections.

#### **5.2.1 Influence of corrosion of lap-spliced steel on the flexural performance of RC beams**

All beams with corroded steel reinforcement showed a reduction in flexural capacity as summarized in Table 5.1. The general trend observed was a greater flexural capacity on non-lap spliced beams than that of lap spliced beams. The flexural behaviour of SANS 10100-1 lap-spliced beams was observed to be similar to that of Eurocode 2, as the failure of all lap-spliced beams occurred suddenly and was reached immediately after the widening of the side longitudinal crack, followed by the spalling of concrete cover in the

lapped zone and slipping of longitudinal bars. As previously mentioned in chapter 4, measurements were taken after removal of the entire concrete cover in the corroded region to check the extent of bar slip. The slippage of steel reinforcement was measured to range between 3 to 8 mm on SANS 10100-1 beams. While on Eurocode 2 beams, steel slippage was ranging between 2 and 7 mm. The slipping of longitudinal steel bars was attributed to steel reinforcement corrosion which resulted in bond degradation at concrete-steel interface and reduction of anchorage capacity at the splice zone.

**Table 5. 1: Reduction in flexural capacity due to corrosion**

<b>Beam Types</b>	<b>Design code</b>	<b>Reduction in flexural capacity (%)</b>	<b>Loss in steel cross-sectional area (%)</b>
Non-spliced corroded beams	SANS 10100-1	9 – 16	15 – 48
	Eurocode 2	9 – 13	26 – 38
Lap-spliced beams	SANS 10100-1	58 – 70	15 – 22
	Eurocode 2	44 – 53	27 – 29

### 5.2.2 Flexural ductility of steel corrosion-damaged RC beams

The mid-span deflection was considered as an important parameter to analyse the ductility of corroded beams. During flexural tests, mid-span deflection was recorded at the yield load and failure load to determine the ductility to evaluate the impact of steel reinforcement corrosion.

When both non-lap spliced and lap-spliced corroded beams were compared with reference beams, the trend of the results indicated a reduction in stiffness on all lap-spliced corroded beams with increasing mid-span deflections at a loading less than that applied on reference beams. This is despite the lower corrosion rate on lap-spliced beams compared to non-lap spliced beams.

The general trend was a reduction of flexural ductility of corroded beams with increasing steel cross-sectional loss. It was noted that non-lap spliced beams carried more load after yielding of steel reinforcement before the failure load was reached, while lap-spliced beams failed immediately after yielding of steel reinforcement.

### **5.2.3 Failure mode of steel corrosion-damaged RC beams**

Different structural behaviour of RC beams was observed during flexural tests. The failure mode of corroded non-spliced beams for both SANS 10100-1 and Eurocode 2 remained a ductile flexural failure, but the plastic behaviour after yielding of steel reinforcement was reduced compared to observations made on non-lapped spliced reference beams. For lap-spliced beams, the steel reinforcement corrosion changed the failure mode from ductile to brittle flexural failure.

The non-lap spliced beams failed due to crushing of concrete in the compression zone, followed immediately by a failure of longitudinal steel reinforcement in the tension zone. While the lap-spliced beams failed without crushing of concrete in the compression zone. The failure on lap-spliced beams occurred suddenly and was reached immediately after the widening of the side longitudinal crack within the lap-splice region.

### **5.2.4 Practical implications of the study findings**

The results from this study found that the corrosion of steel reinforcement has a major effect on the flexural strength of RC beams. The general trend observed was the reduction of flexural capacity of corroded RC beams with increasing mid-span deflection. The effect of steel reinforcement corrosion was observed to be even more critical in beams reinforced with lap-spliced steel as they indicated a great reduction in the ductility, with failure of lap-spliced beams changing from ductile to a brittle flexural mode. The steel reinforcement corrosion in RC beams reinforced with lap-spliced steel raises a serious concern about the safety and reliability of RC structures situated in aggressive environments, as the brittle failure mode might result in a sudden collapse without any significant warnings.

Generally, the flexural behaviour of beams designed according to the two standards (SANS 10100-1 and Eurocode 2) was observed to be similar, with non-lap spliced beams showing a greater flexural capacity than lap spliced beams despite the high corrosion degree on non-lap spliced beams. When non-lap spliced corroded SANS 10100-1 beams were compared with the non-lap spliced corroded Eurocode 2 beams, it was SANS 10100-1 beams that showed a higher load-carrying capacity. The failure loads of SANS 10100-

1 non-spliced corroded beams were about 5% higher than those of Eurocode 2 beams. While on the comparison of lap-spliced corroded beams, it was Eurocode 2 beams that provided a higher load-carrying capacity than SANS 10100-1 beams. The failure loads of Eurocode 2 lap-spliced corroded beams were about 29% higher than those of SANS 10100-1 beams.

It should be pointed out that that lap-spliced beams used in this study contained no transverse steel reinforcement in the splice zone. Transverse steel reinforcement should be provided in the spliced region to provide some confinement to lap-spliced bars, improve flexural ductility of RC beams and minimise bond degradation at the concrete-steel interface.

During the analysis and design of RC beams, it was observed that Eurocode 2 recommends a higher characteristic strength of steel than SANS 10100-1, as a result, a more economic design was achieved due to the less amount of tension reinforcement obtained on Eurocode 2 design. Despite the higher steel cross-sectional area loss experienced by Eurocode 2 lap-spliced beams, compared to SANS 10100-1 lap-spliced beams. Eurocode 2 lap-spliced beams produced an improved ductility compared to SANS 10100-1 design. However, the failure mode remained brittle.

The outcome of this study will enable structural designers to take into consideration the above factors when designing RC flexural members exposed to the chloride environment, as a brittle failure should be avoided. RC members should be designed to undergo large deflections that can provide warning of failure and prevent a total collapse of the structure.

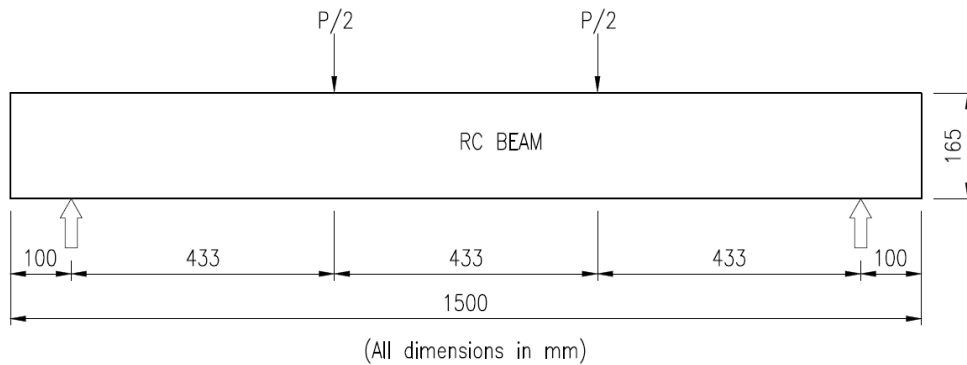
### **5.3 Recommendations for future studies**

Based on the findings of this study, the following topics are recommended for future studies:

1. The influence of the amount of transverse reinforcement in the spliced region on flexural ductility of RC beams.
2. A combined effect on shear and tensile steel reinforcement corroded under loading.
3. The effect of steel cross-sectional area loss on the yield strength of the corroded steel bars.

## APPENDIX A: SPECIMEN DESIGN

### A.1 SANS 10100-1 design



#### DIMENSIONS

Span (l)	=	1.3	m
Width (b)	=	0.1	m
Depth (D)	=	0.165	m

#### Loading

Live load	=	21	kN
Dead load	=	Beam self weight	
Self weight (w)	=	$24 \times \text{width} \times \text{depth}$	
Self weight (w)	=	0.396	kN/m

#### Ultimate loads

$P = 1.6 \times \text{Live load}$	=	33.6	kN
$w = 1.2 \times \text{Dead load}$	=	0.475	kN/m

#### Forces

$$\text{Bending moment (M)} = \{(w \times l^2)/8 + (P/2 \times l/3)\}$$

$$\text{Bending moment (M)} = 7.38 \text{ kN.m}$$

$$\text{Shear Force (V)} = \{(w \times l)/2 + (P/2)\}$$

$$\text{Shear Force (V)} = 17.11 \text{ kN}$$



**REINFORCED CONCRETE BEAM DESIGN ( RECTANGULAR SECTIONS ONLY )**

**Fill In The Yellow Blocks Accordingly**

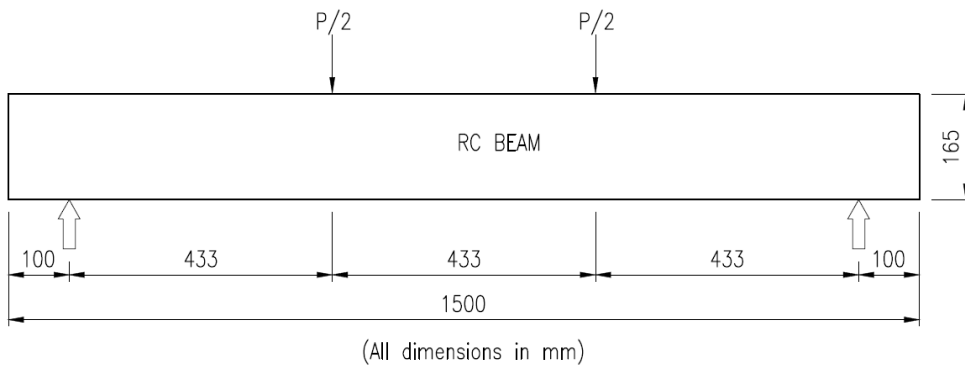
Reference	Calculations	Output
Assumed  table 3  table 2 3.3.3.2	<b>DIMENSIONS</b>	
	Span (mm) =	1300
	Width (mm) =	100
	Depth (mm) =	165
	Cover (mm) =	20
	Main.Reinf.φ =	10
	Links diameter =	6
	<b>PROPERTIES</b>	
	Fy (Mpa) =	450
	Fyv (Mpa) =	250
Fyc (Mpa) =	276.9	
Fcu (Mpa) =	50	
γm =	1.4	
	<b>MOMENT &amp; SHEAR AT ULTIMATE LIMIT STATES</b>	
	Mu (kN.m) =	7.38
	Vu (kN) =	17.11
	d' =	31
T10	<b>Deflection</b>	
	Mark with x where applicable	
	<b>Support conditions</b>	<b>ratio</b>
x	Truly simply supported beams	16
	Simply supported beams with nominally restrained ends	20
	Beams with one end continuous	24
	Beams with both ends continuous	28
	Cantilevers	7
	<b>ratio =</b>	16
Checked.....		

**REINFORCED CONCRETE BEAM DESIGN ( RECTANGULAR SECTIONS ONLY )**

Reference	Calculations	Output	
SABS0100 4.3.3.4.1	<b>MOMENT &amp; SHEAR GIVEN</b>		
	Mu (kN.m) = 7.38		
	Vu (kN.m) = 17.11		
	Assumed d (mm) = 134		
	Calculated d (mm) = 134	therefore d= 134	d (mm) = 134
	Mr (concrete) = 14.0057	kN.m	
	$K = M / b \times d^2 \times f_{cu}$		
	K = 0.082	<b>No Compression reinf. required</b>	
	K' = 0.156		
	$Z = d \{ 0.5 + ( 0.25 - k / 0.9 )^{1/2} \}$	K = 0.082	
	Z = 120.376		
	Zmax = 0.95d	Therefore use Z as 120.376 mm	Z (mm) = 120.37602
	Zmax = 127.3	mm	
	<b>Area of Tension Reinforcement Required</b>		
	As = M / 0.87x Z x fy		
Required As = 156.597 mm <sup>2</sup>	Use 2Y10	Tensile bars = 2Y10	
Min. As = 21.45 mm <sup>2</sup>	Area Used 157 mm <sup>2</sup>	A (mm <sup>2</sup> ) = 157	
Max. As = 660 mm <sup>2</sup>			
<b>Area of Compression Reinforcement Required</b>			
d' = 31			
K = 0.082			
As' = ( K - K' ) fcu x b x d <sup>2</sup> / 0.87 x fy ( d - d' )			
As' ( compression ) = not applicable mm <sup>2</sup>	As = 156.597 mm <sup>2</sup>		
As = K' x fcu x b x d <sup>2</sup> / 0.87 x fy x Z + As' fcy / fy			
As = not applicable mm <sup>2</sup>			

4.3.4	<b>SHEAR</b>					
4.3.4.1	Shear stress - $v = V / b \times d$ $v =$	$v$ should not exceed $0.75(f_{cu})^{1/2}$ or 4.75 Mpa 1.277	OK does not exceed maximum stresses	$0.75(f_{cu})^{1/2} =$	5.30330086	
	$vc = (0.75/\gamma_m) \times (f_{cu}/25)^{1/3} \times (100 \times A_s / b_v \times d)^{1/3} \times (400/d)^{1/4}$ 400 / d	should not be taken as less than 1 2.99			2.99	
	$100 \times A_s / b_v \times d$	should not be taken as greater than 3 1.17	< 3 OK	$A_s =$	157.00	mm <sup>2</sup>
4.3.4.1.2	$vc =$	0.935	MPa			Fail provide shear reinf.
4.11.4.5.3	Nominal Reinforcement (Links) high-yiel steel links $A_{sv} / S_v = 0.0012 \text{ bt}$ $S_v =$ mild steel links $A_{sv} / S_v = 0.002 \text{ bt}$ $S_v =$	not applicable	mm	$A_{sv} =$	6	57
		not applicable	mm			
4.3.4.1.3	Reinforcement (Links) $(A_{sv} / S_v) > b (v - vc) / 0.87 f_{yv}$ $A_{sv}/s_v$ required = $S_v < \text{or} =$  $A_{sv} = a_v.b_v(v - 2d.vc / a_v)/0.87f_{yv}$ $A_{sv} =$	0.157 360.050  21.0		Max spacing =	100.5	mm
				> or =	42.7	mm <sup>2</sup>
						Reduce spacing to 50 mm to ensure beams do not fail in shear at loading greater than theoretical load
Checked.....						

## A.2 Eurocode 2 design



### DIMENSIONS

Span (l)	=	1.3	m
Width (b)	=	0.1	m
Depth (D)	=	0.165	m

### Loading

Live load	=	21	kN
Dead load	=	Beam self weight	
Self weight (w)	=	$25 \times \text{width} \times \text{depth}$	
Self weight (w)	=	0.413	kN/m

### Ultimate loads

$P = 1.5 \times \text{Live load}$	=	31.5	kN
$w = 1.35 \times \text{Dead load}$	=	0.557	kN/m

### Forces

$$\text{Bending moment (M)} = \{(w \times l^2)/8 + (P/2 \times l/3)\}$$

$$\text{Bending moment (M)} = 6.94 \text{ kN.m}$$

$$\text{Shear Force (V)} = \{(w \times l)/2 + (P/2)\}$$

$$\text{Shear Force (V)} = 16.11 \text{ kN}$$

**REINFORCED CONCRETE BEAM DESIGN ( RECTANGULAR SECTIONS ONLY )**

**Fill In The Yellow Blocks Accordingly**

Reference	Calculations	Output
Eurocode 2	<b>DIMENSIONS</b> Span (mm) = 1300 Width (mm) = 100 Depth (mm) = 165 Cover (mm) = 20	
Assumed	Main.Reinf. $\phi$ = 8 Links diameter = 6	
3.2.2	<b>PROPERTIES</b> $F_{yk}$ (Mpa) = 500 $F_{yv}$ (Mpa) = 250 $F_{yc}$ (Mpa) = 276.9 $F_{ck}$ (Mpa) = 50 $\gamma_m$ = 1.4	
table 3.1	<b>MOMENT &amp; SHEAR AT ULTIMATE LIMIT STATES</b>  $M_u$ (kN.m) = 6.94 $V_u$ (kN) = 16.1 $d'$ = 30	
T7.4N	<b>Deflection</b> Mark with x where applicable	
	<b>Support conditions</b>	<b>ratio</b>
x	Simply supported beams, one or two way spanning	20
	Beams with one end continuous	26
	Beams with both ends continuous	30
	Slab supported on columns without beams (flat slab)	24
	Cantilevers	8
	<b>ratio =</b>	20
Checked.....		

6.2.2	<p><b><u>SHEAR</u></b></p> <p><b>Applied Shear Force (<math>V_{ED}</math>):</b> <span style="float: right;"><math>V_{Rd \cot \theta = 2.5} = 5.51</math></span></p> <p><math>V_{ED} = 16.1</math> kN</p> <p><b>Beam shear resistance:</b></p> <p><math>v_{min} = 0.15 \times d \times b \times (f_{ck})^{1/2}</math></p> <p><math>v_{min} = 14.319</math> kN <span style="color: red;"><b>Fail provide shear reinf.</b></span></p> <p><b>Maximum possible shear force:</b></p> <p><math>V_{EDmax} = 16.1</math> kN <span style="float: right;">Try 2 legs of R <span style="border: 1px solid black; background-color: yellow; padding: 2px;">6</span></span></p> <p><math>Asv = 57</math></p> <p><b>Angle of strut is between 22 and 45</b></p> <p><b>Beam shear resistance:</b></p> <p><b>Nominal Reinforcement (Links)</b></p> <p><b>high-yiel steel links</b></p> <p><math>s = (A_{sv} \times f_{yk}) / 0.08 \times b \times (f_{ck})^{0.5}</math></p> <p><math>s = 499.824</math> mm</p> <p><b>mild steel links</b></p> <p><math>s = (A_{sv} \times f_{yv}) / 0.08 \times b \times (f_{ck})^{0.5}</math></p> <p><math>Sv = 249.912</math> mm</p> <p><b>Reinforcement (Links)</b></p> <p><b>Restrict spacing to <math>0.75 \times d</math></b> <span style="float: right;">Max spacing = <b>101.25</b> mm</span></p> <p style="color: red; text-align: right;"><b>Reduce spacing to 50 mm to ensure beams do not fail in shear at loading greater than theoretical load</b></p>	
Checked.....		

## APPENDIX B: DETAILS OF AGGREGATES AND CONCRETE MIX DESIGN

### B.1 Fine aggregate grading analysis and grading curve

Table B. 1: Grading analysis of Fine Aggregate

Diameter (mm)	Mass of Sieve (g)	Mass of Sieve & Soil (g)	Soil Retained (g)	Soil Retained (%)	Soil Passing (%)
6.70	468.3	468.30	0.0	0.0	100.0
4.75	454.2	467.40	13.2	2.6	97.4
2.36	420.7	601.48	180.8	36.2	61.2
1.18	450	570.64	120.6	24.1	37.1
0.60	414.5	465.94	51.4	10.3	26.8
0.30	323.8	360.76	37.0	7.4	19.4
0.15	348.9	378.37	29.5	5.9	13.5
0.075	494.9	526.86	32.0	6.4	7.1
Pan	449.4	484.36	35.0	7.0	0.0
<b>TOTAL:</b>			<b>499.4</b>	<b>100</b>	

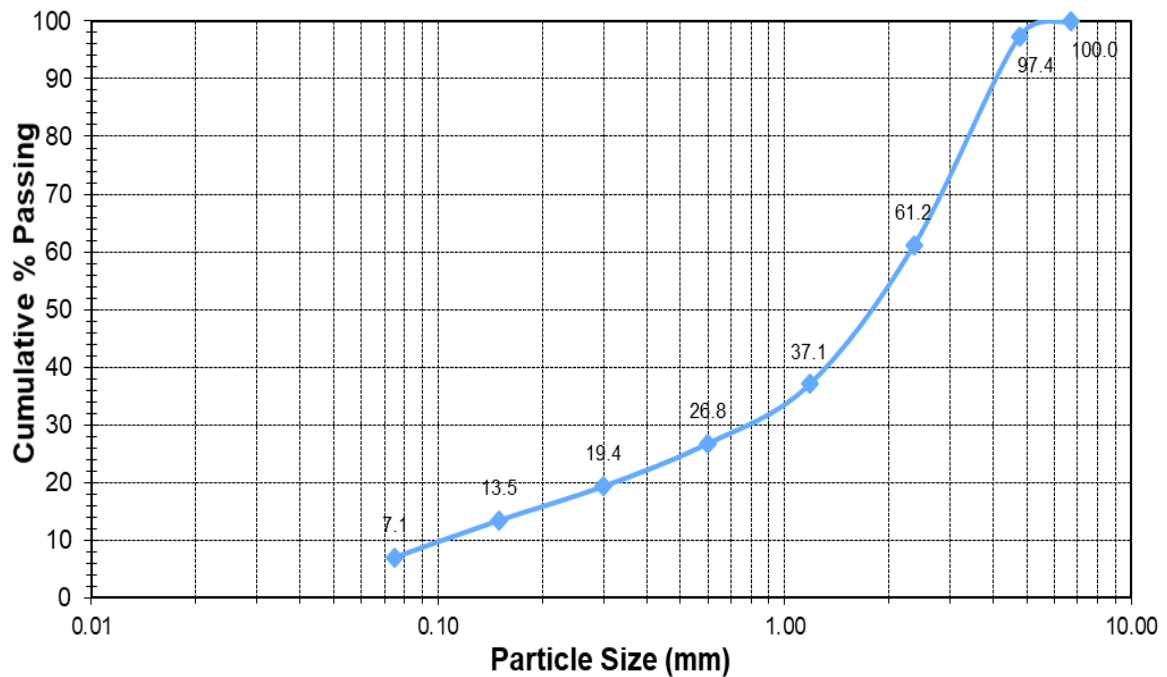
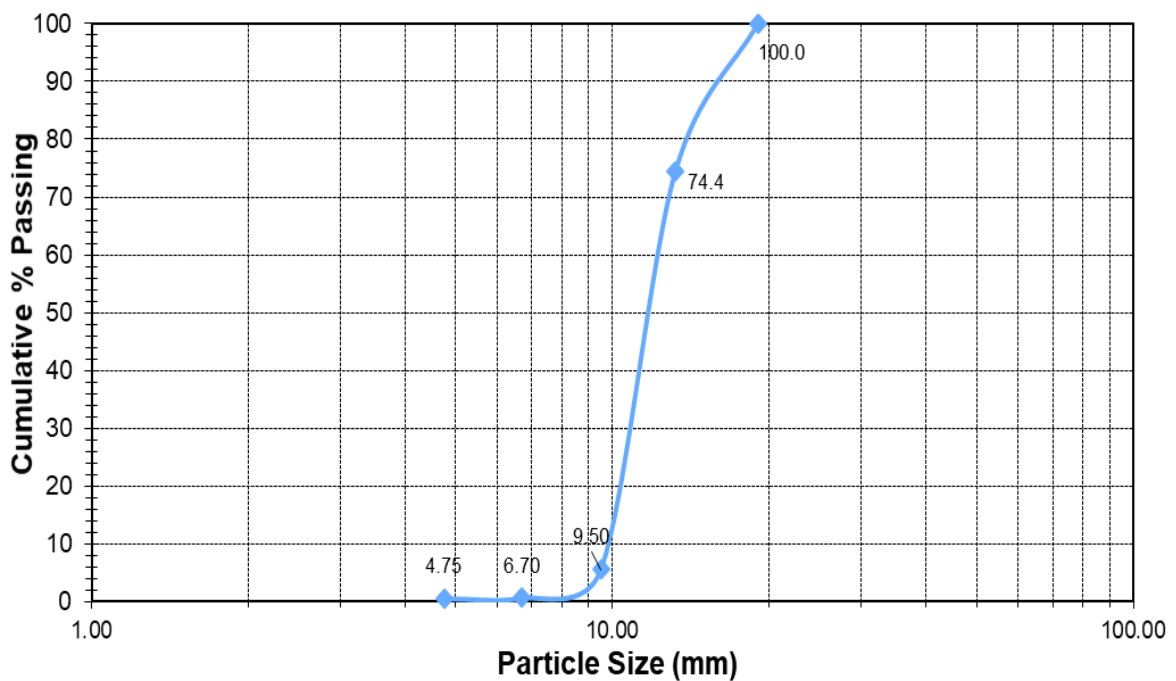


Figure B. 1: Grading curve of fine aggregate

## B.2 Coarse aggregate grading analysis and grading curve

**Table B. 2: Grading analysis of Coarse Aggregate**

Diameter (mm)	Mass of Sieve (g)	Mass of Sieve & Soil (g)	Soil Retained (g)	Soil Retained (%)	Soil Passing (%)
19.00	1591.7	1591.7	0.0	0.0	100.0
13.20	1446.6	2213.2	766.6	25.6	74.4
9.50	1436.4	3502.3	2065.9	68.9	5.6
6.70	1593.2	1741.7	148.5	5.0	0.6
4.75	454.2	457.6	3.4	0.1	0.5
Pan	1119.4	1134.0	14.6	0.5	0.0
<b>TOTAL:</b>			<b>2999</b>	<b>100</b>	



**Figure B. 2: Grading curve of coarse aggregate**



### B.3 Concrete Mix Design

The concrete mix design is based on the volumetric mix design from the Cement and Concrete Institute (C&CI) method.

#### Step 1: Water Cement Ratio

<b>Material</b>	<b>kg</b>		Cement		WC ratio	<b>0.5</b>
Cement	<b>390</b>	100.0%	extenders			
Extender	<b>0</b>	0.0%	FA	Fly ash		
	390		GGBS	ground granulated blastfurnace slag		

#### Step 2: Water Content

Water requirement of concrete mixes (13.2 mm stone, 75mm Slump) – no adjustment made

W req **195**

#### Step 3: Cement Content

**Cement Content**

CC = Water requirement /WC ratio

CC = **390.0** kg/m<sup>3</sup>

#### Step 4: Stone Content

**Stone content**

St = CBDst (K-0.1 FM)

St = **1004.55**

St = mass of stone in 1 m<sup>3</sup> of concrete (kg)

CBDst = dry compacted bulk density of stone

determined in accordance with SABS Method 845:1994 (kg/m<sup>3</sup>)

K = a factor that depends on the nominal size of the stone and the workability of concrete

FM = fineness modulus of sand

**1810**

**0.9**

**3.45**

**Table: Values of K for determining stone content**

Approx. Slump (mm)	Compaction		K			
			Nominal maximum size of stone (mm)			
			9.5	13.2	19	26.5
75-150	Hand compaction		0.75	0.84	0.94	1.00
25-100	Moderate vibration		0.80	0.90	1.00	1.06
0-25	Heavy vibration		1.00	1.05	1.05	1.10

#### Step 4: Sand Content

**Sand Content**

Volume of sand = 1 - [ volume of cement + volume of stone + volume of water]  
or mass of sand /RDs

$$= R_Ds * 1000 [1 - C/R_{Dc} - St/R_{Dst} - \text{water}/1000]$$

C = mass of cement per m<sup>3</sup> of concrete (kg)

390.00

St = mass of stone per m<sup>3</sup> of concrete (kg)

1004.55

R<sub>Ds,c,st</sub> = particle relative density, sand, con & stone

2.94	R <sub>Ds</sub>
3.12	R <sub>Dc</sub>
1.81	R <sub>Dst</sub>

**SC= 367.50**

Summary	kg/m <sup>3</sup>
<b>Cement</b>	<b>390.0</b>
<b>Stone</b>	<b>1004.6</b>
<b>Sand</b>	<b>367.5</b>
<b>Water</b>	<b>195.0</b>
	1957.1

7.8 bags of cement

Proportions by bags

50.0 kg

128.8 kg

47.1 kg

25.0 l

**Note:** There was an error on the relative density for sand. The correct value is 2.94.

## APPENDIX C: EXPERIMENTAL RESULTS

### C.1 Compressive Strength and Density Results

**Table C. 1: 7 day Compressive strength results**

Element	Cube Number	Date of Cast	Test Date	Test Age (days)	Mass (g)	Compressive Strength		Ave. Compressive Strength (MPa)
						Load (kN)	Strength (MPa)	
EC2 & SANS-NS-NC B1	1	27 June 2019	04 July 2019	7	2430.4	364.6	36.5	<b>36.8</b>
EC2 & SANS-NS-NC B2	2	27 June 2019	04 July 2019	7	2448.2	368.4	36.8	
EC2 & SANS-NS-NC B3	3	27 June 2019	04 July 2019	7	2454.5	370.2	37.0	
EC2 & SANS-S-NC B1	1	05 July 2019	12 July 2019	7	2432.3	294.5	29.5	<b>30.6</b>
EC2 & SANS-S-NC B2	2	05 July 2019	12 July 2019	7	2440.5	314.4	31.4	
EC2 & SANS-S-NC B3	3	05 July 2019	12 July 2019	7	2438.4	309.3	30.9	
EC2 & SANS-NS-C B1	1	12 July 2019	19 July 2019	7	2436.1	330.8	33.1	<b>36.0</b>
EC2 & SANS-NS-C B2	2	12 July 2019	19 July 2019	7	2441.7	377.6	37.8	
EC2 & SANS-NS-C B3	3	12 July 2019	19 July 2019	7	2458.4	370.1	37.0	
EC2 & SANS-S-C B1	1	16 July 2019	23 July 2019	7	2470.3	312.4	31.2	<b>31.8</b>
EC2 & SANS-S-C B2	2	16 July 2019	23 July 2019	7	2445.6	322.3	32.2	
EC2 & SANS-S-C B3	3	16 July 2019	23 July 2019	7	2460.2	318.7	31.9	

**Table C. 2: 28 day Compressive strength results**

Element	Cube Number	Date of Cast	Test Date	Test Age (days)	Mass (g)	Compressive Strength		Ave. Compressive Strength (MPa)
						Load (kN)	Strength (MPa)	
EC2 & SANS-NS-NC B1	4	27 June 2019	25 July 2019	28	2536.2	574.8	57.48	<b>56.4</b>
EC2 & SANS-NS-NC B2	5	27 June 2019	25 July 2019	28	2493.9	560	56	
EC2 & SANS-NS-NC B3	6	27 June 2019	25 July 2019	28	2435.2	556.4	55.64	
EC2 & SANS-S-NC B1	4	05 July 2019	02 August 2019	28	2569.7	507.4	50.74	<b>54.6</b>
EC2 & SANS-S-NC B2	5	05 July 2019	02 August 2019	28	2482.8	539.2	53.92	
EC2 & SANS-S-NC B3	6	05 July 2019	02 August 2019	28	2464.5	591.4	59.14	
EC2 & SANS-NS-C B1	4	12 July 2019	09 August 2019	28	2437	575	57.5	<b>58.0</b>
EC2 & SANS-NS-C B2	5	12 July 2019	09 August 2019	28	2501.8	587	58.7	
EC2 & SANS-NS-C B3	6	12 July 2019	09 August 2019	28	2468.5	577.5	57.75	
EC2 & SANS-S-C B1	4	16 July 2019	13 August 2019	28	2436.1	535	53.5	<b>53.0</b>
EC2 & SANS-S-C B2	5	16 July 2019	13 August 2019	28	2441.7	532	53.2	
EC2 & SANS-S-C B3	6	16 July 2019	13 August 2019	28	2458.4	522	52.2	

## C.2 Corrosion Acceleration Tests

### C 2.1 Estimation of required current inducing corrosion

- a. Required current for 10 mm diameter bars – Assume 20% loss on the area corresponding to NaCl pond:**

*Theoretical mass loss ( $M_{th}$ ) = bar mass  $\times$  affected length  $\times$  0.2  $\times$  1000*

$$M_{th} = 0.613 \times 0.5 \times 0.2 \times 1000$$

$$M_{th} = 61.30 \text{ g}$$

$$I = \frac{M_{th} \times z \times F}{M \times t \times 86400}$$

$$I = \frac{61.30 \times 2 \times 96500}{56 \times 5 \times 86400}$$

*Therefore  $I = 0.489 \text{ A}$*

- b. Required current for 8 mm diameter bars – Assume 20% loss on the area corresponding to NaCl pond:**

*Theoretical mass loss ( $M_{th}$ ) = bar mass  $\times$  affected length  $\times$  0.2  $\times$  1000*

$$M_{th} = 0.392 \times 0.5 \times 0.2 \times 1000$$

$$M_{th} = 39.20 \text{ g}$$

$$I = \frac{M_{th} \times z \times F}{M \times t \times 86400}$$

$$I = \frac{39.20 \times 2 \times 96500}{56 \times 5 \times 86400}$$

*Therefore  $I = 0.313 \text{ A}$*

## C 2.2 Corrosion degree results

Tables C.3 and C.4 present the corrosion degree results for SANS 10100-1 beams and Eurocode 2 beams respectively.

**Table C. 3: SANS 10100-1 beams corrosion degree results**

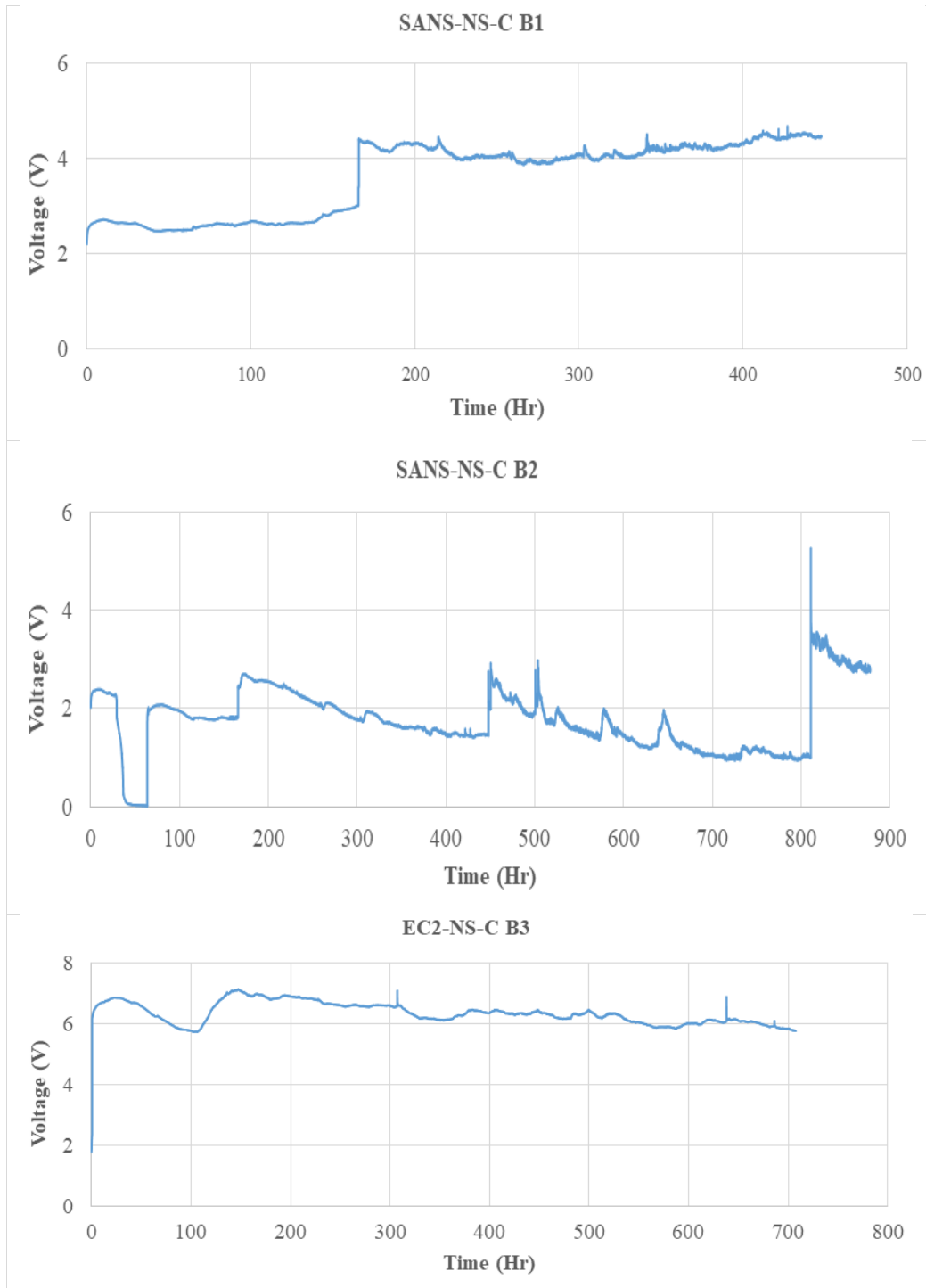
Specimen	Bar Number	Start Date	End Date	No. of Days	Initial dia. (mm)	Final dia. (mm)	Cross sect. area loss (%)	Average corr. Degree (%)
SANS-NS-C B1	1	27-Aug-19	16-Sep-19	20	10	5.3	71.9	47.8
	2	27-Aug-19	16-Sep-19	20	10	8.74	23.6	
SANS-NS-C B2	1	27-Aug-19	01-Oct-19	35	10	9.22	15.0	14.6
	2	27-Aug-19	01-Oct-19	35	10	9.26	14.3	
SANS-NS-C B3	1	27-Aug-19	01-Oct-19	35	10	8.74	23.6	31.2
	2	27-Aug-19	01-Oct-19	35	10	7.82	38.8	
SANS-S-C B1	1	15-Oct-19	23-Nov-19	39	10	8.9	20.8	14.5
	2	15-Oct-19	23-Nov-19	39	10	8.71	24.1	
	3	15-Oct-19	23-Nov-19	39	10	9.42	11.3	
	4	15-Oct-19	23-Nov-19	39	10	9.9	2.0	
SANS-S-C B2	1	19-Oct-19	19-Nov-19	31	10	7.8	39.2	21.9
	2	19-Oct-19	19-Nov-19	31	10	8.56	26.7	
	3	19-Oct-19	19-Nov-19	31	10	9.76	4.7	
	4	19-Oct-19	19-Nov-19	31	10	9.12	16.8	
SANS-S-C B3	1	29-Oct-19	09-Jan-20	72	10	9.46	10.5	17.4
	2	29-Oct-19	09-Jan-20	72	10	9.18	15.7	
	3	29-Oct-19	09-Jan-20	72	10	8.84	21.9	
	4	29-Oct-19	09-Jan-20	72	10	8.86	21.5	

**Table C. 4: Eurocode 2 beams corrosion degree results**

<b>Specimen</b>	<b>Bar Number</b>	<b>Start Date</b>	<b>End Date</b>	<b>No. of Days</b>	<b>Initial dia. (mm)</b>	<b>Final dia. (mm)</b>	<b>Cross sect. area loss (%)</b>	<b>Average corr. Degree (%)</b>
EC2-NS-C B1	1	18-Sep-19	15-Oct-19	27	8	7.2	19.0	37.7
	2	18-Sep-19	15-Oct-19	27	8	4.1	73.7	
	3	18-Sep-19	15-Oct-19	27	8	7.14	20.3	
EC2-NS-C B2	1	18-Sep-19	07-Oct-19	19	8	7.24	18.1	25.5
	2	18-Sep-19	07-Oct-19	19	8	6.9	25.6	
	3	18-Sep-19	07-Oct-19	19	8	6.56	32.8	
EC2-NS-C B3	1	18-Sep-19	18-Oct-19	30	8	6.44	35.2	34.5
	2	18-Sep-19	18-Oct-19	30	8	6.76	28.6	
	3	18-Sep-19	18-Oct-19	30	8	6.21	39.7	
EC2-S-C B1	1	07-Oct-19	09-Nov-19	33	8	6.78	28.2	27.9
	2	07-Oct-19	09-Nov-19	33	8	6.84	26.9	
	3	07-Oct-19	09-Nov-19	33	8	6.84	26.9	
	4	07-Oct-19	09-Nov-19	33	8	6.48	34.4	
	5	07-Oct-19	09-Nov-19	33	8	7.44	13.5	
	6	07-Oct-19	09-Nov-19	33	8	6.32	37.6	
EC2-S-C B2	1	04-Oct-19	30-Oct-19	26	8	6.9	25.6	27.0
	2	04-Oct-19	30-Oct-19	26	8	6.84	26.9	
	3	04-Oct-19	30-Oct-19	26	8	7.3	16.7	
	4	04-Oct-19	30-Oct-19	26	8	7.2	19.0	
	5	04-Oct-19	30-Oct-19	26	8	6.02	43.4	
	6	04-Oct-19	30-Oct-19	26	8	6.68	30.3	
EC2-S-C B3	1	04-Oct-19	29-Oct-19	25	8	6.48	34.4	29.0
	2	04-Oct-19	29-Oct-19	25	8	6.12	41.5	
	3	04-Oct-19	29-Oct-19	25	8	7.24	18.1	
	4	04-Oct-19	29-Oct-19	25	8	7.14	20.3	
	5	04-Oct-19	29-Oct-19	25	8	6.58	32.3	
	6	04-Oct-19	29-Oct-19	25	8	6.82	27.3	

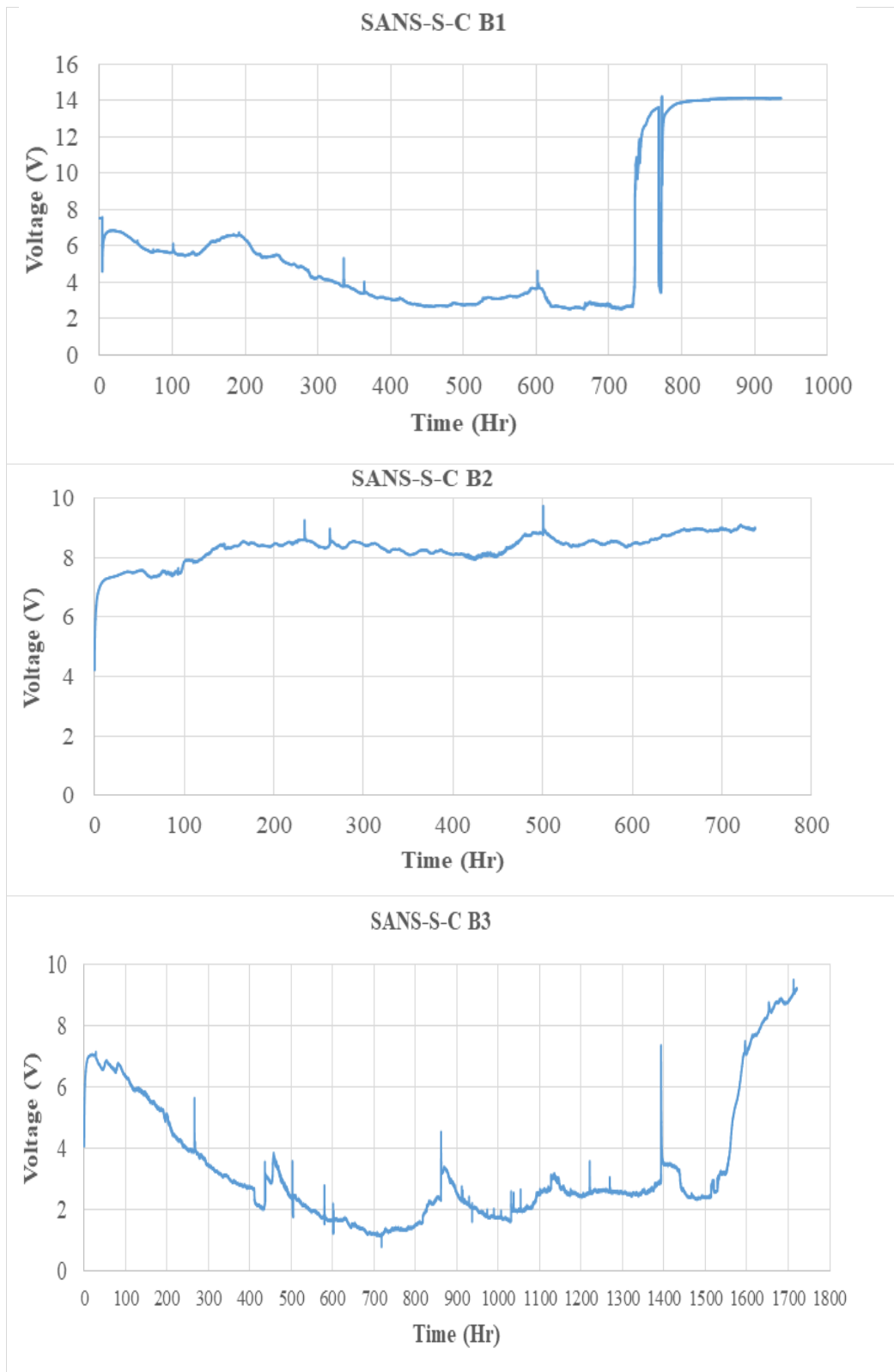
### C 2.3 Voltage-time curves

Figure C.1 to Figure C.4 present the Voltage vs Time (V-T) curves for various beams.



**Figure C. 1: Voltage-Time curve for SANS 10100-1 non-spliced beams**





**Figure C. 2: Voltage-Time curve for SANS 10100-1 lap-spliced beams**

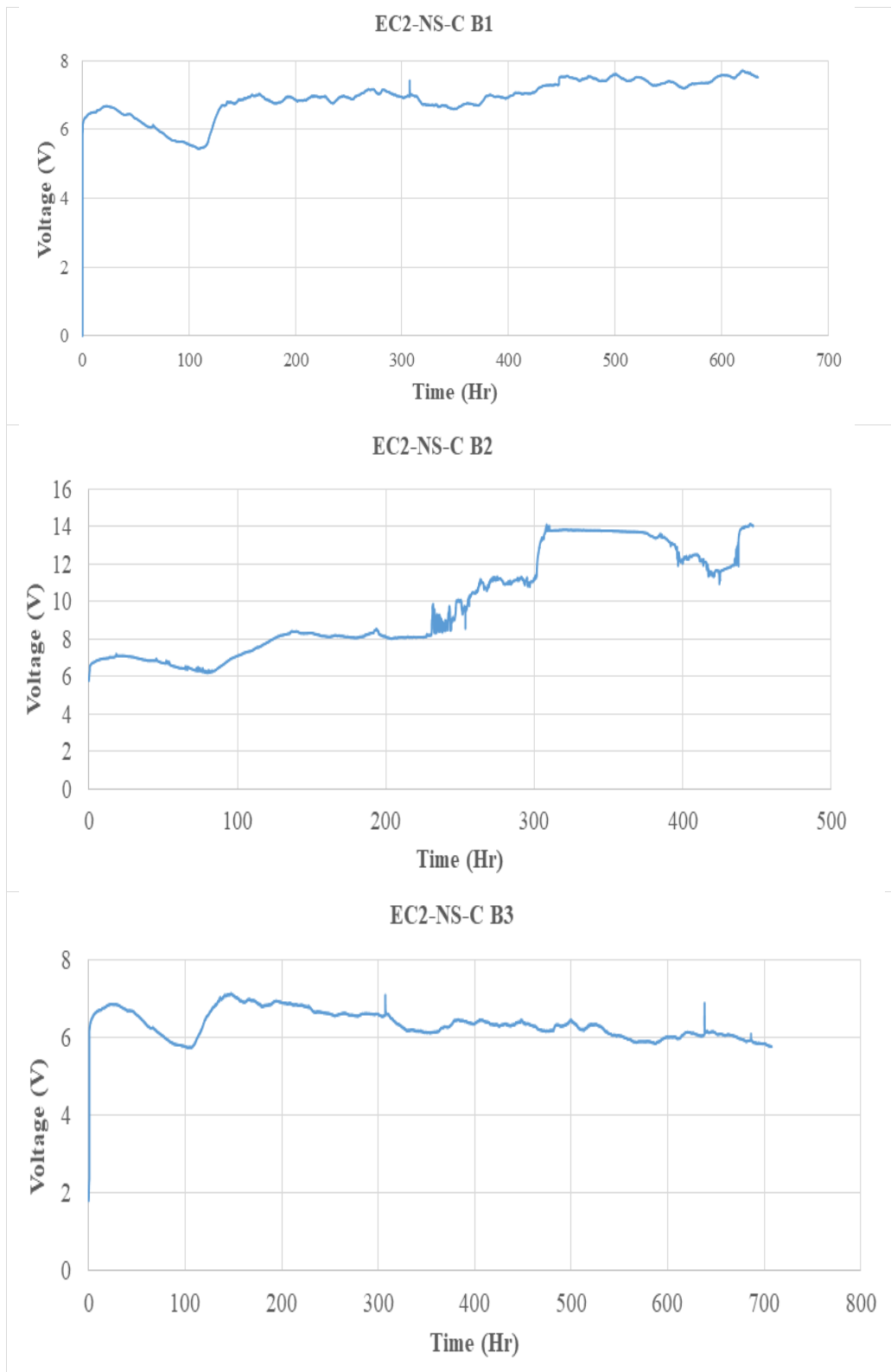


**Figure C. 3: Voltage-Time curve for Eurocode 2 non-spliced beams**

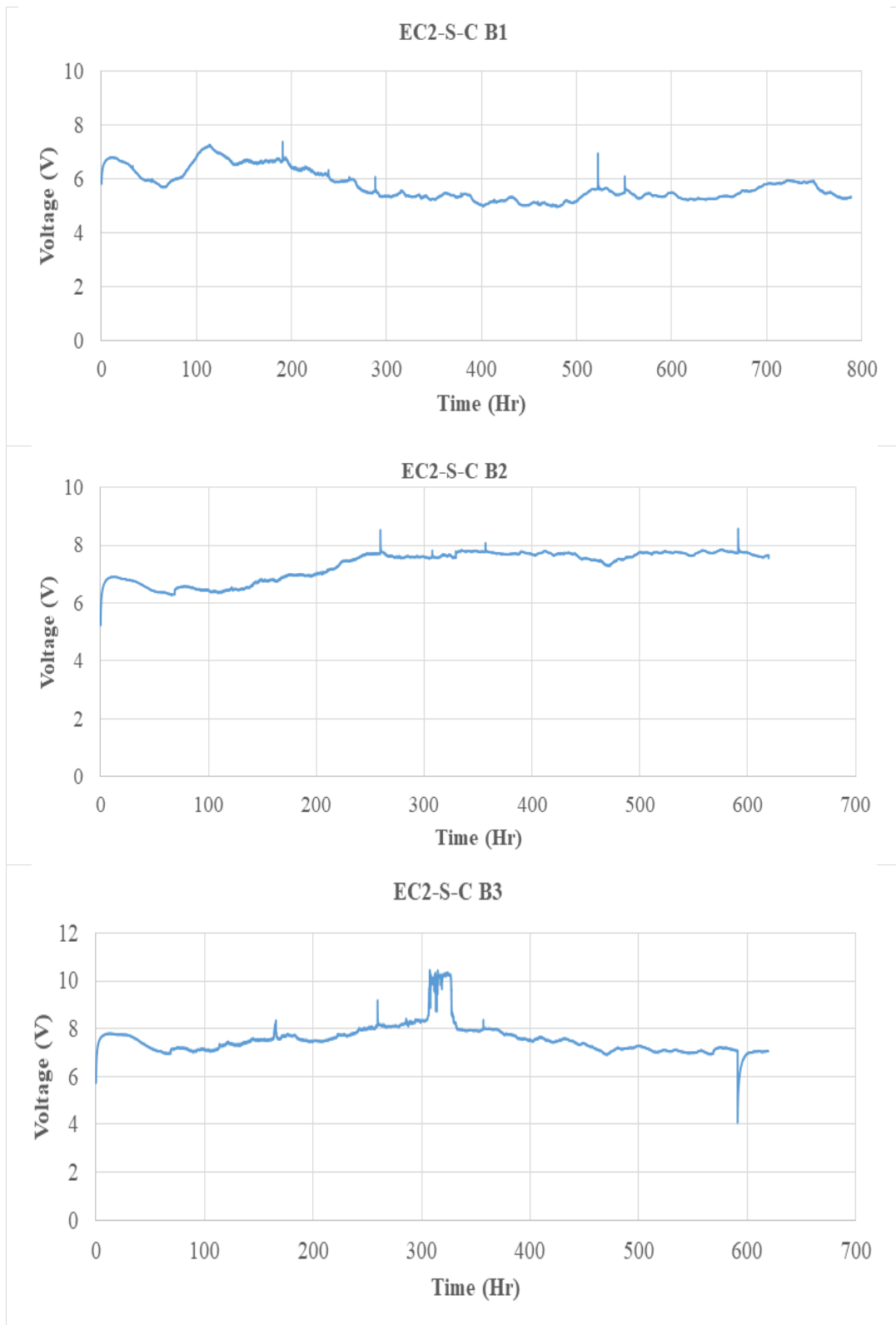


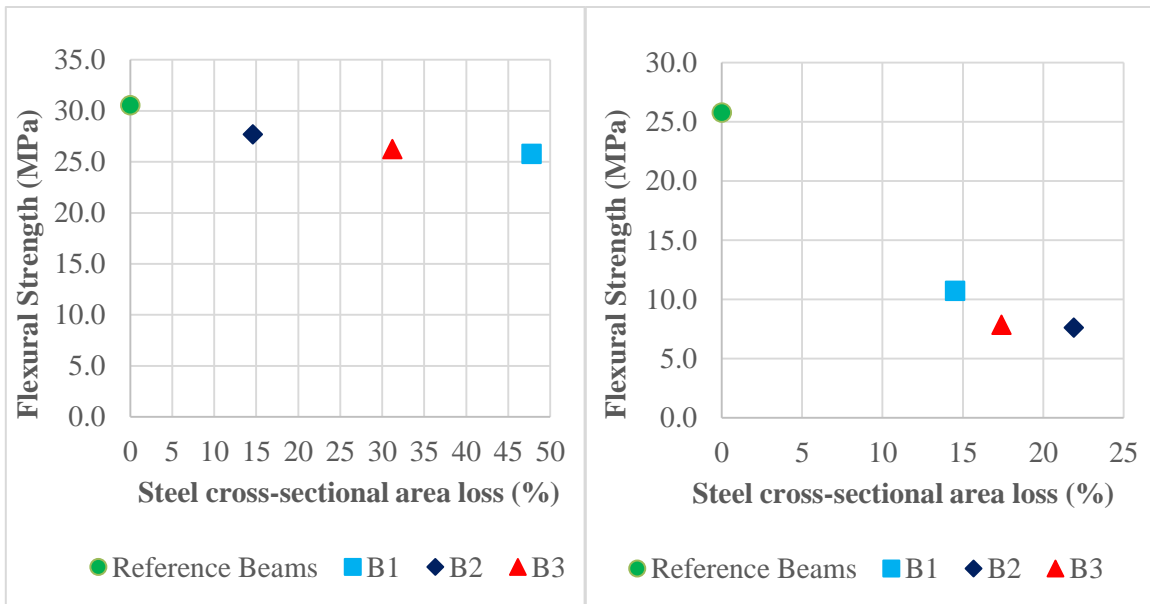
**Figure C. 4: Voltage-Time curve for Eurocode 2 lap-spliced beams**

## C 2.4 Theoretical vs Experimental load

**Table C. 5: Theoretical and experimental load-carrying capacity of control RC beams**

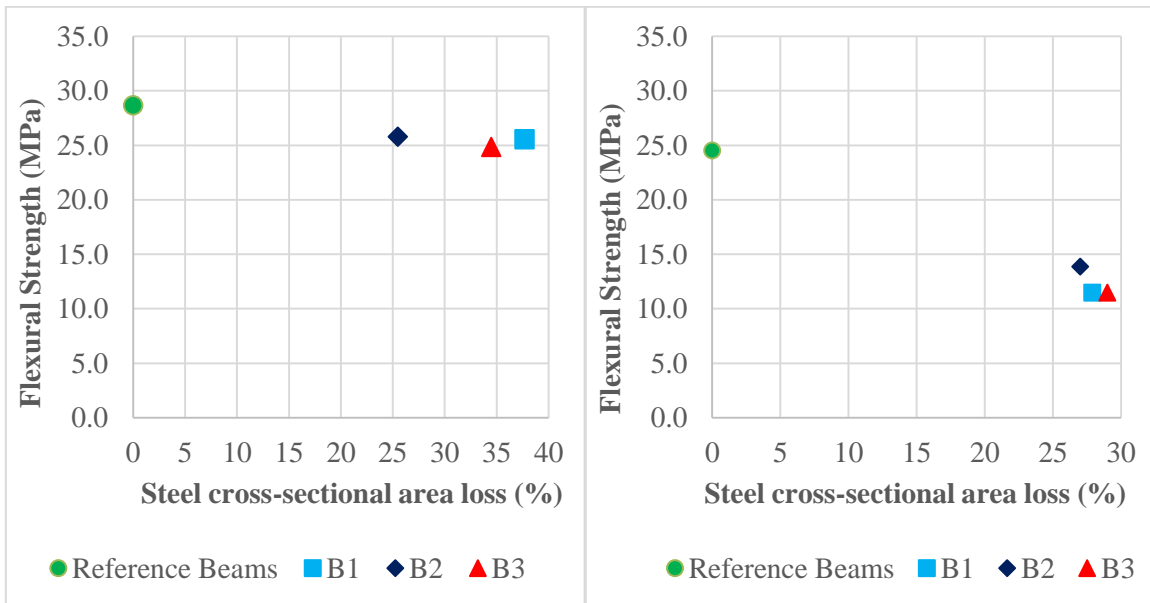
Beam Type	Ultimate load (kN)		Variance (%)
	Theoretical (kN)	Experimental (kN)	
SANS-NS-NC B1	56	64	14.3
SANS-NS-NC B2	56	64	14.3
SANS-NS-NC B3	56	64	14.3
EC2-NS-NC B1	36.5	60	64.4
EC2-NS-NC B2	36.5	60	64.4
EC2-NS-NC B3	36.5	60	64.4
SANS-S-NC B1	55.8	52.5	-5.9
SANS-S-NC B2	55.8	54	-3.2
SANS-S-NC B3	55.8	55	-1.4
EC2-S-NC B1	36.5	52	42.5
EC2-S-NC B2	36.5	52	42.5
EC2-S-NC B3	36.5	50	37.0

### C 2.5 Flexural strength vs corrosion results



a) SANS-NS-C

b) SANS-S-C



c) EC2-NS-C

d) EC2-S-C

**Figure C. 5: Flexural strength and steel cross-sectional loss**

### C 2.6 Ductility vs corrosion results

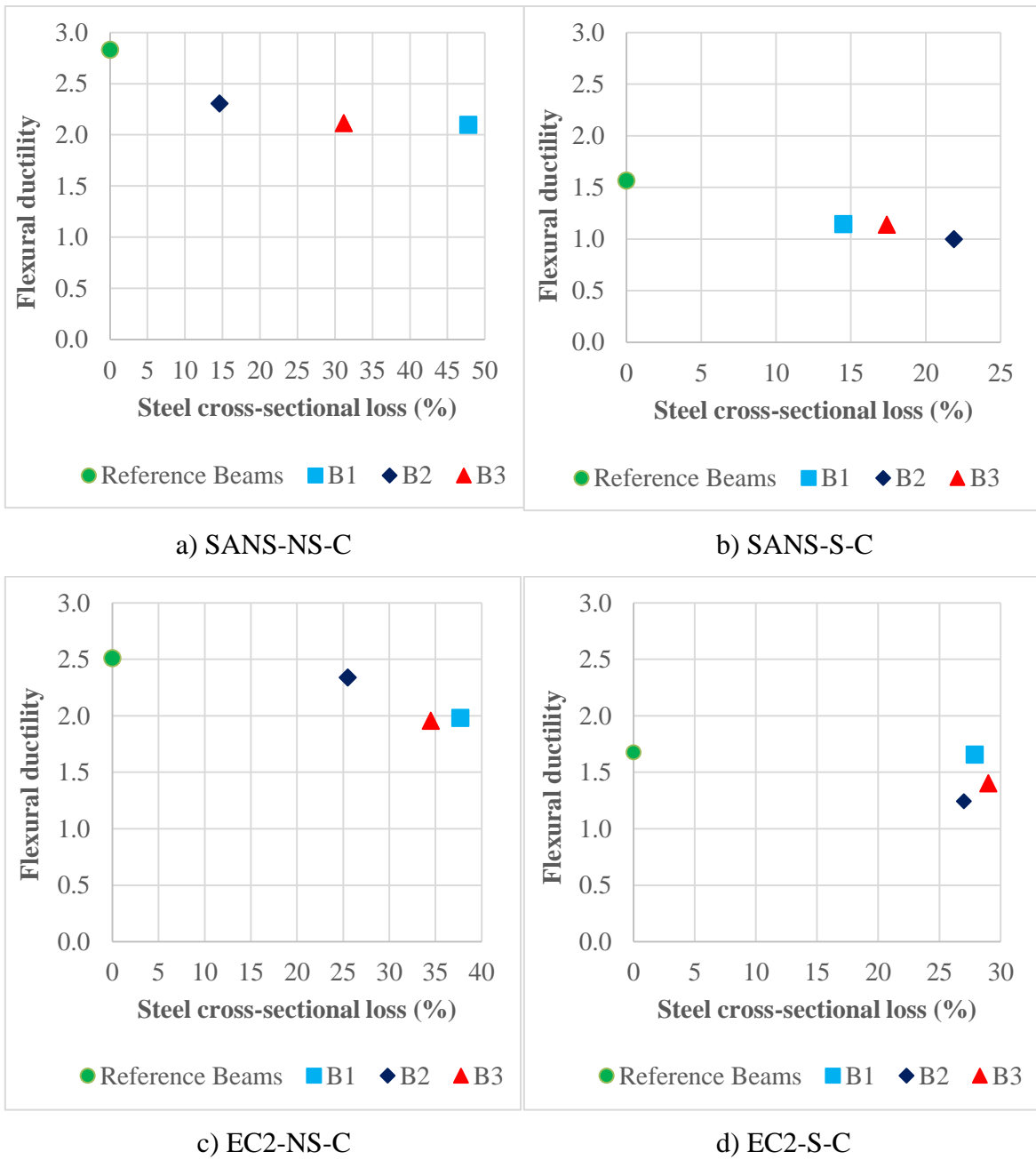


**Figure C. 6: Flexural ductility and steel cross-sectional loss**

## School of Civil Engineering and Environmental Engineering Ethics Committee: Ethics Waiver



**HUMAN RESEARCH ETHICS COMMITTEE  
(NON-MEDICAL)**

Registration number: REC-101114-044

### **SCHOOL OF CIVIL AND ENVIRONMENTAL ENGINEERING ETHICS COMMITTEE**

Ethics clearance number: CEECW 720130 2019

01 April 2019

Re: Anele Emanuel Mahlawe (720130)

To whom it may concern,

Anele Emanuel Mahlawe (720130) is currently registered as a Masters of Science in Engineering student at the School of Civil and Environmental Engineering, University of the Witwatersrand, Johannesburg. This letter is to confirm that, at the time of writing, Anele Mahlawe does not need ethical clearance for his study entitled 'Effect of corrosion of lap-spliced steel reinforcement on the flexural strength of reinforced concrete beams'. This decision has been reached based upon a description of the project supplied by Anele Mahlawe to the School of Civil and Environmental Engineering Ethics Committee, constituted as a subcommittee of the University Human Research Ethics Committee (Non-Medical), which has been evaluated by the subcommittee chair. This decision has then been ratified by the University Human Research Ethics Committee (Non-Medical). If, however, Anele Mahlawe changes the methods of data collection and analysis for this project, this decision may no longer be valid. If such changes take place, this should be communicated to the School of Civil and Environmental Engineering Ethics Committee.

Please feel free to contact me should you require any further information.

Thank you.

Yours sincerely,

A handwritten signature in black ink, appearing to read 'John Ndiritu'.

Prof John Ndiritu, School Ethics Chair

Shaun Schoeman (Senior Administrative Officer)  
Solomon Mahlangu House, 10<sup>th</sup> Floor, Room 10004, Jorissen Street, Braamfontein, Johannesburg  
Private Bag 3, Wits 2050  
T + 27(0)11 717 1408 | E [Shaun.Schoeman@wits.ac.za](mailto:Shaun.Schoeman@wits.ac.za) | [hrec-medical.researchoffice@wits.ac.za](mailto:hrec-medical.researchoffice@wits.ac.za)  
[www.wits.ac.za/research/about-our-research/ethics-and-research-integrity/](http://www.wits.ac.za/research/about-our-research/ethics-and-research-integrity/)